CANADIAN THESES

THÈSES CANADIENNES

NOTICE

The quality of this microfiche is heavily dependent upon the quality of the original thesis submitted for microfilming. Every effort has been made to ensure the highest quality of reproduction possible.

If pages are missing, contact the university which granted the degree.

Some pages may have indistinct print especially if the original pages were typed with a poor typewriter ribbon or if the university sent us an inferior photocopy.

Previously copyrighted materials (journal articles, published tests, etc.) are not filmed.

Reproduction in full or in part of this film is governed by the Canadian Copyright Act, R.S.C. 1970, c. C-30. Please read the authorization forms which accompany this thesis.

AVIS

La qualité de cette microfiche dépend grandement de la qualité de la thèse soumise au microfilmage. Nous avons tout fait pour assurer une qualité supérieure de reproduction.

S'il manque des pages, veuillez communiquer avec l'université qui a conféré le grade.

La qualité d'impression de certaines pages peut laisser à désirer, surtout si les pages originales ont été dactylographiées à l'aide d'un ruban usé ou si l'université nous a fait parvenir une photocopie de qualité inférieure.

Les documents qui font déjà l'objet d'un droit d'auteur (articles de revue, examens publiés, etc.) ne sont pas microfilmés.

La reproduction, même partielle, de ce microfilm est soumise à la Loi canadienne sur le droit d'auteur, SRC 1970, c. C-30. Veuillez prendre connaissance des formules d'autorisation qui accompagnent cette thèse.

THIS DISSERTATION
HAS BEEN MICROFILMED
EXACTLY AS RECEIVED

LA THÈSE A ÉTÉ
MICROFILMÉE TELLE QUE
NOUS L'AVONS REÇUE

NL 339 (r. 86/01)

Canada

PERMISSION TO MICROFILM — AUTORISATION DE MICROFILMER

- Please print or type — Écrire en lettres moulées ou dactylographier

Full Name of Author — Nom complet de l'auteur

ROBERT MICHAEL ST. LOUIS

Date of Birth — Date de naissance	Country of Birth — Lieu de naissance
14 NOVEMBER 1958	U.S.A.

Permanent Address — Résidence fixe

703 TURIN ST.
ROME, N.Y. 13440
U.S.A.

Title of Thesis — Titre de la thèse

GEOCHEMISTRY OF THE PLATINUM GROUP ELEMENTS IN THE
TULAMEEN COMPLEX, BRITISH COLUMBIA

University — Université

UNIVERSITY OF ALBERTA

Degree for which thesis was presented — Grade pour lequel cette thèse fut présentée

M.Sc.

Year this degree conferred — Année d'obtention de ce grade	Name of Supervisor — Nom du directeur de thèse
1984	R. D. MORTON AND B.E. NESBITT

Date	Signature
10 APRIL, 1984	

NL-91 (4/77)

THE UNIVERSITY OF ALBERTA

"Geochemistry of the platinum group elements in theTulameen Ultramafic Complex, British

Columbia"

by

Robert Michael St. Louis

A THESIS

SUBMITTED TO THE FACULTY OF GRADUATE STUDIES AND RESEARCH

IN PARTIAL FULFILMENT OF THE REQUIREMENTS FOR THE DEGREE

OF Master of Science

Department of Geology

EDMONTON, ALBERTA

Spring, 1984

THE UNIVERSITY OF ALBERTA

RELEASE FORM

NAME OF AUTHOR   Robert Michael St. Louis

TITLE OF THESIS   "Geochemistry of the platinum group elements in theTulameen

Ultramafic Complex, British Columbia"

DEGREE FOR WHICH THESIS WAS PRESENTED   Master of Science

YEAR THIS DEGREE GRANTED   Spring, 1984

Permission is hereby granted to THE UNIVERSITY OF ALBERTA LIBRARY to

reproduce single copies of this thesis and to lend or sell such copies for private,

scholarly or scientific research purposes only.

The author reserves other publication rights, and neither the thesis nor

extensive extracts from it may be printed or otherwise reproduced without the

author's written permission.

(SIGNED) ....

PERMANENT ADDRESS:

703 TURIN ST.
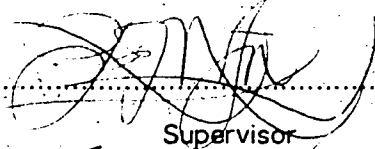
ROME, N.Y. 13440

U.S.A.
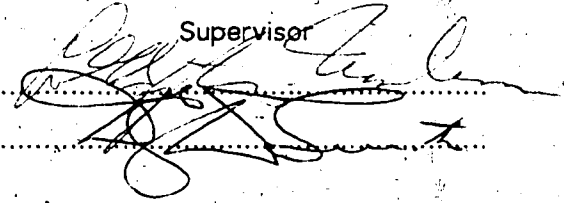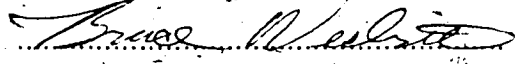
DATED ..APRIL 9.........19 84

THE UNIVERSITY OF ALBERTA

FACULTY OF GRADUATE STUDIES AND RESEARCH

The undersigned certify that they have read, and recommend to the Faculty
of Graduate Studies and Research, for acceptance, a thesis entitled "Geochemistry of the
platinum group elements in theTulameen Ultramafic Complex, British Columbia" submitted
by Robert Michael St. Louis in partial fulfilment of the requirements for the degree of
Master of Science.

....
Supervisor

....
Supervisor

....

Date ....

Dedication

This thesis is dedicated to my family,

particularly Terry and Michelle,

for all they have put up with during

the slaying of this albatross,

and to Mr. Ernie North

for his invaluable help, guidance, and friendship.

Abstract

The platinum group elements (PGE) are distributed roughly according to the degree of differentiation in the Tulameen Complex, with the highest PGE contents in dunitic rocks and the lowest in gabbroic rocks. Exceptions to this are Pd, which appears to be restricted to the least mafic units, and Os, which is present only in rocks that are enriched in magnetite or chromite. In addition, Ru is not present in concentrations that are quantifiable by the analytical techniques used.

Serpentinite and serpentinite-dunite have PGE contents that are substantially higher than the PGE contents of dunite and peridotite. This, together with the fact that serpentinized rocks contain more sulfide minerals than their unaltered equivalents, suggests that the PGE and base metals are remobilized during serpentinization.

Rocks containing 20 to 100 volume percent chromite have the highest noble metal contents of any of the lithologies sampled. These samples, which contain massive, nodular, and schlieren chromite in dunite, have PGE enrichments of one to two orders of magnitude relative to rocks containing accessory or no chromite. In addition, discrete platinum group minerals (PGMs) were observed only in chromite-rich samples. The PGMs occur as cubic inclusions in chromite, dominantly Pt-Fe alloys (Type 1), and as anhedral grains, mainly sperrylite, interstitial to chromite (Type 2). The Type 2 PGMs are often associated with serpentine and Fe-Ni sulfides, especially pentlandite.

Textural and lithochemical data suggest that chromite collected the PGE from the melt as inclusions or droplets adhered to the growth surfaces of chromite grains; with very little isomorphous substitution of the PGE into the chromite lattice. These data also indicate that most of the PGE form discrete PGE-rich phases at the high temperatures associated with the crystallization of chromite. These phases include alloys, sulfides, and possibly monosulfide solid solution (Mss).

The ranges of concentration of the PGE in the Tulameen Complex overlap the ranges for other Alaskan-type complexes. The exceptions are Ru, which is below the limits of quantification by the analytical techniques used, and Pd, which is apparently depleted in the Tulameen Complex. "Overall" averages for Pt, Os, and Pd in the Tulameen

Complex, weighted on the number of samples, agree with the literature values for these elements in Alaskan-type complexes, while the averages for Rh and Ir are substantially lower in the Tulameen Complex.

Acknowledgements

This thesis would not have been possible without the assistance and cooperation of many people. My supervisors, Roger Morton and Bruce Nesbitt, are given my heartfelt thanks for suggesting and financially supporting a research topic that proved to be a challenge. The financial support given by the British Columbia Ministry of Energy, Mines and Petroleum Resources is gratefully acknowledged. The Faculty of Pharmacy and the University of Alberta SLOWPOKE Facility are given my deepest thanks for allowing me to use their facilities, without which this thesis would not have been possible. In particular, Dr. L. G. Stephens-Newsham is thanked for teaching me the fundamentals of neutron activation analysis, and for allowing me to utilize the facilities under his direction. Peter Ford and Dennis Ng at the University of Alberta SLOWPOKE Facility are thanked for providing useful discussions and assistance with the neutron activation analysis aspects, especially in terms of the irradiation of samples and the sorting out of hardware problems. John Duke shared his invaluable expertise in neutron activation analysis, which greatly improved the analytical part of this research.

Alex Stelmach, Wayne Day, and Dr. H. Baadsgaard had many helpful comments regarding the fire-assay procedure. Alex is also thanked for placing the countless orders for laboratory materials and Dr. Baadsgaard for providing me with the laboratory space I required, for which I am especially grateful.

Dr. D. G. W. Smith deserves many thanks for his help in many of the microprobe aspects, and is thanked in particular for allowing me to make good use of the facilities under his direction. Steve Launspach and Dave Tomlinson gave me valuable assistance with the microprobe analyses and data reduction. Frank Dmitrov is acknowledged for helping with many of the cartographic details. Dr. C. Scarfe is thanked for providing me with the material I used to make my Pt, Rh, and Pd microprobe standards.

A number of people outside this department gave much needed assistance. Dr. Richard Alcock provided the nickel powder used, and steered me away from using a faulty analytical procedure. Dr. Louis Cabri gave me the Os and Ir metals required for use as microprobe standards and made helpful suggestions regarding a variety of aspects

Table of Contents

List of Tables

List of Figures

PGE	platinum group elements
PGM	platinum group mineral
NAA	neutron activation analysis
INAA	instrumental neutron activation analysis
Mss	monosulfide solid solution
fO_2	oxygen fugacity
fS_2	sulfur fugacity
g	grams
μg	micrograms
μl	microliters
m	meters
cm	centimeters
mm	millimeters
km	kilometers
ml	milliliters
mg	milligrams
μb	microbarns
mb	millibarns
b	barns
ppm	parts per million
ppb	parts per billion
nA	nanoamperes
kV	kilovolts
keV	kiloelectron volts
FWHM	full width half maximum
Ge(Li)	lithium-drifted germanium
NaI	sodium iodide
MCA	multichannel analyzer

min.	minutes
wks.	weeks
hr.	hour
wtd. x	weighted mean
SABS	South African Bureau of Standards
M	molar
mil	thousandths of an inch
°C	degrees Celsius
HCl	hydrochloric acid
NiS	nickel sulfide, as produced during the fire-assay preconcentration
H_2S	hydrogen sulfide
OsO_4	osmium tetroxide
r.p.m.	revolutions per minute
λ	decay constant
σ	thermal or effective cross-section
$\varnothing$	neutron flux
E	detector efficiency
B^-	beta (negative)
B^+	beta (positive)
E.C.	electron capture
n	neutrons
ol	olivine
sp	serpentine
cb	carbonates
cpx	clinopyroxene
hb	hornblende
pl	plagioclase
kf	K-feldspar
qz	quartz
cl	chlorite

ep	epidote
bt	biotite
at	actinolite
tc	talc
ct	chromite
mt	magnetite
py	pyrite
po	pyrrhotite
pn	pentlandite
vi	violarite
ilm	ilmenite
rt	rutile
hm	hematite
cp	chalcopyrite

I. INTRODUCTION

The Tulameen Ultramafic Complex is located approximately 200 km east of Vancouver, British Columbia, and 50 km north of the Canada-United States border, along the eastern margin of the Coast and Cascade geological belt (Figure 1). The Complex covers an area of almost 60 km², and has been tentatively dated as Late Triassic (Findlay, 1969). The Tulameen Complex intrudes metavolcanic and metasedimentary rocks of the Triassic Nicola Group and is unconformably overlain along its eastern margin by the Tertiary Princeton Group, which consists of terrestrial, coal-bearing sedimentary and volcanic rocks (Rice, 1947; Findlay, 1963, 1969). The Eagle Granodiorite, part of the Coast Intrusions, lies to the west. The Tulameen Complex is largely concordant with the regional northwest-trending structural grain.

The Tulameen River area has been known as a gold and platinum producer for over 100 years (Raicevic and Cabri, 1976). This district is interesting in that it is one of the few areas in Canada in which nuggets of the platinum group elements (PGE) are found in placers. Cabri et al. (1973), Cabri and Hey (1974), and Raicevic and Cabri (1976) examined platinum group minerals (PGMs) from the Tulameen placers. They recognized one new PGM, tulameenite, and established some of the PGE chemistry and mineralogy in the Tulameen material. Essentially all of the noble metal production in this area has been from placers. No hard-rock mining of platinum has been attempted, partially because of the lack of information regarding the distribution of the PGE within the Complex. The purpose of this project is to document the distribution of the PGE in the Tulameen Complex and to determine any mineralogical, geochemical, and petrological associations. The major contribution of this study is the enhancement of the body of knowledge concerning the PGE in Alaskan-type ultramafic complexes. Most of the information available at present is the result of work in the U.S.S.R., with very little research of this type published with regards to North American examples.

Some 61 samples from the Tulameen Complex have been analyzed for the PGE and other elements in the present study, with a total of 90 analyses carried out for the PGE. Most of these samples were taken in the northern part of the complex, as exposure is limited south of Olivine Mountain.

1

120° 45'

Tulameen

River

Princeton

BRITISH

COLUMBIA

km

0   5   10

Kamloops
Princeton
Vancouver

Tertiary

Miocene or later
PLATEAU BASALT

Miocene or earlier
PRINCETON GROUP

Cretaceous

KINGSVALE, PASAYTEN,
and SPENCE BRIDGE GPS.

Triassic

Upper Triassic
NICOLA GROUP

Sedimentary and Volcanic Rocks

Cretaceous

Upper Cretaceous or later
LIGHTNING CREEK and
OTTER INTRUSIONS

Jurassic

Jurassic or later
COAST INTRUSIONS

Triassic

Upper Triassic
MAFIC/ULTRAMAFIC ROCKS
(TULAMEEN COMPLEX)

Figure 1: Location and local geology (after Rice, 1947; and Findlay, 1969).

A. Geology of the Tulameen Complex

A brief overview of the geology of the Tulameen Complex is given here, with special attention to the major oxide and sulfide mineral occurrences. For a more detailed account of the geology and petrology of this complex, the reader is referred to Findlay (1963, 1969).

Petrology of the Complex

The Tulameen is an Alaskan-type or zoned intrusion, such as is common in southeastern Alaska and in the Ural Mountains of the U.S.S.R. The few Alaskan-type intrusions in Canada are found mainly in the north-central area of British Columbia.

Although the Alaskan-type intrusions are tectonically similar to Alpine complexes, they differ in their structure and lithochemistry (Wyllie, 1967). Alaskan-type intrusions characteristically lack orthopyroxene, have no feldspars in the ultramafic units, and contain highly magnesian olivine, on the order of Fo_{75} to Fo_{93} (Wyllie, 1967). The pyroxene is usually a calcic species, and in the case of the Tulameen is diopsidic augite. The Tulameen also shows cryptic zoning, with the bulk Fe/Mg ratio increasing from the core to the margins (Findlay, 1963, 1969). The gabbroic rocks in the Tulameen Complex are alkalic, whereas those of other Alaskan-type peridotites are tholeiitic (Findlay, 1969). In addition, both the ultramafic and gabbroic rocks of the Tulameen suite are undersaturated in silica (Findlay, 1969). A major characteristic of the Alaskan-type complexes is the crudely-developed concentric zoning of their lithologies, which generally follows a pattern of dunite in the core, with successive shells of minor peridotite, olivine clinopyroxenite, hornblende and/or magnetite clinopyroxenite, and gabbroic rocks on the margin.

The geology of the Tulameen Complex is shown in Figure 2. It should be noted that the contacts between the ultramafic units are usually gradational, while the contacts between the ultramafic and gabbroic rocks are typically well-defined.

Dunite in the Tulameen Complex occurs in the northwest end of the area and is also elongated to the northwest. It is composed of olivine, 50 percent or less serpentine and magnetite, 2 to 20 percent chromite, and less than 10 percent clinopyroxene. A peridotite containing 45 to 90 percent olivine/serpentine and clinopyroxene, is present but does not constitute a mappable unit (Findlay, 1963). Olivine clinopyroxenite partly

4
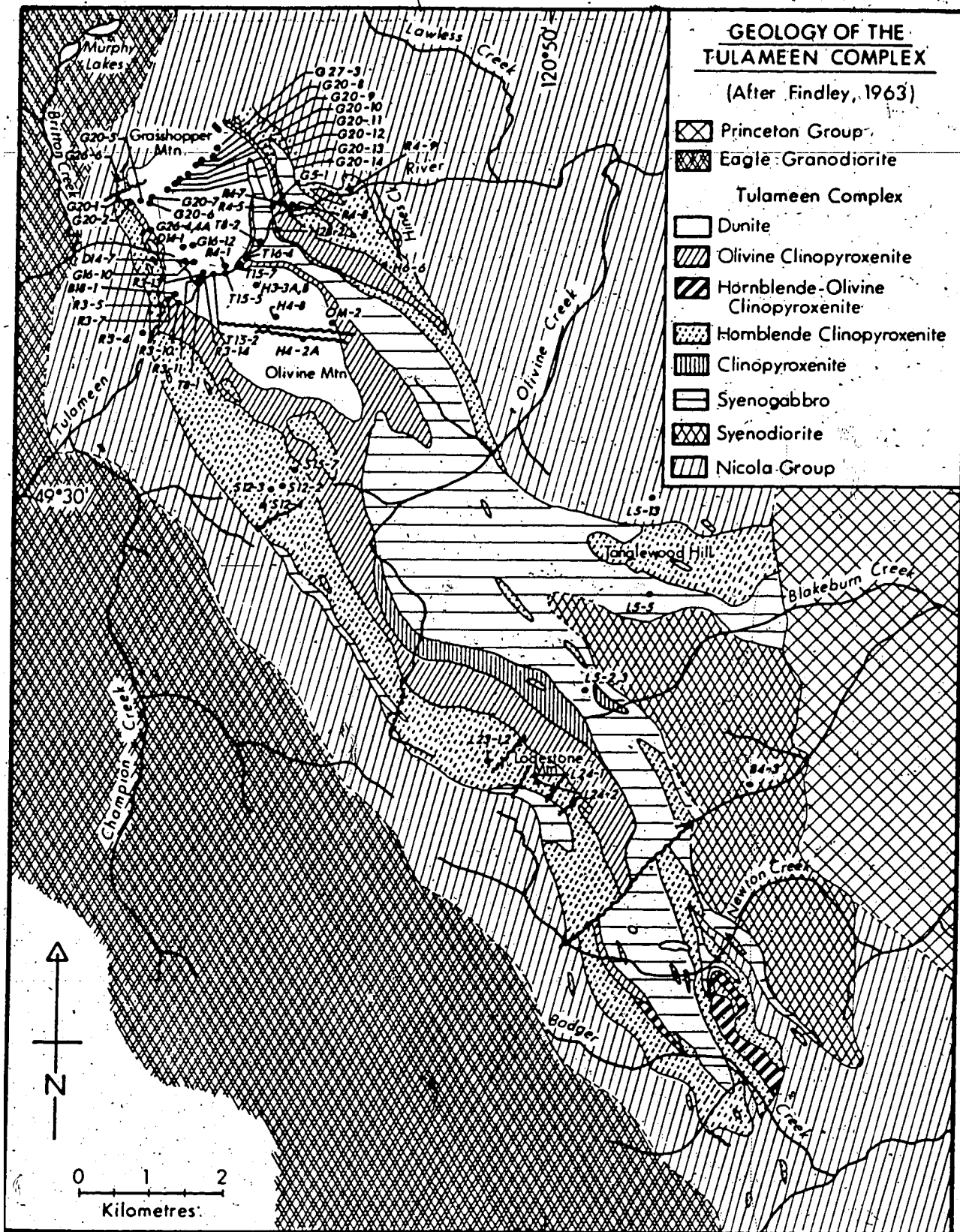
Figure 2: Generalized geology of the Tulameen Complex (after Findlay, 1963).

Legend:

GEOLOGY OF THE TULAMEEN COMPLEX

(After Findley, 1963)

- Princeton Group
- Eagle Granodiorite

Tulameen Complex
- Dunite
- Olivine Clinopyroxenite
- Hornblende-Olivine Clinopyroxenite
- Hornblende Clinopyroxenite
- Clinopyroxenite
- Syenogabbro
- Syenodiorite
- Nicola Group

envelopes the dunite unit in the southern part of the dunite mass and extends southward as a single zone. It consists of 70 to 80 percent clinopyroxene, 10 to 25 percent olivine/serpentine, some magnetite, and minor chromite. For the purposes of this paper, serpentinite is defined as any rock containing greater than 85 volume percent serpentine and no primary silicates. The remaining 15 volume percent is usually comprised of carbonates, talc, and actinolite, with carbonates more abundant than talc or actinolite. Serpentinite-dunite is any rock with greater than 70 volume percent serpentine and which, on the basis of serpentine textures and remnant olivine grains, is considered to have been dunite originally. Hornblende clinopyroxenite comprises the outermost unit around much of the complex. It contains 30 to 75 percent clinopyroxene, 5 to 70 percent hornblende, 5 to 25 percent magnetite, and accessory biotite. Gabbroic rocks, syenogabbro and syenodiorite, comprise a large mass along the eastern part of the complex. The syenogabbro contains 30 to 50 percent clinopyroxene, 25 to 35 percent plagioclase, 15 to 20 percent K-feldspar, and minor biotite and magnetite. The syenodiorite contains 10 to 25 percent clinopyroxene and hornblende, 35 to 55 percent andesine plagioclase (An$_{40}$), 15 to 35 percent K-feldspar, and accessory biotite, magnetite, and apatite (Findlay, 1963). These two gabbroic units are typically saussuritized and where altered are difficult to distinguish in outcrop. In addition, a variety of other lithologies are present in the Tulameen Complex including hornblendite, clinopyroxenite, mafic/ultramafic pegmatites, and hybrid or mixed rocks (Findlay, 1963; 1969).

Accessory minerals of the Complex

Chromite in the Tulameen Complex is Fe-rich (Findlay, 1969) and generally occurs as disseminated grains in dunite and to a lesser extent in olivine clinopyroxenite, and usually constitutes less than 20 volume percent of the rock. Massive chromite occurs sporadically throughout the dunite as small (less than 0.5 m) pods, lenses, veins, and schlieren. There appears to be no systematic distribution of the chromite within the complex (Findlay, 1963).

Magnetite is present in all the rock units of the Tulameen Complex, although it is most common in the hornblende clinopyroxenite. In dunite and olivine clinopyroxenite magnetite is generally the product of serpentinization. In hornblende clinopyroxenite

magnetite typically constitutes less than 25 percent of the rock (Findlay, 1963, 1969). However, near the summit of Lodestone Mountain and on Tanglewood Hill magnetite is locally observed to constitute greater than 50 percent of the rock. Eastwood (1959) gives a detailed account of the magnetite occurrences on Lodestone Mountain and Tanglewood Hill. Magnetite in these areas is concentrated in small (typically less than one m) pods and lenses. There are numerous other areas within the hornblende clinopyroxenite where the magnetite content is higher than 25 percent, although the areal extent of these patches is not as great as the extent of the pods on Lodestone Mountain and Tanglewood Hill.

Serpentine is ubiquitous in dunite and olivine clinopyroxenite and is generally localized along boundaries of olivine grains. Carbonates usually accompany serpentine minerals in varying proportions. In most instances serpentine is volumetrically greater than the carbonates. The degree of serpentinization increases towards contacts and shear zones. The greatest development of serpentine in the Tulameen Complex has been observed near the summit of Grasshopper Mountain where up to 100 percent of the rock may be serpentinized (Findlay, 1963).

Sulfides occur throughout the complex but are generally too fine-grained to be observed in hand specimen. Fresh dunite and peridotite contain very few sulfides, whereas serpentinized rocks have minor amounts of sulfides disseminated throughout them. Microscopic sulfides (mostly pentlandite and violarite) also occur interstitial to chromite grains in massive, nodular, and schlieren chromite. There are scattered occurrences of macroscopically visible sulfides, chalcopyrite, pyrrhotite, and pyrite, in hornblende clinopyroxenite, gabbroic rocks, and hornblendite dikes. The greatest concentrations of sulfides are observed in hornblendite dikes north of Tanglewood Hill and northwest of Grasshopper Mountain. None of the known sulfide occurrences in the Tulameen Complex contain economic concentrations of base or precious metals (Findlay, 1963).

Previous work on the PGE in the Tulameen Complex

Findlay (1963, 1965) reports the results of some analyses for the PGE in the Tulameen Complex, and found the greatest concentrations of Pt in the dunite and peridotite, with the highest value of 0.225 grams per ton (20.4 ppb assuming short tons) in dunite on Olivine Mountain. Chromite segregations within the dunite on Grasshopper Mountain gave the highest Pt content recorded by Findlay (1963, 1965) of 7.34 grams per ton (6657 ppb), with Pt enriched in the magnetic fraction relative to the non-magnetic fraction. Findlay (1963) detected Pd in only one sample, which was a disseminated sulfide sample in hornblende clinopyroxenite from the Tulameen River approximately 0.5 km from the eastern margin of the intrusion. No other PGE were detected by Findlay (1963, 1965).

Although Findlay's (1963, 1965) research is the only work carried out on hard-rock PGE in the Tulameen Complex, other workers have examined the placers associated with the intrusion with regard to their PGE contents and the mineralogy of the PGE. Of the studies on the placers, that of Raicevic and Cabri (1976) is one of the most complete, although much needed additional information has been provided by Cabri et al. (1973) and Cabri and Hey (1974).

B. PGE in Alaskan-type complexes

Most of the work concerning the distribution and concentration of the PGE in Alaskan-type complexes has been carried out by researchers in the U.S.S.R., who have examined a number of intrusions in the Ural Mountains and the Aldan Shield. Fominykh and Khvostova (1970) have given the most comprehensive compilation of PGE data from ultramafics in the Urals. In addition, Razin and Khvostova (1965), Razin et al. (1965), Razin and Khomenko (1969), Razin (1968), Begizov et al. (1975), and Khvostova et al. (1976) have made significant contributions to the body of information regarding the PGE in Alaskan-type intrusions.

Table 1 gives the average PGE content of the Alaskan-type, Alpine, Stillwater and Bushveld complexes in parts per billion (ppb). These values are taken from lithologies that are not classified as noble metal ores. Those horizons that are considered PGE ores, especially in the Stillwater and Bushveld complexes, contain values that are up to an order

Table 1: Average PGE contents (in ppb) of some types of ultramafic complexes (after Crocket, 1981). Approximate ranges of values for all Alaskan-type complexes are given in parentheses.

COMPLEX	Ru	Rh	Pd	Os	Ir	Pt
Alaskan (overall)	0.65 (0.5-1.0)	19 (0.7-29)	32 (8-45)	3.7 (0.8-7.0)	9.6 (3-13)	43 (10-105)
Alaskan (Alaska, excluding Salt Chuck)	---	29	32	---	---	54
Alaskan (U.S.S.R.)	0.65	4.4	32	3.7	9.6	82
Alpine (overall)	6.1	3.0	6.7	5.1	3.8	9.1
Stillwater[1]	230	160	960	---	66	535
Stillwater[2]	---	9	44	---	---	20
Bushveld[3]	577	---	---	90	77	--
Bushveld[4]	4.3	---	---	0.42	0.35	--

[1]Data for the ultramafic zone, peridotite member. Average for nine chromitite horizons.
[2]Basal zone orthopyroxene cumulates which are 25 percent sulfide-bearing.
[3]Chromitite from the Upper Critical Zone.
[4]Orthopyroxene from the Critical, Transition and Lower zones.

of magnitude higher (Crocket, 1981).

Alaskan-type complexes tend to have PGE contents greater than Alpine complexes, although the Pt/(Pt+Pd) ratio in Alaskan-type complexes tends to be somewhat lower than that of the Alpine type (Naldrett and Cabri, 1976). However, the Pt/(Pt+Pd) ratios of both these types of ultramafic complexes are substantially higher than is observed in large layered complexes (Naldrett and Cabri, 1976; Raicevic and Cabri, 1976). This ratio is on the order of 0.68 for Alaskan-type complexes, 0.73 for Alpine complexes, and 0.51 for large layered intrusions, excluding heavily mineralized zones (Naldrett and Cabri, 1976).

The Soviet researchers have, for the most part, directed their attention to the concentration and distribution of the PGE in chromite and the role that chrome spinels play in the petrogenesis of PGE deposits. The results of their work indicate enrichments of the PGE of at least 100 times in massive and schlieren chromites versus rocks containing accessory chromite (Fominykh and Khvostova, 1970).

The data base for PGE concentrations and distributions in Alaskan-type complexes from North America is very small compared to that of occurrences in the U.S.S.R. It is apparent from an examination of the available data, largely from intrusions in Alaska, that the general abundance levels of the PGE are essentially the same in Alaskan-type intrusions in Alaska and the Soviet Union (Crocket, 1979; 1981). The Americans have been mainly concerned with the correlation of lithochemistry, oxide and sulfide content, and lithology with PGE contents (Clark and Greenwood, 1972).

A major problem with the North American data arises from the analytical techniques employed, which usually utilize small (less than 10 g) samples. As a result, spurious data are often obtained due to the inhomogeneity in distribution of the noble metals (Crocket, 1979). Also, the determination of all six PGE is often not possible due to the various nuclear and chemical procedures employed in the analyses (Crocket, 1979). However, the Soviet data are often difficult to evaluate, as detailed descriptions of the analytical procedures employed are often lacking in the literature.

II. PLATINUM GROUP MINERALS IN THE TULAMEEN COMPLEX

Discrete, *in situ* platinum group minerals (PGMs) have been observed only in samples of massive chromite taken from the dunite. This is to be expected, as the close relationship between the PGE and chromite in Alaskan-type complexes is well-documented (Razin and Khomenko, 1969; Naldrett and Cabri, 1976; Crocket, 1981).

The PGM phases observed in Tulameen chromites, as well as the ideal compositions of those phases, are given in Table 2. The identification of these minerals was based upon the relative abundances of the elements in each grain as determined from energy dispersive spectra obtained with ARL/EMX and ARL/SEMQ microprobes. In addition, the sulfides observed in association with the PGMs were analyzed by microprobe via the energy dispersive technique, and all appear to be pentlandite.

A number of attempts were made to obtain quantitative analyses of the Tulameen PGMs by energy dispersive analysis. An Ortec energy dispersive spectrometer fitted on the ARL/EMX was used. This spectrometer, which employs an Ortec Si(Li) detector, has a resolution at the 5.9 keV photopeak of Mn Kα of 154 eV full width half maximum (FWHM) at a count rate of 1000 counts per second. Spectra of 1024 channels are acquired with an Ortec 6220 multichannel analyzer (MCA), and the data stored on cassette tapes using a Texas Instruments 700. Data reduction was performed with EDATA2 (Smith and Gold, 1979) on the University of Alberta AMDAHL 470 v/6 computer after transmission of the spectra from the TI 700 to the mainframe.

A standard block containing the PGE, as pure elements and binary alloys, was prepared, and overlap coefficients for the PGE and eight other elements were calculated for use in analyses with the ARL/EMX microprobe, by means of the EDATA2 program. These overlap coefficients are shown in Appendix IX. However, a number of instrumental problems made quantitative analysis difficult, and these, combined with a decrease in the beam resolution over time, resulted in the abandonment of analyses via the EMX.

Wavelength dispersive analysis was then attempted using the ARL/SEMQ, which has very good beam resolution. Again, a number of instrumental problems cropped up during the analyses. As a result, no quantitative analyses of the Tulameen PGMs are presented in this thesis. It must be emphasized that the main purpose of the microprobe work was to identify the PGMs, not to provide complete analyses. Also, none of the

Table 2: PGM phases observed in Tulameen chromites.

Mineral	Ideal Formula	Minor Elements Detected
Tulameenite	Pt_2FeCu	Sb, Ni
Pt-Fe alloys	Pt_xFe	Rh, Ni, Cu, S
Stumpflite	PtSb	Pd, Ru
Geversite	$PtSb_2$	Pd, Ru
Genkinite	$(Pt,Pd)_4Sb_3$	Rh, S
Sperrylite	$PtAs_2$	Ru, S, Sb (Fe)
Platinum	Pt	Fe, Ni (Ir)
Irarsite	IrAsS	Rh, Sb, Cu

instrumental problems encountered were insurmountable, but it seemed unncecessary to pursue this type of analysis in the light of the data required for this study.

As can be seen in Table 2, there are more species of Pt minerals than minerals of the other PGE, with irarsite as the only Ir phase identified. All of the PGE, except Os, have been detected in the Tulameen PGMs, and As, Sb, and Fe were found to be the most commonly occurring accessory elements. Among the PGMs, Pt-Fe alloys, sperrylite, and irarsite are the most abundant. It should be noted that a number of Pt-Fe species are reported in the literature, but their specific names are dependent upon their structure (Cabri and Feather, 1975). No attempts were made to obtain X-ray data for the phases observed in this study.

The PGMs in the chromite samples occur as euhedral to subhedral inclusions in chromite grains (Type 1), and as anhedral grains interstitial to chromite (Type 2). They are typically less than 30 microns in diameter, and pentlandite, violarite, occasionally bravoite, and serpentine are the minerals most often associated with the PGMs. It should be noted that there are very few sulfide minerals included within chromite grains; most are found interstitial to chromite.

Figure 3 illustrates an example of the Type 1 PGM totally enclosed within a chromite grain. There are at least seven PGM phases within this noble metal grain, with Pt-Fe alloys, geversite, stumpflite, and irarsite being the major phases, although the Type 1 PGMs are most often Pt-Fe alloys. Other phases observed in the Type 1 PGMs include platinum, tulameenite, and genkinite. The shape of this grain most likely indicates strong spinel structural control during the growth of the chromite. Grains such as this are believed to represent PGE-rich droplets that have been entrapped during primary crystallization of the chromite. The Type 1 PGMs are the most commonly observed PGMs in Tulameen chromites.

The second major type of PGM observed in Tulameen chromites is shown in Figure 4. As can be seen in this example, the Type 2 PGMs are interstitial to chromite grains. Associated with these PGMs are serpentine, which comprises the bulk of the interstitial material, pentlandite, and a little violarite. The PGMs in this example are mainly sperrylite, with some irarsite. Sperrylite is the most common Type 2 PGM observed in chromite samples from the Tulameen Complex, although Pt-Fe alloys, irarsite, and

10 microns

Figure 3: Polyphase Type 1 PGM grain totally enclosed within a chromite grain. Reflected light, in oil.

H
10 microns

Figure 4: Type 2 PGMs interstitial to chromite. The bulk of the interstitial material is serpentine, and the dominant sulfide in this area is pentlandite. Reflected light, in oil.

tulameenite have also been observed in Type 2 PGMs. An important aspect of the Type 2 PGMs in Figure 4 is the apparent paragenesis of the PGMs and Fe-Ni sulfides. The PGMs in this instance rim the area predominated by pentlandite. Grains such as those shown in Figure 4 are taken to represent material that possibly began as alloys or as a monosulfide solid solution (Mss) (Kullerud et al., 1969) or some other sulfide phase, at relatively high temperature which on cooling exsolved the phases observed in Figure 4. PGMs associated with sulfides in the Howland Reef of the Stillwater Complex have been attributed to a similar origin (Bow et al., 1982). It is important to note that not all of the Type 2 PGMs are associated with sulfides.

A third type of PGM has been observed only rarely. These are PGMs which occur as anhedral inclusions within chromite, and appear texturally to have been exsolved from the chromite (Figure 5). There may also be substantial amounts of PGE that are not visible microscopically and which have been incorporated into the chromite lattice. These cryptocrystalline phases are also included in the Type 3 classification. As can be seen in Figure 5, these grains are generally located towards the center of chromite grains and appear to be localized along defects within the chromite. The examples of the Type 3 PGMs in the Tulameen chromites were too small to quantitatively analyze by microprobe.

Based upon these observations it is felt that there are three major types of PGE mineralization associated with massive, magmatic chromite in the Tulameen Complex:

Type 1 are PGMs, typically Pt-Fe alloys, that have cubic shapes and are included within chromite grains;

Type 2 are PGMs, usually sperrylite, interstitial to chromite grains which are in some instances associated with Fe-Ni sulfides;

Type 3 PGMs are those which occur as inclusions within chromite grains but appear to have been exsolved from chromite.

H
10 microns

Figure 5: Type 3 PGM (right of center) exhibiting possible exsolution texture within a chromite grain. Note the small Type 1 PGM to the left of center. Reflected light, in oil.

III. ANALYTICAL METHODS

When analyzing the noble metals in typical geological samples, the analytical technique employed must be capable of measuring sub-ppb concentrations. A number of techniques, such as atomic absorption, X-ray fluorescence, and spectrophotometric methods, are generally not sensitive enough to detect low levels of the noble metals (Beamish and Van Loon, 1972; Crocket and Cabri, 1981). In addition, the heterogeneity of noble metal distribution within the materials to be assayed requires large samples, on the order of 30 to 50 grams, for representative analyses (Crocket and Cabri, 1981; Harris, 1982).

Neutron activation analysis (NAA) offers a number of advantages over many other techniques. One of its major assets is the high sensitivity inherent in the method (Gijbels, 1971; Beamish and Van Loon, 1972; Crocket and Cabri, 1981). This, combined with a suitable concentrating procedure, results in a very precise and sensitive analytical tool.

The preconcentration procedure using a fire-assay with nickel sulfide as the collector first described by Robert et al. (1971) and Robert and van Wyk (1975) and later adapted for use with NAA by Hoffman et al. (1978) has been utilized in this study. A modified version of the nickel sulfide technique was used for the analysis of samples rich in chromite (Borthwick and Naldrett, pers. comm.). During the early stages of this research a radiochemical technique, involving post-irradiation treatment of 0.5 to 1.0 gram samples was used (Nadkarni and Morrison, 1974). However, it became apparent that the small sample size did not result in representative analyses (Hoffman, 1978; R.A. Alcock, pers. comm.). In addition, this technique could not be used to determine Rh and Pd, which produce radionuclides with short half-lives (i. e., short-lived radionuclides). The nickel sulfide technique, which allows for samples of up to 50 grams, combined with careful crushing and splitting of the sample and subsequent NAA, provides a fairly simple and effective means of assaying for all six PGE and gold.

A detailed account of the nickel sulfide fire-assay procedure, as modified for this study, is given in Appendix I. The procedure for the analysis of samples rich in chromite is given in Appendix II, a description of the crushing and splitting technique in Appendix III, and a discussion of the NAA aspects is given in Appendix IV.

A. Sample preparation via the nickel sulfide fire-assay

The nickel sulfide method entails fusing approximately 50 grams of powdered rock, via two 25 gram aliquots, with a sodium borate-sodium carbonate flux for 1.25 hours, and producing two nickel sulfide assay buttons. These buttons are crushed, dissolved in concentrated HCl, and filtered using membrane filters. The two buttons from each sample are treated independently throughout the procedure. After filtration, the two membrane filters from each sample are packaged in one polyethylene envelope for irradiation. The procedure for chromite-rich samples is the same, except that a different flux (lithium tetraborate-sodium carbonate) is used in a two hour fusion (Borthwick and Naldrett, pers. comm.). Also, one 30 g aliquot of each sample is used, instead of two 25 g aliquots. All chromite-rich samples were analyzed in duplicate.

B. Limits of detection and quantification: NiS technique

Tables 3(a) and 3(b) give the limits of detection and quantification for the modified version of the nickel sulfide technique used in this study, and the limits for the procedure used to analyze chromite-rich samples. These limits have been calculated according to the method of Currie (1968). For typical ultramafic rocks, the limits for Pt, Ir, Rh, and Au were calculated from 31 analyses of Tulameen samples, and Os, Ru, and Pd from eleven analyses of the South African noble metals standard SARM 7. The SARM 7 analyses were used because Ru, Os, and Pd were not detected in enough Tulameen samples to provide statistical reliability in the calculations. The limits for Pt, Ir, Rh, and Au by the procedure used with chromite-rich samples have been calculated from the seven duplicate analyses performed on Tulameen samples. The limits for Ru and Pd were calculated from three SARM 7 analyses. The limits for Os via the chromite-rich technique have been calculated from Tulameen chromite samples and the three SARM 7 analyses, as Os was not quantified in all the Tulameen chromite samples. As can be seen from Table 3, the limits for all the metals except Pd, Ru, and Os are very low. The relatively high limits for these three elements, which do not activate as well as the other noble metals, is a result of their nuclear properties. Also, the SARM 7 material has a noble metal content that is much higher than most Tulameen samples. This higher noble metal content results in higher backgrounds during counting, and hence slightly higher limits than would be found if the

Table 3(a): Limits of detection and quantification at the 90 percent confidence level for the noble metals as determined by the nickel sulfide preconcentration procedure used with NAA. The limits for Pt, Ir, Au, and Rh have been calculated from the analyses of 31 Tulameen samples; Os, Ru, and Pd limits have been calculated from 11 analyses of SARM 7. All limits have been calculated by the method of Currie (1968).

Element	Limit of Detection (ppb)	Limit of Quantification (ppb)
Rh	0.2±0.2	0.7±0.6
Pd	18.0± 7.9	56.8±26.1
Os	10.4± 8.5	31.8±26.1
Pt	0.2±0.2	0.7±0.7
Au	0.02±0.02	0.06±0.06
Ir	0.06±0.13	0.2±0.4
Ru	34.6±32.2	106.7± 99.4

Table 3(b): Limits of detection and quantification at the 90 percent confidence level for the noble metals as determined by the procedure used for samples rich in chromite. All limits except those for Pd and Ru have been calculated from seven duplicate analyses of Tulameen chromitites and chromite-rich samples; Pd and Ru limits have been calculated from three SARM 7 analyses via the same analytical technique.

Element	Limit of Detection (ppb)	Limit of Quantification (ppb)
Rh	0.9±1.1	2.7±3.5
Pd	46.2±13.9	146.1±48.4
Os	11.3±10.1	34.7±31.1
Pt	61.2±83.4	187.1±254.7
Au	0.1±0.2	0.4±0.6
Ir	0.9±1.2	2.9±3.7
Ru	29.2±12.6	91.1±40.5

limits had been calculated from Tulameen samples.

The uncertainties associated with the limits listed in Table 3 are very high because the background activity, usually produced from Ni, Br, Cl, PGE, and Au, is variable from sample to sample. The background activity results in increased uncertainty in the photopeak of interest, and therefore imposes more uncertainty in the value obtained for that element. Thus, in some instances the limits of detection and quantification may be at their maximum, while in others the limits will be at their minimum.

C. Neutron activation analysis

All irradiations performed for this study were done in the University of Alberta SLOWPOKE II reactor, and all counting done with the gamma spectroscopy equipment at that facility. The nickel sulfide preconcentration procedures were utilized for the analysis of the noble metals, and the elements Mn, Mg, V, Ti, Al, Fe, Co, Cr, Ni, and Sc were analyzed by instrumental NAA (INAA).

In INAA, no pre- or post-irradiation chemical treatment of the samples is employed. In this work approximately 200 mg of rock powder were sealed in an irradiation vial, irradiated, and counted with Ge(Li) detectors. This method is obviously preferable to methods involving chemical treatment, as there is less chance of sample contamination, and the time and effort required per sample is comparatively small. The major limitation of INAA is that it is not as sensitive as techniques that employ chemical concentration because high background activities are usually produced.

Table 4 lists the nuclear reactions and data for the elements of interest. In those cases where two or more photopeaks are used for any given radionuclide (i.e., the 296, 308, and 468 keV peaks for ^{192}Ir), the weighted mean of the results for those peaks, as determined during data reduction, was used as the value for the particular element in question. Table 5 gives the irradiation and counting schemes used for the various groups of elements.

Two different detectors were used for counting. One, an Ortec Win[15] coaxial Ge(Li), has a resolution at the 1332 keV photopeak of ^{60}Co of 2.1 keV full width half maximum (FWHM), peak-to-Compton ratio of 53:1, and a relative efficiency of 18.5 percent (relative to a 3" x 3" NaI crystal). The other, a Canberra 413R, is a closed-end

Table 4. Nuclear reactions and nuclear data for the production of radionuclides used in this study. All data except the effective cross-sections are from Gijbels (1971), Nadkarni and Morrison (1974), Chart of the Nuclides (1977), and Lederer and Shirley (1978). (Cross-sections denoted with [1] are thermal cross-sections).

Element	Reaction	Cross-section (barns)	Half-life	Isotopic Abundance	Photopeaks Used (keV)
Pt	^{199}Pt(n, γ)^{199}Pt(β)^{199}Au	7.14	3.14 days	7.2	158, 208
Au	^{197}Au(n, γ)^{198}Au	166	2.69 days	100	412
Ir	^{191}Ir(n, γ)^{192}Ir	912	74.2 days	37.3	296, 308, 468
Os	^{190}Os(n, γ)^{191}Os	8.89	15.3 days	26.4	129
Ru	^{102}Ru(n, γ)^{103}Ru	1.55	39.4 days	31.6	497
Rh	^{103}Rh(n, γ)^{104m} Rh	800[1]	4.35 min.	100	51, 77, 97
Pd	^{108}Pd(n, γ)^{109m} Pd	0.2[1]	4.67 min.	26.7	188
Pd	^{108}Pd(n, γ)^{109}Pd	12[1]	13.43 hour	26.7	88, 600
Mg	^{26}Mg(n, γ)^{27}Mg	0.03[1]	9.46 min.	11.01	1014
Al	^{27}Al(n, γ)^{28}Al	0.24[1]	2.24 min.	100	1779
Ti	^{50}Ti(n, γ)^{51}Ti	0.14[1]	5.75 min.	5.2	320
V	^{51}V(n, γ)^{52}V	4.9[1]	3.76 min.	99.75	1434
Cr	^{50}Cr(n, γ)^{51}Cr	17[1]	27.72 days	4.35	320
Fe	^{54}Fe(n, p)^{54}Mn	1.3[1]	312.5 days	5.8	835
Mn	^{55}Mn(n, γ)^{56}Mn	13.3[1]	2.58 hour	100	1811
Sc	^{45}Sc(n, γ)^{46}Sc	13[1]	83.8 days	100	890
Ni	^{58}Ni(n,p)^{58}Co	2.2[1]	70.8 days	68.3	811
Co	^{59}Co(n, γ)^{60}Co	19[1]	5.27 year	100	1173, 1332

Table 5: Irradiation / decay / counting scheme used for the various elements analyzed in this study.

Elements	Thermal Neutron Flux (n / cm² / s)	Irradiation Period (min.)	Decay Period	Counting Period (min.)	Counting Geometry (cm)
Rh, Pd	1×10^{12}	2	2 min.	5	3
Pt, Au	1×10^{12}	240	5 days	60	1
Ir, Os, Ru	1×10^{12}	240	2 wks.	120	1
Al, Mg, Mn, Ti, V	1×10^{11}	4	6 min.	5	6
Fe, Cr, Co, Ni, Sc	1×10^{12}	120	2 wks.	120	1

coaxial Ge(Li), with resolution of 1.88 keV FWHM, peak-to-Compton ratio of 38:1, and a relative efficiency of 10.3 percent (all measurements made at the 1332 keV ^{60}Co photopeak).

The Win^{15} Ge(Li) is used with a Nuclear Data ND660 multichannel analyzer (MCA), which incorporates an LSI-11 minicomputer. The 413R Ge(Li) is used with a Canberra Series 80 MCA. Spectra of 4096 channels are stored on floppy disks. Both MCA's have peak search capabilities, and the ND660 is also capable of performing data reduction online with the LSI-11.

D. Data reduction

Three data reduction programs were used to process the NAA data. Peak searching of the spectra was carried out on the MCA used to acquire the individual spectra. Peak searching for Rh, Pd, Al, Mn, Mg, V, and Ti was done with the program PREP10 on the ND660 LSI-11 (Apps, 1978). The Series 80 has built-in functions for peak searching, and was used for Pt, Au, Ir, Os, and Ru. Two of the programs, DATRED and ALETC, require peak searching seperately from data reduction, while the third program, NAARUN, performs the peak search in addition to data reduction by means of PREP10 (Apps and Apps, 1981). DATRED, listed in Appendix VIII, and ALETC were written by the author and J. Duke (pers. comm.) for use with the University of Alberta AMDAHL 470 v/6 mainframe computer. NAARUN operates on the LSI-11 system of the ND660 (Apps and Apps, 1981). The only corrections applied in data reduction were the live time/clock time and pulse pile-up corrections, which were applied only in the case of short-lived radionuclides.

E. Discussion

In order to determine the suitability and accuracy of the nickel sulfide techniques, a total of fourteen analyses of the South African noble metals standard SARM 7 were performed. The results of these analyses, as well as the recommended values, are given in Table 6. Eleven of these analyses were performed utilizing the sodium borate fusion, and the remaining three analyses were obtained via the procedure used for chromite-rich samples. SARM 7 is not the ideal material to test the yields from the of analysis of

Table 6. Results from the analyses of the South African noble metals standard SARM 7, as determined in this study by the nickel sulfide preconcentration procedure with NAA. SABS indicates the recommended values as quoted by the South African Bureau of Standards. wtd. x indicates the weighted mean of the analyses performed for this study, and CT1, CT2, and CT3 are the results from the chromite-rich procedure. Values in ppm at 95 percent confidence limits.

Sample	Rh	Pd	Pt	Au	Ir	Os	Ru
1	0.23±0.02	1.72±0.14	3.91±0.45	0.24±0.01	0.079±0.001	0.07±0.03	0.44±0.08
2	0.18±0.01	1.39±0.11	3.35±0.28	0.05±0.00	0.071±0.001	0.06±0.02	0.43±0.03
3	0.23±0.01	1.98±0.16	4.79±0.48	0.25±0.01	0.078±0.001	0.04±0.02	0.45±0.05
4	0.27±0.02	1.84±0.15	4.82±0.52	0.26±0.01	0.084±0.001	0.05±0.02	0.46±0.06
5	0.21±0.01	1.11±0.09	4.35±0.46	0.07±0.00	0.081±0.001	0.05±0.02	0.44±0.05
6	0.23±0.02	1.68±0.13	3.84±0.10	0.09±0.00	0.082±0.001	0.07±0.02	0.46±0.04
7	0.28±0.02	1.69±0.13	4.01±0.17	0.07±0.00	0.086±0.001	0.07±0.02	0.48±0.04
8	0.22±0.01	1.82±0.14	3.96±0.19	0.15±0.01	0.084±0.001	0.07±0.02	0.47±0.05
9	0.24±0.02	1.29±0.10	3.53±0.21	0.09±0.00	0.080±0.001	0.06±0.02	0.45±0.03
10	0.22±0.01	1.41±0.11	3.51±0.19	0.10±0.00	0.079±0.001	0.07±0.02	0.47±0.03
11	0.26±0.02	1.98±0.16	3.99±0.33	0.23±0.01	0.087±0.001	0.07±0.02	0.48±0.05
wtd. x	0.22±0.01	1.52±0.04	3.83±0.06	0.15±0.01	0.081±0.001	0.06±0.01	0.46±0.02
SABS	0.24±0.01	1.53±0.03	3.74±0.05	0.31±0.02	0.074±0.012	0.06±0.01	0.43±0.06
CT1	0.24±0.01	1.82±0.15	4.14±0.22	0.26±0.01	0.076±0.001	0.05±0.02	0.22±0.03
CT2	0.24±0.01	1.83±0.15	4.28±0.25	0.24±0.01	0.082±0.001	0.05±0.02	0.24±0.04
CT3	0.24±0.01	1.88±0.15	4.10±0.23	0.25±0.01	0.086±0.001	0.06±0.02	0.29±0.04
wtd. x	0.24±0.01	1.84±0.09	4.17±0.14	0.25±0.01	0.080±0.001	0.06±0.01	0.25±0.02

chromite-rich samples, but no chromitite standard was available for use in this study. In addition to analyzing SARM 7, another test of the yields through the chromite-rich fusion procedure was made by analyzing a sample with a relatively low chromite content (approximately 25 volume percent) by both fusion procedures (sodium borate and lithium tetraborate). A comparison of the data obtained for this sample (G26-4#1, 2, and 3) shows that although only Rh, Ir, and Au were quantified, the values for these three elements are substantially higher in the analyses by the lithium tetraborate fusion (G26-4#2, 3). Thus, it appears that the yields via the lithium tetraborate fusion are much closer to 100 percent for chromite-rich samples than is the case with the sodium borate fusion.

As can be seen from the data in Table 6, good agreement between the recommended and measured values was obtained for all elements except gold when the sodium borate fusion is used. However, the SARM 7 material is not suitable as a gold standard, as the distribution of gold in SARM 7 tends to be erratic (E. Hoffman, S. J. Barnes, pers. comm.,). The CANMET gold standard MA-2 arrived too late to check the gold yields by the preconcentration techniques used, so all gold values reported in this paper should be considered qualitative. The yields by the lithium tetraborate fusion, as determined by the analyses of SARM 7, are not as good as the yields via the sodium borate fusion. Rh, Ir, and Os show essentially 100 percent recoveries by this fusion, but Ru is only about 50 percent recovered. Oddly enough, Pd and Pt are high compared to the recommended values.

On the basis of these observations regarding the analysis of SARM 7 it appears that the sodium borate fusion produces results that are much closer to the accepted values for a given sample than does the lithium tetraborate fusion. The exception to this is in the case of chromite-rich samples, where the lithium tetraborate fusion gives higher yields, although it is difficult to determine if even these yields are close to 100 percent without a chromitite standard.

An evaluation of the sampling technique was also made. The first ten samples for assay were analyzed in triplicate, the results of which are given in Table 7. Although the replicates for each sample do not always fall within error of one another, the data given in Table 7 indicate that the crushing and splitting technique utilized provides reasonably

Table 7: Results of triplicate analyses of ten Tulameen samples. Only the four elements listed were detected in these samples. The gold values should be considered qualitative. All values are given in ppb at the 95 percent confidence level. BLQ indicates elements below the limit of quantification.

Sample	Rh	Ir	Pt	Au
T8-1#1	0.8±0.3	1.7±0.1	87.3±10.9	0.2
T8-1#2	1.3±0.1	1.8±0.1	94.1±12.3	0.7
T8-1#3	1.3±0.2	1.1±0.1	103.7±10.4	0.1
D14-1#1	1.7±0.3	0.7±0.1	18.5±12.9	0.8
D14-1#2	0.9±0.2	0.7±0.1	19.8±10.7	0.5
D14-1#3	0.6±0.1	0.5±0.1	18.3±9.4	0.1
T15-2#1	1.5±0.2	1.0±0.1	106.0±10.2	0.3
T15-2#2	1.5±0.1	1.2±0.1	112.2±9.6	0.1
T15-2#3	1.6±0.1	1.4±0.1	144.1±10.8	0.1
T15-7#1	3.7±0.3	4.5±0.1	403.1±18.3	0.3
T15-7#2	3.8±0.3	3.7±0.1	383.5±16.6	0.2
T15-7#3	3.8±0.3	3.8±0.1	380.2±17.4	0.9
G16-10#1	0.6±0.1	0.9±0.1	26.1±7.7	0.9
G16-10#2	0.9±0.1	0.9±0.1	25.4±6.6	0.8
G16-10#3	0.7±0.1	0.9±0.1	32.3±7.3	0.4
G20-6#1	1.3±0.1	0.7±0.1	41.5±9.6	0.4
G20-6#2	1.1±0.1	0.8±0.1	26.5±10.9	0.1
G20-6#3	1.5±0.2	0.7±0.1	31.2±19.7	0.3
G20-8#1	2.7±0.2	1.9±0.1	191.1±12.8	0.5
G20-8#2	2.8±0.2	2.4±0.1	211.0±12.6	0.6
G20-8#3	2.6±0.2	2.3±0.1	198.9±12.4	0.7
OM-2#1	2.2±0.3	1.2±0.1	144.8±9.2	0.3
OM-2#2	2.5±0.2	1.2±0.1	141.1±10.3	0.7
OM-2#3	2.4±0.2	1.0±0.1	136.6±10.9	0.2
R3-10#1	2.4±0.2	0.2±0.1	60.0±8.9	0.3
R3-10#2	3.5±0.3	0.3±0.1	75.9±11.7	0.8
R3-10#3	2.9±0.3	0.2±0.1	62.5±9.6	0.1
H4-8#1	0.3±0.1	0.2±0.1	BLQ	0.2
H4-8#2	0.2±0.1	0.1±0.1	BLQ	BLQ
H4-8#3	0.3±0.1	BLQ	BLQ	BLQ

representative aliquots of each sample for assay. Also, the seven chromite-rich samples taken from the Tulameen Complex were analyzed in duplicate. The results of these analyses are given in Table 8. In general there is good agreement between the replicates for each sample, although the values do not always fall within error of one another. This is probably the result of a pronounced nugget effect in the chromite-rich samples, which contain PGMs on the order of 10 to 30 μ in size. The 30 g sample size used is not large enough to correct for these distribution effects in all samples. If larger samples were used, the high noble metal contents of these samples would result in errors during NAA (pulse pile-up, self-shielding, and self-absorption). For the purposes of this study, the weighted mean of the duplicate analyses for each chromite-rich sample is used as the most reliable result for those samples.

Ten whole rock samples were analyzed in duplicate to determine the reproducibility of the INAA procedure and the sampling technique. The results of these analyses are given in Table 9. It should be noted that the values for MgO have been corrected for the $^{27}Al(n,p)^{27}Mg$ interference. As can be seen from the data in Table 9, the samples taken for whole rock analysis appear to be representative and the analyses are reproducible. Three USGS rock standards, DTS-1, PCC-1, and AGV-1, were analyzed to check the accuracy of the whole rock INAA via the short irradiation. The results of these analyses indicated that the values for MgO and TiO_2 needed slight corrections. All the other elements determined were found to give accurate results. Duke (1983) analyzed USGS rock standards to determine the reliability of the long-irradiation INAA and found that the results were satisfactory.

Table: 8. Duplicate analyses of chromite-rich samples from the Tulameen Complex. All values are given in ppb at 95 percent confidence limits. BLQ indicates that the element is below the limit of quantification in that sample. 'wtd. x' is the weighted mean for each set of duplicates, which should be considered to be the most reliable value for each sample. An approximate mode for chromite in each sample is given.

Sample	Chromite, mode %	Rh	Os	Ir	Pt	Au
D14-7#1		74.7±3.8	29.7±16.9	185.1±0.5	4582.7±79.6	2.2±0.1
D14-7#2		78.7±3.9	BLQ.	204.0±0.6	5224.3±89.8	2.8±0.2
wtd. x	90	76.6±2.7	29.7±16.	192.8±0.4	4865.0±59.6	2.3±0.1
G16-12#1		6.5±0.5	BLQ	32.3±0.3	141.4±28.6	1.6±0.1
G16-12#2		5.2±0.5	BLQ	22.4±0.2	163.8±27.6	1.2±0.1
wtd. x	25	5.9±0.4	BLQ	25.4±0.2	152.9±19.9	1.4±0.1
G26-4#2		3.3±0.3	BLQ	10.1±0.1	BLQ	1.5±0.1
G26-4#3		2.6±0.3	BLQ	10.2±0.1	BLQ	1.9±0.1
wtd. x	25	2.9±0.2	BLQ	10.2±0.1	BLQ	1.7±0.1
G26-4A#1		16.3±1.2	BLQ	274.2±0.6	BLQ	3.6±0.2
G26-4A#2		11.8±1.0	BLQ	74.2±0.4	63.5±44.0	1.99±0.01
wtd. x	50	13.6±0.8	BLQ	135.7±0.3	63.5±44.0	1.9±0.1
H3-3A#1		3.7±0.3	BLQ	13.0±0.2	96.7±22.9	1.5±0.1
H3-3A#2		3.8±0.4	BLQ	7.02±0.15	91.4±22.6	1.45±0.07
wtd. x	35	3.7±0.2	BLQ	9.2 ±0.1	94.1±16.1	1.5±0.1
H3-3B#1		20.3±1.1	17.1±7.3	74.3±0.4	1425.6±43.3	7.9±0.2
H3-3B#2		24.5±1.5	11.6±7.1	59.1±0.4	1522.2±43.2	11.4±0.4
wtd. x	80	21.8±0.9	14.3±5.	66.7±0.3	1474.0±30.6	8.6±0.2
H4-2A#1		148.9±6.3	78.4±18.	234.3±0.6	13856.3±90.1	42.4±1.2
H4-2A#2		145.3±6.2	67.4±16.9	235.8±0.6	13826.8±90.4	36.2±1.1
wtd. x	90	147.1±4.4	72.4±12.4	235.1±0.4	13841.6±63.8	39.1±0.8

Table 9. Duplicate whole rock analyses of Tulameen samples, expressed in ppm except where noted as percent. All values given at 95 percent confidence limits.

Sample	Sc	Cr₂O₃	FeO (%)	NiO	Co	TiO₂ (%)	MgO (%)	MnO	V₂O₅	Al₂O₃ (%)
R4-7#1	1.5±0.2	26±2	1.3±0.1		10±1	0.18±0.07	1.8±1.0	150±32	122±10	14.6±0.1
R4-7#2	1.4±0.2	19±2	1.4±0.1		10±1	0.16±0.07	3.9±1.0	155±29	124±12	14.1±0.1
T8-1#1	4.8±0.6	4967±289	8.2±0.4	1377±56	119±5	0.04±0.04	43.8±2.5	1516±157	21±3	0.57±0.01
T8-1#2	4.9±0.2	5105±297	8.4±0.4	1380±56	122±5	0.04±0.05	43.6±2.6	1530±159	22±3	0.57±0.01
B18-1#1	4.0±0.5	6768±392	9.4±0.4	1474±62	137±6		46.5±2.6	1826±189	14±3	0.25±0.01
B18-1#2	4.4±0.5	7529±437	10.2±0.4	1445±57	149±6		47.9±2.7	1927±199	15±3	0.28±0.01
D14-1#1	4.6±0.6	3655±212	10.7±0.4	1519±56	152±6		47.8±2.7	1927±196	10±3	0.21±0.01
D14-1#2	4.3±0.6	3397±201	9.9±0.4	1436±37	142±6		46.8±2.6	1939±197	7±2	0.20±0.00
G20-6#1	7.1±0.9	4169±242	8.4±0.3	1557±59	120±5	0.07±0.05	44.3±2.5	1486±154	42±3	0.81±0.01
G20-6#2	6.9±0.8	4167±242	7.4±0.3	1458±57	117±5		44.1±2.5	1488±154	45±4	0.83±0.01
G20-8#1	3.8±0.5	6730±391	9.1±0.3	1286±59	123±5		39.3±2.2	1809±187	19±3	0.26±0.01
G20-8#2	3.9±0.5	7208±418	9.8±0.4	1388±58	130±6		40.6±2.2	1883±192	20±3	0.28±0.01
L5-13#1	106±13	19±4	12.2±0.7		51±2	1.01±0.08	11.9±1.2	1674±173	805±12	5.91±0.04
L5-13#2	100±12	18±4	10.9±0.7		48±2	0.98±0.08	13.1±1.2	1716±178	840±12	6.2±0.1
G26-6#1	82±10	12±4	20.2±0.7		79±3	1.48±0.09	11.3±1.2	1786±185	1524±16	6.19±0.04
G26-6#2	83±10	18±4	20.2±0.7		80±3	1.52±0.09	10.8±1.2	1902±197	1562±17	6.3±0.1
H6-6#1	0.9±0.1	20±2	1.5±0.2		106±4			18±5	17±2	0.41±0.01
H6-6#2	0.6±0.1	17±2	1.3±0.2		98±4			17±5	18±2	0.43±0.01
S15-7#1	96±12	98±8	21.9±0.8		190±8	1.07±0.09	11.2±0.9	1795±186	1378±15	3.17±0.02
S15-7#2	88±11	88±7	20.8±0.7		166±7	1.10±0.07	11.3±1.2	1788±185	1381±15	3.18±0.02

IV. DISTRIBUTION OF THE NOBLE METALS IN THE TULAMEEN COMPLEX

A. General relationships

The average noble metal contents of the various lithologies in the Tulameen Complex are given in Table 10. In addition to analyzing the lithologies typical of the Tulameen Complex, samples were grouped on the basis of their relative enrichment in oxides and sulfides. The three classes, magnetite-rich, chromite-rich, and sulfide-rich, were determined by visual macroscopic inspection of the samples. To be considered magnetite- or chromite-rich, a sample must contain at least 10 volume percent of the oxide in question. The magnetite-rich samples usually have significant amounts of ilmenite and other Fe-Ti and Ti oxides associated with the magnetite. Sulfide-rich samples are those with macroscopically visible sulfides disseminated throughout the sample, as opposed to the more typical ultramafic samples which have very few or no macroscopically visible sulfides. The sulfides most commonly observed in these samples are pyrrhotite, chalcopyrite, and pyrite.

The magnetite-, chromite-, and sulfide-rich samples are restricted in terms of the lithologies in which they occur. Chromite-rich samples were found only in the dunite: three from near Olivine Mountain summit (samples H3-3A, H3-3B, H4-2A) and four from the west flank of Grasshopper Mountain (G16-12, G26-4, G26-4A, D14-7). Magnetite-rich samples were collected from the hornblende clinopyroxenite southwest of Olivine Mountain summit (S12-2, S12-3, S12-4) and near the summit of Lodestone Mountain (L23-1, L23-2, L24-1, L24-2). Sulfide-rich samples were collected from hornblendite dikes near Grasshopper Mountain (G26-6) and Tanglewood Hill (L5-13), in hornblende clinopyroxenite southwest of Olivine Mountain summit (S15-7) and northeast of Olivine Mountain summit (H6-6), in syenogabbro between Lodestone Mountain and Tanglewood Hill (L5-2, L5-3, L5-5) and in syenodiorite east of Lodestone Mountain summit (B4-3).

The data in Table 10 have been heavily biased towards dunite, peridotite, and their altered equivalents. The reason for this is two-fold: dunite has long been noted as the major host of the PGE in Alaskan-type intrusions (Razin, 1968), and dunite is the dominant lithology in the well-exposed, northern end of the Tulameen Complex. Although

Table 10: Weighted mean values, on the basis of number of samples, of the noble metals by lithology. The number of samples in each case is given in parentheses. BLQ indicates below limit of quantification.

ppb at 95 % confidence limits

Lithology	Pt	Ir	Au	Os	Pd	Rh
Dunite and peridotite	55.9±1.7 (30)	0.103±0.001 (33)	0.174±0.002 (33)	BLQ	BLQ	1.01±0.02 (31)
Serpentinite and serpentinite-dunite	150.4±3.6 (10)	2.62±0.01 (11)	0.22±0.01 (10)	2.6±1.1 (2)	BLQ	1.47±0.05 (11)
Dunite, peridotite, serpentinite, and serpentinite-dunite	72.8±1.5 (40)	0.105±0.001 (44)	0.209±0.002 (43)	2.6±1.1 (2)	BLQ	1.13±0.02 (42)
Olivine clinopyroxenite and clinopyroxenite	33.7±3.6 (2)	0.15±0.01 (1)	0.20±0.01 (2)	BLQ	BLQ	0.45±0.06 (2)
Hornblende clinopyroxenite and hornblendite	16.4±5.9 (1)	0.10±0.01 (1)	0.30±0.01 (1)	BLQ	24.5±15.9 (1)	0.1±0.1 (1)
Magnetite-rich	37.6±2.8 (7)	0.25±0.01 (4)	0.19±0.01 (7)	1.9%0.4 (5)	42.9±17.8 (1)	0.34±0.05 (5)
Syenogabbro and syenodiorite	24.4±5.1 (2)	0.10±0.01 (3)	0.10±0.01 (1)	BLQ	BLQ	0.2±0.1 (1)
Sulfide-rich	43.9±3.3 (4)	0.13±0.01 (3)	1.15±0.01 (5)	1.8±1.0 (1)	55.3±7.2 (5)	0.23±0.05 (3)
Chromite-rich	837.5±10.8 (6)	24.9±0.1 (7)	2.01±0.03 (7)	23.1±4.5 (3)	BLQ	47.8±0.1 (7)
Average[1]	8.79±0.92	0.032±0.002	0.039±0.002	0.39±0.11	14.47±3.29	0.09±0.02
Average[2]	57.7±1.1	0.106±0.001	0.204±0.002	1.98±0.38	49.2±6.2	0.89±0.02

[1] weighted on the volume percentages of the lithologies
[2] weighted on the number of samples of each lithology

hornblende clinopyroxenite, hornblendite, syenogabbro, and syenodiorite comprise the bulk of the Tulameen Complex, they are volumetrically less important than the dunite in the principal area of study. Olivine clinopyroxenite and clinopyroxenite constitute the least volume of the Tulameen Complex in the principal study area, and have been sampled accordingly. On the basis of the number of samples of each lithology analyzed it is apparent that statistically large sample populations have been produced only for the dunite / peridotite and serpentinite / serpentinite-dunite in this study.

Ruthenium was not quantified in any of the samples analyzed, and Os and Pd were found to be present in a relatively small proportion of the total number of samples analyzed (eight and seven samples respectively, excluding chromite-rich samples). Of the remaining noble metals, Au and Rh were quantified most often, followed by Ir and Pt. This distribution is probably a function of the very low limits of quantification for Au, Rh, and Ir, and may be due to the low limits of quantification and the relatively high abundance of Pt.

B. Lithological relationships

In the Tulameen Complex, dunite, peridotite, serpentinite, and serpentinite-dunite have the greatest Pt, Au, Ir, Os, and Rh contents compared with the other major lithologies (see Table 10). Palladium appears to be concentrated in hornblende clinopyroxenite, hornblendite, and the gabbroic units of the complex. It is interesting to note that no Pd was detected in any of the dunite, peridotite, or altered equivalents of these rocks. Overall, olivine clinopyroxenite and clinopyroxenite have the lowest noble metal contents, and together with the dunite, have the fewest PGE (Pt, Ir, and Rh only) quantified, although this may be a function of sampling.

Figure 6 presents a ranking of the lithological groups given in Table 10 on the basis of the average noble metal content. Samples rich in chromite have not been included in this figure and will be discussed later. Data for sulfide- and magnetite-rich samples have been included with the lithologies in which they occur. This was done because the values obtained from these two classes were not substantially different from the data for the lithologies (hornblende clinopyroxenite, hornblendite, gabbros) so they imparted little bias to the data in Figure 6. A major exception to this is Os in the magnetite-rich rocks. If the
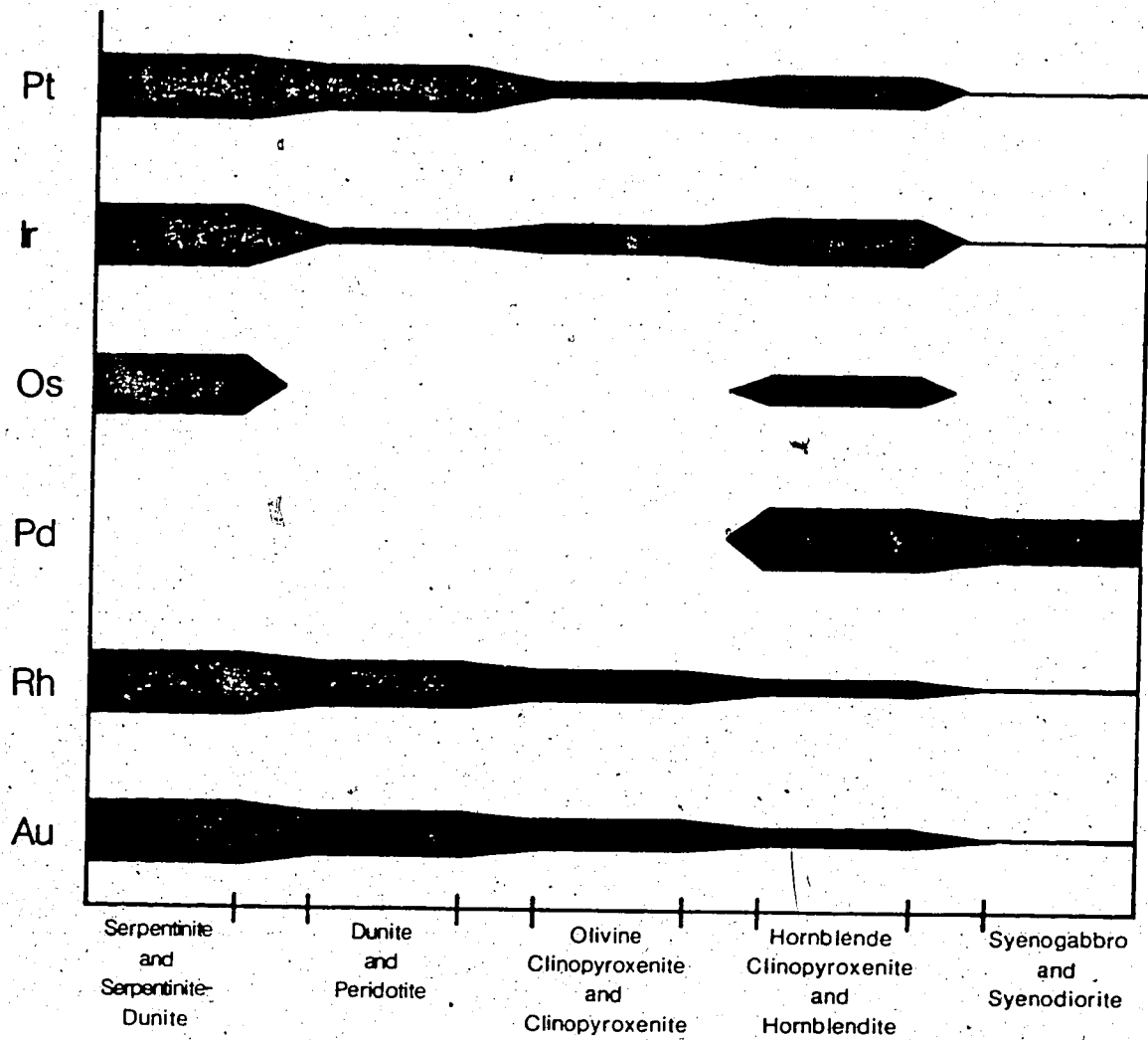
Figure 6: Relative abundances of the noble metals in the Tulameen Complex according to lithology. Chromite-rich samples have been excluded.

data for the magnetite-rich samples had not been included in the hornblende clinopyroxenite and hornblendite data; there would be no Os recorded for these lithologies. Another exception is that some of the sulfide-rich gabbroic rocks contain substantial enrichments in gold relative to typical gabbros. The highest gold content in the sulfide-rich gabbroic rocks is 239 ppb, but gabbros with little or no sulfides have a high value of only 2.9 ppb, This is not surprising, as most of the sulfides observed in the gabbroic rocks of the Tulameen Complex are late and appear to have accompanied the alteration of these rocks (mainly saussuritization). Thus, it is most likely that the higher (239 ppb) gold contents of *some* of the sulfide-rich gabbroic rocks in the Tulameen Complex are due to the presence of sulfides. The chromite-rich samples are discussed separately because the noble metal contents of these samples are substantially higher than the noble metal contents of the other lithologies.

Assuming that the serpentinite and serpentinite-dunite are equivalent to dunite and peridotite, the noble metals are distributed according to the degree of differentiation, with the highest noble metal contents in the most mafic rocks. As can be seen in Figure 6, Rh, Pt, and Au show strong positive correlations with the mafic characteristics of the rocks. Osmium and Ir are concentrated in the serpentinized and hornblende-rich rocks, although Ir is present in all the rock types analyzed. Palladium appears to be restricted to the least mafic units of the complex.

C. Relationships with magnetite-, sulfide-, and chromite-rich samples

Sulfide- and magnetite-rich samples

As can be seen from Table 10, the sulfide- and magnetite-rich rocks have approximately equal noble metal contents. Also, the values given for these two classes of samples are not significantly different from the averages for gabbroic and hornblende-rich rocks given in Table 10, with the exception of Os and Au.

It would appear from the data in Table 10 that magnetite-rich hornblende clinopyroxenite samples tend to be enriched in Os relative to hornblende clinopyroxenites without anomalous amounts of magnetite. If we accept the geochemical coherence of Ru, Ir, and Os (Crocket, 1981) then we should expect to see these magnetite-rich hornblende

clinopyroxenites enriched in Ru and Ir in addition to Os. A slight enrichment in Ir is observed in these samples, but no Ru was quantified.

There are essentially no published data concerning the distribution, concentration, and mode of occurrence of Os in magnetite-rich hornblende clinopyroxenites from Alaskan-type complexes. In fact, the author was not able to find data for Os in typical hornblende clinopyroxenites from these intrusions. Razin (1971) points out that the mineral "osmite" (given as Os, Ir: probably osmiridium) occurs with magnetite in some Uralian dunites. Clark and Greenwood (1972) note strong Pt enrichments in magnetite separates versus olivine separates from the same sample. They did not analyze for Os, and gave no indication as to the behavior of the other PGE in magnetite from dunite, let alone from hornblende clinopyroxenite.

Chromite-rich samples

It is obvious from an examination of the data in Table 10 that with the exception of Pd the chromite-rich samples are greatly enriched in the noble metals over the other lithologies sampled. This is expected, as the Soviet Alaskan-type complexes show PGE enrichments in chromite-rich samples, although Pd is reported to be enriched in addition to the other PGE in these samples (Fominykh and Khvostova, 1970; Naldrett and Cabri, 1976; Crocket, 1981). Table 11 gives a synopsis of the published data for the noble metals in chromite schlieren and segregations in Alaskan-type complexes from occurrences in the Ural and Aldan Shield areas in the U.S.S.R. These data have been selected on the basis of the elements analyzed: many authors have not analyzed for all six PGE, so their data have not been included. Only two listings for gold, both from Kraka, were found in the available literature.

The data in Table 11 indicate that the PGE range from the tens of ppb to hundreds of ppm, while gold appears to be present in the low ppb concentrations in the Soviet chromite-rich samples. The analyses of chromite-rich samples from the Tulameen Complex, given in Tables 8 and 10, show a range from the low ppb to tens of ppm. Thus, to a first approximation, the Tulameen chromite-rich samples are depleted in the PGE by an order of magnitude compared with Alaskan-type complexes in the U.S.S.R. In addition, Ru and Pd were not quantified in any of the Tulameen chromite-rich samples, yet they are

Table 11: Typical noble metal values for chromite-rich samples from occurrences in the Ural and Aldan Shield areas of the U.S.S.R. Values are in ppb.

	High	Low	Mean	Source
Pt	390,000	1,100	156,560	1
	7,000	3,000	5,400	2
	6,000	3,000	4,000	3
Ir	4,300	86	1,687	1
	4,000	3.2	3,000	2
	9,000	2,000	4,000	3
Os	6,100	42	2,194	1
	90	60	80	2
	90	50	75	3
Rh	680	64	479	1
	3,000	400	1,600	2
	7,000	200	2,700	3
Pd	46,000	580	18,356	1
	1,600	500	1,000	2
	600	200	500	3
Ru	480,000	65	99,277	1
	70	40	53	2
	60	30	45	3
Au	1.7	0.4	1.1	4

Sources of data:

[1] Fominykh and Khvostova (1970)
[2] Razin and Khvostova (1965)
[3] Razin et al. (1965)
[4] Sobolev et al. (1974)

present in the Soviet intrusions in concentrations that are certainly above the limits of quantification for these two elements by the analytical technique used in this study.

It is difficult to make meaningful comparisons between the noble metal contents of the Soviet chromite-rich samples and similar samples from the Tulameen Complex because of the distinct differences in the data for these two groups. Possible reasons for these differences may be a depletion in these elements in the Tulameen Complex relative to the Soviet intrusions, or they may reflect differences in the sampling and/or analytical techniques employed by the author versus those employed by the Soviets.

D. Comparisons with other Alaskan-type complexes

Two "overall" averages for each of the noble metals in the Tulameen Complex are given in Table 10. Chromite-rich rocks have not been included in these averages because of their low abundance in the Tulameen Complex. Hornblende-rich and gabbroic rocks constitute the major proportions of Alaskan-type complexes (Taylor and Noble, 1960; Wyllie, 1967), so any overall averages should take this into account. However, the averages based on lithological volumes given in Table 10 may be in error because of the small sample populations for the hornblende-rich and gabbroic rocks. The averages weighted on the number of samples, although biased towards dunite, peridotite, and their altered equivalents, appear to be more in agreement with the published data. As a result, these sample-weighted averages are plotted with the range of concentration for each of the PGE in Figure 7, which shows the relationships between the PGE contents of the Tulameen Complex and other Alaskan-type complexes (exclusive of chromite-rich samples).

As can be seen in Figure 7, the ranges of concentration for the PGE in the Tulameen Complex, except Ru, overlap the ranges for other Alaskan-type complexes. Ruthenium was not present in quantifiable concentrations in any of the Tulameen samples analyzed. This is probably a function of the high limits of detection and quantification for Ru via the analytical technique used, and does not necessarily reflect anomalously low Ru contents in the Tulameen Complex. Crocket (1979) and others have suggested that the very low levels of abundance of Ru in Alaskan-type complexes may result in erroneous analyses for that element.
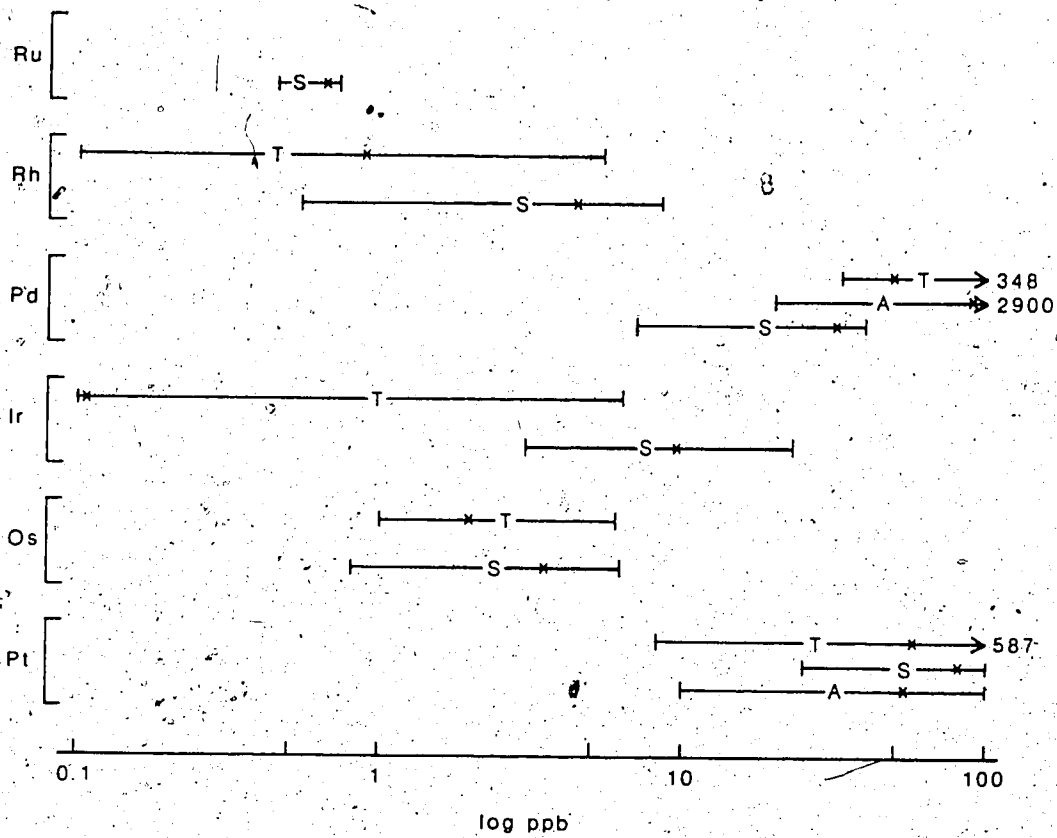
Figure 7: Ranges and average values for the PGE in Alaskan-type complexes, with data for the Tulameen Complex as determined in this study (after Crocket, 1981). Elemental data denoted by "A" are for intrusions in the U.S.A., "S" for occurrences in the U.S.S.R., "T" for the Tulameen Complex, and mean values indicated by "x". The mean values for the Tulameen Complex have been weighted on the number of samples of each lithology. It should be noted that the Tulameen data do not include the analyses of chromite-rich samples.

The average Ir and Rh abundances in the Tulameen Complex are low compared to the published data by between one and two orders of magnitude, and the average value for Ir is approximately one tenth that of Rh in the Tulameen Complex. Chemically and crystallographically, Ir and Rh should behave coherently during crystallization and presumably during initial melting (Berlincourt et al., 1981; Crocket, 1981). If the published values for Rh and Ir in Alaskan-type complexes are accurate, Ir is usually enriched in these intrusions relative to Rh. In the Tulameen Complex, the Rh content is about eight times the Ir content, yet both are low compared to Alaskan-type complexes in general, although they have essentially equal ranges in terms of their concentrations.

Unfortunately there are few published data concerning the distribution and concentration of gold in Alaskan-type intrusions. Naldrett and Cabri (1976) quote an average gold content in Ural dunites of 1.2 ppb, and an average of 2.6 ppb for Ural pyroxenites. The range in Au values given by Naldrett and Cabri (1976) is 1.2 to 75 ppb for Alaskan-type complexes, with a value of 2 ppb as the preferred average for dunites. Sobolev et al. (1974) suggest that the average Au values are 0.7 ppb in dunites, 1.2 ppb in peridotites, 2.7 ppb in pyroxenites, and 8.4 ppb in gabbros. A comparison of these data with the data presented in Table 10 shows that the Au contents reported in this study are substantially lower than those of other Alaskan-type complexes, although the literature data base is too small to provide certainty. The values given in Table 10 also indicate that the overall Au contents of Tulameen samples are much lower than those of peridotites from the ocean floor (4.4 to 10 ppb) and alpine peridotites (0.6 to 165 ppb), and are about the same as those of spinel lherzolites (0.03 to 1.2 ppb) and garnet lherzolites (0.03 to 0.09 ppb) (Crocket and Chyi, 1972; Crocket and Teruta, 1977; Mitchell and Keays 1981). However, the Au data from this study may not truly reflect the primary Au contents of the ultramafic rocks in the Tulameen Complex because the analytical techniques were not tested against a reliable gold standard.

V. DISCUSSION

A. Correlation of the PGE with whole-rock chemistry

All samples analyzed for the noble metals were also analyzed for other trace elements as well as some major and minor elements (Mg, Al, Fe, Cr, Ni, Ti, Co, Sc, Mn, V) to determine if any geochemical tracers could be used as indicators of PGE enrichment. Element-by-element correlations for the ten elements listed above plus the six noble metals quantified were obtained using the MIDAS statistical package on the University of Alberta AMDAHL 470/v6 computer. Two data sets were analyzed: one consisting of all samples except those rich in chromite, and the other consisting only of the chromite-rich samples. All correlations were made after the data had been log transformed, except MgO and MnO, which have relatively normal distributions. It should be noted that MgO has a bimodal distribution, which tends to affect all the correlations made with that oxide.

General lithochemical relationships.

Table 12 gives the element-by-element correlations for all elements analyzed, except the noble metals, in which the correlation coefficients are better than ±0.79. As with the noble metals discussed in the previous sections, these data are biased towards dunite, peridotite, and their altered equivalents. No attempt was made to weight the data towards the more volumetrically abundant gabbroic and hornblende-rich rocks.

Only one correlation involving NiO (with Sc) was deemed to be of a significant value. This is due to the low (less than one weight percent) levels of Ni in the Tulameen Complex, and is also a function of the relatively low number of samples in which Ni was quantified (37). Nonetheless, the fairly strong negative correlation with Sc is consistent with their geochemical relationship.

The strong positive correlation of MgO with Cr_2O_3 in samples that are not chromite-rich is expected, as most of the Cr_2O_3 is found in the dunite. The strongly negative correlation of these two oxides in chromite-rich samples indicates both the lack of forsterite in these samples and a relative MgO deficiency in Tulameen chromites. All the other correlations with MgO that are significant are indicative of the tendency for Mg to partition into the early differentiates.

40

Table 12: Best element-by-element correlations observed in Tulameen samples, exclusive of the noble metals and chromite-rich samples. Correlations for chromite-rich samples are given in italics. All oxides and elements, except MnO and MgO, have been log transformed.

	Al₂O₃	Sc	TiO₂	Cr₂O₃	V₂O₅	MnO	FeO	Co
Al₂O₃					0.89			
		0.82			*0.99*	*0.83*	*0.84*	
Sc					0.88			
	0.93					*0.83*		
TiO₂					0.95			
		0.99			*0.98*			
Cr₂O₃	-0.79							
	0.97	*0.87*			*0.97*	*0.83*	*0.86*	
V₂O₅		*0.96*				*0.83*		
NiO		-0.82						0.79
FeO			0.86					
		0.89	*0.95*		*0.90*			
Co			-0.94					
MgO	-0.91	-0.80		0.88	-0.91			0.79
	-0.97	*-0.93*	*-0.81*	*-0.98*	*-0.98*	*-0.84*	*-0.92*	

The FeO correlations also reflect the partitioning of Fe during differentiation. Most of the Fe in the Tulameen Complex is associated with hornblende clinopyroxenite, so the strong positive correlation with TiO_2 is not surprising. In chromite-rich samples, the positive correlations of FeO with TiO_2, V_2O_5, MnO, Sc, and Cr_2O_3 are also to be expected, as Alaskan-type intrusions tend to have Fe-rich chromites (Crocket, 1981; others).

No significant correlations of Cr_2O_3 with other oxides or elements were obtained from the "chromite-poor" samples, except for a negative correlation with Al_2O_3. As with Ni, this is most likely due to the strong partitioning of Cr into the earliest differentiates, and is further influenced by the relatively low and constant abundance of Cr in the Tulameen Complex.

TiO_2 correlates extremely well with Sc, FeO, and V_2O_5. This is especially true in the case of the chromite-rich samples, and is a reflection of the tendency for the Tulameen chromites to be Fe-rich.

Cobalt is correlated best with MgO and TiO_2. These correlations are taken as indicative of the partitioning of Co into early differentiates.

Thus, an examination of the data in Table 12 shows that the Tulameen Complex does not deviate from what would be expected of a differentiated ultramafic intrusion in terms of its whole-rock chemistry. The chromite-rich samples from this complex show no strange behavior with respect to the elements listed, except for a tendency to be enriched in Fe and therefore elements that behave geochemically similar to Fe.

Correlations among the noble metals

All correlations involving the noble metals with correlation coefficients greater than ±0.79 are given in Table 13. These data can be sub-divided into two sets: correlations among the noble metals, and correlations between the noble metals and other elements. As can be seen in Table 13, of the six noble metals quantified in this study, all but gold show significant in-group correlations. This would seem to indicate that gold behaves very differently from the PGE during the petrogenesis of Alaskan-type complexes.

Of the PGE, the only correlation obtained from the chromite-poor samples is that of Pt and Pd. This relationship has also been documented by Naldrett and Cabri (1976).

Table 13: Best element-by-element correlations for the noble metals obtained for Tulameen samples. Values for samples rich in chromite are given in italics. All elemental and oxide data, except MnO and MgO, have been log transformed.

	Rh	Os	Pd	Ir
Os	0.97			
Ir	0.92	0.91		
Pt	0.92	0.99	0.86	
MgO	-0.84			-0.95
Al₂O₃	0.87			0.97
Sc	0.95			0.95
TiO₂		0.91		0.93
Cr₂O₃	0.81			0.95
V₂O₅	0.91			0.98
MnO		0.90		0.84
NiO		0.99		
FeO	0.81			0.81

However, the obvious depletion of Pd in the chromite-rich samples results in no correlation of Pt with Pd in such samples. Figure 8 shows six PGE ratios plotted for a number of types of Tulameen samples as well as for some Soviet Alaskan-type intrusions. Figure 8 gives a graphical representation of the differences in the correlation of some PGE with others. Thus, it can be seen that although Pt correlates well with Pd (Pt/(Pd+Pt)) in all Tulameen samples lacking chromite-rich material, the correlation is nil in chromite-rich samples. This contradicts the Soviet data, which indicate that Pd and Pt always positively correlate with one another, regardless of the chromite content.

In the chromite-rich samples, the best correlation is between Pt and Os. This correlation is similar in the Soviet data for chromite-rich rocks (Pt/(Os+Ir+Pt)). In addition, Ir correlates positively with Os, which is also demonstrated by the consistency of the Pt/(Os+Ir+Pt) ratios. However, the Ir/(Os+Ir) ratio indicates that Ir and Os are better correlated in the Tulameen Complex chromite-rich rocks than in similar Soviet samples.

Strong positive correlations are obtained when Os, Ir, and Pt are correlated with Rh. A comparison of the Pt/(Rh+Os+Ir+Pt) ratios for chromite-rich samples and those with accessory chromite indicates that this ratio is slightly higher for Tulameen samples, although the values in the Soviet complexes are not that much lower than the Tulameen values. This indicates that the Pt-Rh, Os-Rh, and Ir-Rh correlations are quite strong and positive in Alaskan-type complexes.

In terms of the overall correlations and PGE ratios, it is obvious that Pt dominates in all ratios except the Pt/(Pd+Pt). In the Tulameen Complex the only exception to this is in the case of samples with accessory or no chromite, which contain approximately equal Pt and Pd contents. The PGE-PGE correlations given in Table 13 show that Pt and Rh are the most commonly correlated PGE, although all the PGE seem to positively correlate with one another to some extent. The obvious exceptions are Pd and Ru, which were not quantified in the chromite-rich samples. The observations given in this section appear to indicate that in the Tulameen Complex, where chromite-rich samples are concerned, all the PGE except Pd and Ru behaved coherently during the differentiation of the complex. In the case of Ru, it may be that the Tulameen melt was depleted in this metal, although it must be considered that the limits of quantification for Ru by the analytical method employed may be responsible for this apparent depletion. For Pd, the only possible

O Dunite and peridotite (Urals: Naldrett and Cabri, 1976)
△ Chromite-rich (Urals, Aldan Shield; Naldrett and Cabri, 1976)
● Tulameen, overall
■ Tulameen, overall with chromite-rich
▲ Chromite-rich (Tulameen)
▼ Dunite, peridotite, and altered equivalents (Tulameen)
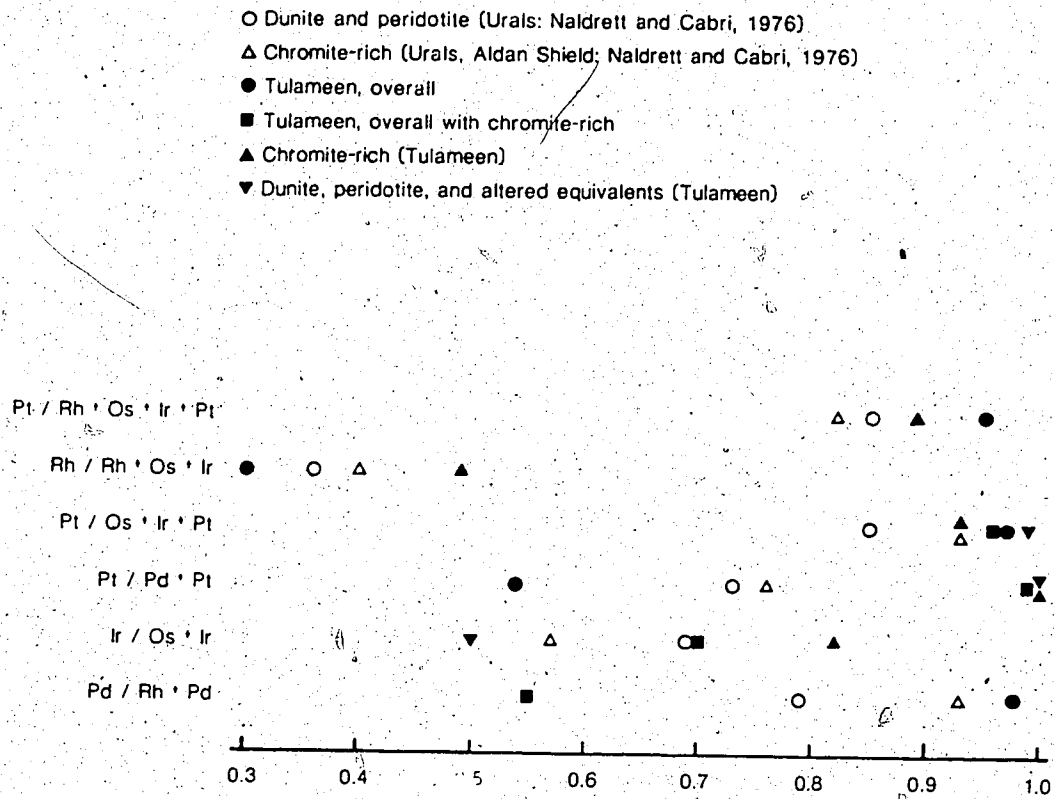
Figure 8: Typical PGE ratios for the Tulameen Complex, as determined in this study, and Alaskan-type complexes in the U.S.S.R. (after Naldrett and Cabri, 1976).

explanations appear to be that of either a depleted melt or almost total partitioning of Pd into later-stage differentiates.

PGE correlations with other elements

Of the six noble metals quantified, only Rh, Os, and Ir show any significant correlations with the non-noble elements analyzed. In samples with accessory or no chromite, the only significant correlation observed is that of Os with TiO_2. This is probably due to the high amounts of Os quantified in the magnetite-rich samples, which contain the greatest Os contents of any of the samples analyzed (except for the chromite-rich samples). It is interesting that Os does not correlate well with FeO or V_2O_5, which are both heavily enriched in the magnetite-rich samples.

Strong negative correlations exist between MgO and Rh, and between MgO and Ir in the chromite-rich samples. This is interesting in that the other PGE do not show any correlation, positive or negative, with MgO in the same samples.

The only correlations with Os that are observed in the chromite-rich samples are with MnO and NiO. The positive correlation with NiO is notable, as none of the other PGE show a correlation with this oxide. The MnO correlation with Os is odd, as Os does not correlate with any of the other principal components of chromite.

The only PGE to correlate positively with FeO are Rh and Ir. This is interesting, as the PGE have pronounced siderophile tendencies (Crocket, 1981). Given that chromites in Alaskan-type complexes are Fe-rich, and the fact that chromite-rich samples contain the greatest PGE contents in these intrusions, we should expect all the PGE quantified in these samples to show strong positive correlations with FeO. Moreover, Rh and Ir are the only PGE that show significant positive correlations with Al_2O_3, Sc, Cr_2O_3, and V_2O_5 in chromite-rich rocks. These three oxides and Sc were shown in a previous section to be major correlations in the "general" lithochemical data. Iridium also correlates well with MnO.

It should be noted that no systematic variations in the whole-rock chemistry of the chromite-rich samples relative to noble metal content were observed. The amount of chromite in the sample appears to have some effect on the noble metal concentration, with higher noble metal contents recorded for samples very rich in chromite. However,

there is no systematic relationship between chromite content and noble metal content in these samples, as samples D14-7 and H4-2A both contain essentially 100 volume percent chromite but have significantly different noble metal contents (see Table 8).

A number of conclusions may be drawn on the basis of these lithochemical observations: Of the PGE, the only elements that show significant positive correlations with the principal components of chromite in chromite-rich samples are Rh and Ir. Thus, there is obviously some petrogenetic relationship between chromite and these two elements. Iridium appears to be slightly better correlated with chromite than is Rh, as the correlation coefficients for Ir with Al_2O_3, Cr_2O_3, and V_2O_5 are all higher than the corresponding Rh values. Also, Ir shows a substantial positive correlation with MnO and TiO_2, which are also enriched in the chromite-rich samples relative to dunite.

Platinum shows no correlation with any of the non-noble elements analyzed, which probably indicates that Pt does not reside in the chromite lattice. This seems to contradict the association of high Pt contents with chromite enrichments. However, this lack of correlation may reflect a preference for Pt to form discrete Pt-rich phases at the high temperatures present during chromite crystallization. The apparent Pt-chromite relationship would then be one of temperature rather than crystal-chemical.

Osmium in chromite-rich rocks correlates well with MnO and NiO, and with TiO_2 in samples containing accessory or no chromite. This may be a reflection of two things: firstly, Os may be partially partitioned between Ni-bearing phases and chromite during the early stages of differentiation. Secondly, Os appears to partition much more readily into Fe and Ti-bearing rocks during the later stages of differentiation (i. e., during the crystallization of hornblende clinopyroxenite containing major amounts of magnetite).

There are a number of possible explanations as to why Pd and Ru were not quantified in any of the chromite-rich samples: these two elements do no partition into the early differentiates; the Tulameen Complex is depleted in terms of these elements in chromite-rich rocks; or their absence is a function of the analytical technique employed. Given the very high abundances of the other PGE in the samples rich in chromite, it seems unlikely that the analytical technique is solely at fault. Also, the fact that Pd was not quantified in any of the dunite, peridotite, or serpentinized rocks cannot be dismissed. Thus, it appears that, at least in the case of Pd, the physical-chemical conditions associated

with the primitive differentiates were unsuitable for this element to partition into the crystalline phase. Ruthenium probably suffers from the combined effects of high quantification limits and a lower abundance in the rocks of the Tulameen Complex.

It is obvious that Au is not appreciably enriched in the chromite-rich rocks compared with rocks containing little or no chromite. In fact, the Au contents of these two classes ███████████ same. Also, since Au shows no significant correlation with any of the ot██████████ quantified, it seems likely that Au is somewhat randomly distribut██████████ Tulameen Complex at fairly constant concentrations, although local enrichme██████████ occur. These local highs may be the result of late-stage alteration, which re-mobilized and possibly introduced some Au, and upon deposition produced the observed anomalies. In addition, the relative consistency in PGE contents between sulfide-rich and sulfide-poor gabbroic rocks in this intrusion can be taken as indicators of either the ineffectiveness of the incorporation of the PGE into epigenetic sulfides or the immobility of the PGE during the alteration of these gabbroic rocks.

B. PGE in serpentinized rocks

Up to this point the dunite/peridotite and serpentinite/serpentinite-dunite have been considered as a single rock type. This has been done because the discussion has centered on the primary distribution of the noble metals. However, it is obvious from the data in Table 10 and Figure 6 that there is a significant difference in the noble metal contents of these two lithological groups; and, therefore, warrants a separate discussion.

As is shown in Table 10 and Figure 6, the PGE are in all cases enriched in serpentinite/serpentinite-dunite relative to dunite/peridotite. In some instances this enrichment is on the order of a factor of ten. Clearly, either the serpentinized rocks contained primary PGE contents higher than that of the dunites and peridotites, or the PGE have been concentrated in the serpentinized rocks during serpentinzation.

Eckstrand (1975) has presented a model for the mobilization and redeposition of a number of elements during serpentinization, and has also given some indication of the conditions of serpentinization. According to this model, during the onset of serpentinization when olivine alters to serpentine and magnetite, reducing conditions predominate. The opaque mineral assemblages that develop under these conditions are

low in sulfur. As the second stage proceeds, which involves the alteration of serpentine to talc, oxidizing conditions exist which result in sulfur-rich opaque mineral assemblages. Many of Eckstrand's (1975) observations have been demonstrated experimentally by Filippidis (1982).

Rucklidge (1972) and Rucklidge and Patterson (1977) have shown that large amounts of chlorine are introduced to the system during serpentinization, mostly from the country rocks. Much of this chlorine appears to be taken up by serpentine minerals, although it seems that cations in olivine (such as Fe) form hydroxychlorides and are taken . into solution (Rucklidge and Patterson, 1977). These hydroxychloride phases are later redeposited as magnetite with the release of water and HCl. The entire process is initiated as acid solutions attack olivine. As the reaction continues, the pH increases and the solution becomes alkaline near the reaction front, but solutions behind the front become more acidic once again, allowing minerals such as magnetite to be deposited. It must be kept in mind that conditions at the reaction front are such that pH's as high as 12 may be encountered (Barnes and O'Neill, 1969).

Groves and Keays (1979) have indicated that S, Au, and Ni are redistributed during serpentinization, but assume the PGE to be immobile under these conditions. Groves and Keays (1979) have observed that the Ni/S and Ni/Fe ratios are higher in the altered rocks than in their precursors. They have also shown that the Pd/Ir ratios are relatively constant between altered and unaltered rocks, which they take as a sign of the lack of redistribution of these elements during alteration. The Ni/Pd ratios in serpentinites are lower than in dunites and serpentinized dunites, indicating the addition of Ni to sulfides in dunite prior to serpentinization (Groves and Keays, 1979). They reason that the Ni released from silicates during serpentinization either left the system entirely or was added to the sulfides in dunite. On the basis of S/Pd ratios, with the assumption of Pd immobility, Groves and Keays (1979) consider that S is added during serpentinization, with some As and S added during carbonatization.

Fuchs and Rose (1974) have given an Eh-pH diagram for the systems $Pt-H_2O-Cl^-$ and $Pd-H_2O-Cl^-$. Their data, at 25° C, indicate that the formation and transport of Pt and Pd as chlorides or hydroxides is possible, with the formation of $PtCl_4^{-2}$ and $PdCl_4^{-2}$ occurring below pH 7. If we assume that the stability fields for these chlorides and hydroxides do

not shift significantly with increasing temperature, then it may be possible to produce these complexes at 350-400° C. If this is true, then the remobilization of the PGE may be possible during serpentinization. If the activity of As and the fS_2 increase in the serpentinizing fluids, the chlorides or hydroxides may be replaced by sulfides or arsenides. Alternatively, changes in the fO_2 or pH may cause the noble metal complexes to become unstable, resulting in the precipitation of the noble metals which may later form compounds with the available chalcogens.

Another possible explanation is that first the chlorides form at low pH, and as serpentinization proceeds and the pH rises, the chlorides are replaced by hydroxides. When fO_2 increases (or pH decreases) at the end of serpentinization, the noble metal hydroxides become sulfides or arsenides.

The author has not performed the calculations required to draw the Eh-pH diagram for these systems at 350-400° C, so the foregoing discussion is pure conjecture. However, it appears from the noble metal distribution data that something has resulted in an enrichment of the PGE in the Tulameen serpentinites. In addition, the differences in the sulfide contents of the dunite/peridotite and serpentinized rocks must be considered. Unaltered dunitic rocks in the Tulameen Complex contain very few sulfides, whereas serpentinized rocks contain minor, but widely disseminated, amounts of sulfides. Also, the fact that the Type 2 PGMs are dominated by sperrylite ($PtAs_2$) may reflect the remobilization of the PGE and their subsequent deposition as chalcogen compounds. It is felt by the author that a relatively simple mechanism of remobilization and enhanced concentration of the PGE, Ni, Fe, As, and S in the altered rocks as a result of serpentinization may be a viable explanation for the observed distributions.

C. Petrogenetic model for the PGE

Chromite-rich rocks in the Tulameen Complex contain the greatest Rh, Ir, Os, and Pt contents of any samples analyzed. The chromite-rich rocks are also the only materials in which discrete PGMs were observed. Although these observations seem to indicate that these four elements are petrogenetically related to chromite, a number of lithochemical factors suggest that this is not strictly the case.

Of the four PGE listed above, the only ones that show substantial correlations with the major components of chromite are Rh and Ir, with Ir more strongly correlated with chromite than is Rh. Osmium shows a mildly positive correlation with some of the principal components of chromite, but not as strongly as Rh and Ir. Platinum shows no correlation with these components, and Pd was not quantified in any of the chromite-rich samples.

On the basis of these observations it is felt that only Rh and Ir have relatively strong petrogenetic relationships with chromite, with Os showing a slight relationship. Platinum appears to be most strongly governed by temperature, so its association with chromite-rich samples is probably thermal rather than crystallochemical. Palladium seems to preferentially partition into the melt during the high temperature stage when massive, nodular, or schlieren chromite is crystallizing.

The observations made with respect to the PGMs that occur in chromite-rich samples support these suggestions. The Type 1 and Type 2 PGMs show very different modes of occurrence and mineralogy, and their textures appear to reflect a temporal relationship with chromite. In the case of Type 1 PGMs, which are dominantly Pt-Fe alloys, it seems quite likely that these PGMs begin as complex Pt-Fe or Pt-Sb droplets in the melt that adhere to the growth surfaces of crystallizing chromites. As the chromite grains continue to crystallize they surround the PGE-rich droplets, which are "shaped" by the chromites to produce cubic-shaped PGM inclusions. This shaping reflects attempts by the chromites to minimize their surface free energies.

The Type 2 PGM, which occur mainly as anhedral grains of sperrylite in a xenomorphic texture interstitial to chromite grains, are commonly associated with serpentine and Fe-Ni sulfides, especially pentlandite. They are never more than partially enclosed by single chromite grains, and rarely are they in direct contact with chromite. Two possible modes of genesis for the Type 2 PGMs are suggested. The first mode is that of PGE which are trapped as droplets in the liquid interstitial to chromite, possibly in a monosulfide solid solution (Mss) with Fe, Ni, and S, as independent PGE-rich droplets, or as metal-rich alloys (similar to the Cu-Fe-Ni alloys given by Kullerud *et al.*, 1969, and Craig and Kullerud, 1969). Although there are few experimental data concerning the system Fe-Ni-S-PGE, Stevens *et al.* (1978) have shown that the system Fe-Ni-Pt behaves quite

similarly to the Fe-Ni-S system. Also, Berlincourt et al. (1981) report that a number of PGE-Fe,Ni-S compounds have been synthesized at temperatures well within those considered relevant to the Fe-Ni-S system. Substitution of some Cu and Co into Mss can occur, with little effect on the phase relations in the Fe-Ni-S system (Craig and Kullerud, 1969). Possibly the same may be true for the PGE. Thus, it appears highly probable that the PGE may be incorporated into immiscible droplets, consisting of sulfides, alloys, or Mss, at relatively high temperatures. From the textural evidence exhibited by some of the Type 2 PGMs it seems that the PGE-Fe-Ni-S may form Mss that exsolves seperate PGMs and Fe-Ni sulfides on cooling. In addition, some PGE may be incorporated into Fe-Ni sulfides (Berlincourt et al., 1981). Also, perhaps due to immiscibility, the PGE/alloys are not completely incorporated into Mss, but through some wetting or adhesive properties adhere to the surfaces of Mss, resulting in the observed textures. The lack of Fe sulfides in association with the Type 2 PGMs may result from Ni enrichment in the liquid phase due to the low sulfur pressures in the ultramafic melt (Craig and Kullerud, 1969).

The second process by which Type 2 PGMs may form is during serpentinization. It has been established that the initial sulfide assemblages formed during serpentinization are sulfur-poor (Eckstrand, 1975). These sulfur-poor sulfides may be formed at the expense of primary sulfur-rich sulfides. The breakdown of the primary sulfides and silicates could cause any contained PGE to be released and perhaps dissolved in the serpentinizing fluids. As serpentinization ends, these PGE are redeposited as discrete PGMs. Since the chromite-rich samples analyzed in this study occur in dunites that are located away from the main areas of serpentinization, the PGE have probably not been transported over large distances. In fact, the distances involved could be on the order of centimeters or less, for all that is required to form these PGMs is the remobilization of most of the PGE that are contained in Fe-Ni sulfides and silicates interstitial to chromite. The high sulfide contents of serpentinized rocks relative to unaltered dunite/peridotite in the Tulameen Complex is probably directly observable evidence of this remobilization.

Thus, the Type 1 and Type 2 PGMs, although spatially related to chromite, are not strictly related to chromite in petrogenetic terms. Type 1 PGMs form at somewhat higher temperatures than Type 2, for they form while chromite is still crystallizing. The Type 2 PGMs form in the liquid interstitial to chromite after chromite has essentially stopped

crystallizing and the temperature has decreased. The reason for the apparent correlation between chromite and the PGE is probably due to strong temperature controls on the initial partitioning of the PGE.

As chromite forms in the melt, it begins to settle because of its greater density. Likewise, the PGE-rich and sulfide droplets formed will have a tendency to settle. Hiemstra (1979) has suggested that the small size of the PGMs and sulfides in the Merensky Reef and UG-2 Reef would cause them to settle in the melt less rapidly than the larger chromite grains. He reasons that they may have settled as composite liquids of PGE and sulfides that were adhered to chromite grains, by a process he calls pepa settling. Hiemstra (1979) proposes that these composite liquids are more likely to wet chromite than silicates, based on textural evidence. In addition to settling as composite droplets adhered to chromite, the PGE may also settle as alloys of Fe (Hiemstra, 1979). The mineralogical and textural data presented in this study combined with the phase relation data tend to suggest that pepa settling, both as PGE droplets/alloys and as composite PGE-sulfide droplets/phases, is a viable mechanism that can be invoked to explain much of the rich primary concentration of the PGE in chromite-rich rocks in the Tulameen Complex.

Hiemstra (1979) points out that although many authors, including Razin (1965) and Naldrett and Cabri (1976) have alluded to a more active role of chromite in the concentration of the PGE, there are no experimental data that indicate the efficiency of such collection. The question arises as to what degree can the isomorphous substitution of the PGE in the chromite structure take place, and how likely are such substitutions to occur?

The strong positive correlations between Rh, Ir, and chromite would seem to indicate that at least these two PGE do substitute into the chromite structure. The literature contains no clear evidence to support such claims, although studies such as that of Grimaldi and Schnepfe (1969) and Gijbels et al. (1974) suggest that Ir and Rh do occupy sites within the chromite lattice. Grimaldi and Schnepfe (1969) argue that Rh occurs entirely within and Pd totally outside the chromite lattice, with Pt distributed both in and out of the chromites. Gijbels et al. (1974) suggest that chromite can effectively concentrate Ru, Os, and Ir in its lattice but expels up to 25 percent of these PGE during

cooling (as in the Type 3 PGMs). Unfortunately the Type 3 PGMs observed in this study were too small and few to allow the author to use microprobe analyses to verify the mineralogy of these phas·

The methods of analysis employed must be considered when discussions of the PGE in chromite are presented. Both the studies mentioned above utilized fusions to break down chromite grains, and their conclusions are based on the apparent amounts of PGE contained in chromite versus PGE outside chromite. These techniques do not allow for the differentiation between PGE contained as inclusions and PGE occupying lattice positions. It is highly probable that the PGE may be present as minute PGM inclusions (Page, 1971). Thus, it is felt by the author that although Rh and Ir may substitute for Cr in chromite, it is most likely that the amount of these elements (and the other PGE) contained in chromite lattice positions is small relative to the PGE contained as PGM inclusions in chromite.

The literature contains conflicting evidence as to the likelihood of PGE incorporation into silicate lattices. As with chromite, the author believes that the PGE are mainly present in silicates, such as olivine, as minute inclusions.

In terms of general lithological relationships, Pt, Ir, and Rh strongly partition into the most mafic differentiates. Osmium partitions into these phases as well, but appears to partition equally as well into magnetite-rich hornblende clinopyroxenite. Osmium also presents a problem because it was not quantified in any of the dunite/peridotite samples but was quantified in serpentinized rocks. This may be an indicator of relatively higher mobility of Os during serpentinization compared with the other PGE. If this is the case, the Os quantified in the serpentinized rocks may be the result of enrichments that are relatively small, but great enough to allow this element to be accurately analyzed in these rocks. Palladium appears to partition only into the late-stage differentiates (hornblende clinopyroxenites and gabbros). Perhaps this is an indicator of a very pronounced siderophile tendency, or it may be that Pd prefers rocks with higher silica and light element contents. Alternatively, Pd may have a very strong temperature dependence in the Tulameen Complex, resulting in greater partitioning of this element into lower temperature, less mafic phases.

The only PGE not observed to occur in all the major Tulameen lithologies are Pd and Os. In addition, the gabbroic rocks contain the lowest PGE contents, with the exception of Pd. This is taken as an indication of two things: firstly, Pd and Os appear to be much more sensitive to differences in temperature and melt chemistry compared with Rh, Ir, and Pt; and secondly, Rh, Ir, Pt, and Os all share similar temperature/chemistry requirements, as they show a substantial decrease with decreasing mafic characteristics of the rocks.

VI. CONCLUSIONS

The PGE are distributed roughly according to the degree of differentiation in the Tulameen Complex, with the highest PGE contents in dunitic rocks and the lowest in gabbroic rocks. The major exception to this trend is Pd, which appears to be strongly partitioned into hornblende clinopyroxenite and gabbroic rocks. Also, Os shows a complex behavior, partitioning into early differentiates rich in chromite, and into hornblende clinopyroxenite.

Rocks containing massive, nodular, or schlieren chromite contain the greatest concentrations of the PGE, except Pd. The association with chromite is taken as an indicator of a strong temperature control on the partitioning of the PGE, not as evidence of crystallochemical relationships. This is not to say that there are no such relationships, but rather that if they do exist their significance is dwarfed by the role of temperature.

The PGE occur in three distinct modes in samples rich in chromite. The first, here called Type 1 PGMs, are present mainly as Pt-Fe alloy inclusions within chromite grains. These inclusions have cubic outlines, indicating that they were entrapped as liquids while chromite was still crystallizing. The chromite grains "shaped" these inclusions in cubic forms to minimize their surface free energies (in the same way that negative crystal fluid inclusions form). The second occurrence, Type 2 PGMs, consist mainly of sperrylite interstitial to chromite grains. These PGMs are often associated with Fe-Ni sulfides, especially pentlandite, and serpentine. The PGE in this case are assumed to have been originally deposited as complex sulfide droplets, alloys, and possibly Mss, and as PGE inclusions in silicates. Some PGE-Fe-Ni sulfides exsolved from an Mss into discrete PGMs and Fe-Ni sulfides, which probably contained some PGE. Many of the PGE sulfides and alloys perhaps adhered to Fe-Ni-S phases, such as Mss, and produced the observed textures on cooling. During serpentinization the PGE contained in silicates and sulfur-rich sulfides were released, transported in solution, and redeposited as discrete PGMs in association with secondary (or late) sulfur-rich sulfides. The third occurrence is noted as Type 3 PGMs, which appear to have been exsolved from chromite during cooling. These PGMs may have been originally deposited in chromite lattice positions, and in fact some PGE may still be present in those lattices.

All three types of PGMs occur in microscopically visible (and presumably smaller) grains. In terms of their paragenesis, it seems that the Type 1 and 3 PGMs are

56

contemporaneous, and Type 2 are slightly later. The model for the concentration of the PGE by chromite assumes that the PGE are more likely to adhere as droplets to growing chromite grains than to silicates. The PGE are probably first present as PGE-rich droplets, alloys, and perhaps Mss, which are swept out of the melt and concentrated by settling chromite grains.

The PGE in rocks with accessory or no chromite were probably deposited as inclusions in silicates and oxides, and in complex Fe-Ni sulfide mixtures or alloys. During serpentinization, much of the PGE held in these minerals, especially silicates and sulfur-rich sulfides, were released and transported as hydroxide or chloride complexes. This remobilization appears to be able to cause significant enrichments of the PGE and sulfides in the serpentinized rocks. The PGE were probably redeposited as minute, discrete PGE sulfides and other chalcogen compounds. The required chalcogens are assumed to be mainly supplied from the country rocks by the serpentinizing fluids.

No Ru was quantified in the Tulameen Complex. This is probably a function of the relatively high limits of quantification for Ru by the analytical techniques used, (106.7 ± 99.4 and 91.1 ± 40.5 ppb) and may also be due to a relative depletion in Ru in the Tulameen magma. Geochemically, in terms of major, minor, and trace elements, the Tulameen Complex is not particularly peculiar. However, the Tulameen Complex is different compared with other Alaskan-type intrusions in that most Alaskan-type complexes are much smaller than the Tulameen Complex, and these intrusions usually occur in fairly close proximity to one another. The Alaskan-type complexes nearest the Tulameen Complex are on the order of 750 to 800 km away, in north-central and northwestern British Columbia. Perhaps these two observations indicate that the genesis of the Tulameen magma was slightly different from the other Alaskan-type complexes in terms of starting materials. This may account for some of the observed differences and discrepancies between the Tulameen PGE data and similar data from other Alaskan-type complexes. In addition, the different analytical techniques used by the author and other researchers could play an important role in producing the observed variations.

In spite of the obvious differences between the PGE characteristics of the Tulameen Complex and those of other Alaskan-type complexes, in general terms the PGE concentrations and distributions are not all that different. The basic lithological patterns

and levels of concentration established for the Tulameen Complex agree reasonably well with the data published for other Alaskan-type complexes.

There is a definite need for more detailed studies of this type to enable us to compare and understand the PGE data in the Alaskan-type complexes better. This study suffers mainly from a deficiency of samples analyzed from all the lithologies except the dunite/peridotite and serpentinite/serpentinite-dunite, so there is still more work that can be done with the PGE in the Tulameen Complex. Only through analyses of the PGE in many different Alaskan-type complexes by proven analytical techniques combined with experimental data concerning the role of silicate, oxide, and sulfide minerals in the genesis of PGE deposits can we hope to begin to understand fully the nature of the PGE in this type of ultramafic intrusion. Such information should result in practical applications, as the Alaskan-type complexes contain potentially economic concentrations of the PGE.

VII. REFERENCES CITED

Apps, M.J., 1978, Development of INAA facilities, *in* University of Alberta SLOWPOKE Facility Ann. Rpt., p 1 1.

------, and Apps, K.S., 1981, NAARUN: a simple to use neutron activation analysis computer program, *in* University of Alberta SLOWPOKE Facility Ann. Rpt., p. R4-R5.

Barnes, I., and O'Neill, J.R., 1969, The relationship between fluids in some fresh alpine ultramafics and possible modern serpentinization, western United States: *Geol. Soc. Am. Bull.*, v. 80, p. 1947-1960.

Beamish, F.E., and van Loon, J.C., 1972, The present status of methods of separating and determining the noble metals: *Minerals Sci. Engng.*, v. 4, p. 3-17.

Begizov, V.D., Borisenko, L.F., and Uskov, Ye. D., 1975, Sulfides and natural solid solutions of platinum metals from ultramafic rocks of the Gusevogorskiy Pluton, Urals: *Doklady Akad. Nauk SSSR*, v. 225, p. 134-137.

Bergerioux, C., Kennedy, G., and Zikovsky, L, 1979, Use of the semi-absolute method in neutron activation analysis: *J. Radioan. Chem.*, v. 39, p. 229-234.

Berlincourt, L.E., Hummel, H.H., and Skinner, B.J., 1981, Phases and phase relations of the platinum-group elements: *in* Cabri, L.J., ed., *Platinum-group elements: mineralogy, geology, recovery*: CIM Spec. Vol. 23, p. 19-45.

Bow, C., Wolfgram, D., Turner, A., Barnes, S., Evans, J., Zdepski, M., and Boudreau, A., 1982, Investigations of the Howland Reef of the Stillwater Complex, Minneapolis Adit area: stratigraphy, structure, and mineralization: *Econ. Geol.*, v. 77, p. 148.1-1492.

Cabri, L.J., and Feather, C.E., 1975, Platinum-iron alloys: a nomenclature based on a study of natural and synthetic alloys: *Can. Miner.*, v. 13, p. 117-126.

------, and Hey, M.H., 1974, Platiniridium: confirmation as a valid mineral species: *Can. Miner.*, v. 12, p. 299-303.

------, Owens, D.R., and LaFlamme, J.H.G., 1973, Tulameenite, a new platinum-iron-copper mineral from placers in the Tulameen River area, British Columbia: *Can. Miner.*, v. 12, p. 21-25.

Chart of the nuclides, 1977, twelfth ed. (revised), San Jose, California, General Electric Company, 53 p.

Clark, A.L., and Greenwood, W.R., 1972, Geochemistry and distribution of platinum-group metals in mafic to ultramafic complexes of southern and southeastern Alaska: *U.S.G.S. Prof. Paper* 800-C, p. C157-C160.

Craig, J.R., and Kullerud, G., 1969, Phase relations in the Cu-Fe-Ni-S system and their application to magmatic ore deposits: *Econ. Geol. Mono.* 4, p. 344-358.

Crocket, J.H., 1979, Platinum-group elements in mafic and ultramafic rocks- A survey: *Can. Miner.*, v. 17, p. 391-402.

--------, 1981, Geochemistry of the platinum group elements, *in* Cabri, L.J., ed., *Platinum-group elements: mineralogy, geology, recovery*: CIM Spec. Vol. 23, p. 47-64.

--------, and Cabri, L.J., 1981, Analytical methods for the platinum-group elements, *in* Cabri, L.J., ed., *Platinum-group elements: mineralogy, geology, recovery*: CIM Spec. Vol. 23, p. 71-82.

--------, and Chyi, L.L., 1972, Abundances of Pd, Ir, Os, and Au: *24th IGC, Section 10*, p. 202-209.

--------, and Teruta, Y., 1977, Palladium, iridium, and gold contents of mafic and ultramafic rocks drilled from the Mid-Atlantic Ridge, Leg 37, Deep Sea Drilling Project: *Can. J. Earth Sci.*, v. 14, p. 777-784.

Currie, L.A., 1968, Limits for qualitative detection and quantitative determination - application to radiochemistry: *Anal. Chem.*, v. 40, p. 586-593.

De Soete, D., Gijbels, R., and Hoste, J., 1972, *Neutron activation analysis*, Elving, P.J., and Kolthoff, I.M., eds., John Wiley and Sons, London, 836 p.

Duke, M.J.M., 1983, *Geochemistry of the Exshaw Shale of Alberta - an application of neutron activation analysis and related techniques*: Unpub. M.Sc. thesis, Univ. Alberta, 186 p.

Eastwood, G.E.P., 1959, Magnetite in Lodestone Mountain stock, *in* British Columbia Department of Mines Ann. Rpt., p. 39-53.

Eckstrand, O.R., 1975, The Dumont serpentinite: a model for control of nickeliferous opaque mineral assemblages by alteration reactions in ultramafic rocks: *Econ. Geol.*, v. 70, p. 183-201.

Filippidis, A., 1982, Experimental study of the serpentinization of Mg-Fe-Ni olivine in the presence of sulfur: *Can. Miner.*, v. 20, p. 567-574.

Findlay, D.C., 1963, *Petrology of the Tulameen Ultramafic Complex, Yale District, British Columbia*: Unpub. Ph.D. thesis, Queen's Univ., 415 p.

--------, 1965, Platinum in the Tulameen Ultramafic Complex, B.C.: *Geol. Surv. Canada Paper 65-2(20)*.

--------, 1969, Origin of the Tulameen ultramafic-gabbro complex, southern British Columbia: *Can. J. Earth Sci.*, v. 6, p. 399-425.

Fominykh, V.G., and Khvostova, V.P., 1970, Platinum content of Ural dunite: *Doklady Akad. Nauk SSSR*, v. 191, p. 184-186.

Fuchs, W.A., and Rose, A.W., 1974, The geochemical behaviour of platinum and palladium in the weathering cycle in the Stillwater complex, Montana: *Econ. Geol.*, v. 69, p. 332-346.

Gijbels, R., 1971, Determination of noble metals by neutron-activation analysis: *Talanta*, v. 18, p. 587-601.

--------, Millard, H.T. Jr., Desborough, G.A., and Bartel, A.J., 1974, Osmium, ruthenium, iridium, and uranium in silicates and chromite from the eastern Bushveld Complex, South Africa: *Geochim. Cosmo. Acta*, v. 38, p. 319-337.

Grimaldi, F.S., and Schnepfe, M.M., 1969, Mode of occurrence of platinum, palladium, and rhodium in chromitite: *U.S.G.S. Prof. Paper* 650-C, p. C149-C151.

Groves, D.I., and Keays, R.R., 1979, Mobilization of ore-forming elements during alteration of dunites, Mt. Keith-Betheno, Western Australia: *Can. Miner.*, v. 17, p. 373-389.

Harris, J.F., 1982, Sampling and analytical requirements for effective use of geochemistry in exploration for gold, *in*, Levinson, A.A., ed., *Precious metals in the northern cordillera*: Assoc. Expl. Geochemists, Spec. Pub. 10, p. 53-68.

Hiemstra, S.A., 1979, The role of collectors in the formation of the platinum deposits in the Bushveld complex: *Can. Miner.*, v. 17, p. 469-482.

Hoffman, E.L., 1978, *The platinum group element and gold content of some nickel sulfide ores*: Unpub. Ph.D. thesis, Univ. Toronto, 173 p.

--------, Naldrett, A.J., Van Loon, J.C., Hancock, R.G.V., and Manson, A., 1978, The determination of all the platinum group elements and gold in rocks and ore by neutron activation analysis after preconcentration by a nickel sulphide fire-assay technique on large samples: *Anal. Chim. Acta*, v. 102, p. 157-166.

Knoll, G.F., 1979, *Radiation detection and measurement*: John Wiley and Sons, New York, 816 p.

Khvostova, V.P., Golovnya, S.V., Chernysheva, N.V., and Bukhanova, A.I., 1976, Distribution of the platinum group metals in chromite ores and ultramafic rocks of the Ray-Iz Massif (Polar Urals): *Geochem. Int.*, v. 13, p. 35-39.

Kruger, P., 1971, *Principles of activation analysis*: John Wiley and Sons, New York, 522 p.

Kullerud, G., Yund, R.A., and Moh, G.H., 1969, Phase relations in the Cu-Fe-S, Cu-Ni-S, and Fe-Ni-S systems: *Econ. Geol. Mono.* 4, p. 323-343.

Lederer, C.M., and Shirley, V., 1978, *Table of isotopes*, seventh edition: John Wiley and Sons, New York, 1523 p.

Mitchell, R.H., and Keays, R.R., 1981, Abundance and distribution of gold, palladium and iridium in some spinel and garnet lherzolites: implications for the nature and origin of precious metal-rich intergranular components in the Upper mantle: *Geochem. Cosmo. Acta*, v. 45, p. 2425-2442.

Muecke, G.K. (ed.), 1980, Short course in neutron activation analysis in the geosciences: Mineral. Assoc. of Canada, Short Course Handbook, v. 5, 279 p.

Nadkarni, R.A., and Morrison, G.H., 1974, Determination of the noble metals in geological materials by neutron activation analysis: *Anal. Chem.*, v. 46, p. 232-236.

‑‑‑‑‑‑, and Morrison, G.H., 1977, Neutron activation determination of noble metals using a selective group separating scheme: *J. Radioanal. Chem.*, v. 38, p. 435-449.

Naldrett, A.J., and Cabri, L.J., 1976, Ultramafic and related rocks: their classification and genesis with special reference to the concentration of nickel sulfides and platinum-group elements: *Econ. Geol.*, v. 71, p. 1131-1158.

Page, N.J., 1971, Sulfide minerals in the G and H chromitite zones of the Stillwater Complex, Montana: *U.S.G.S. Prof. Paper* 694, 20 p.

Raicevic, D., and Cabri, L.J., 1976, Mineralogy and concentration of Au- and Pt-bearing placers from the Tulameen River area in British Columbia: *C.I.M. Bull.*, v. 69, no. 770, p. 111-119.

Rakovic, M., 1970, *Activation analysis*: Iliffe, London, and Academia, Prague, 339 p.

Razin, L.V., 1968, Problem of the origin of platinum metallization of forsterite dunites: *Int. Geology Rev.*, v. 13, n. 5, p. 776-788.

‑‑‑‑‑‑, and Khomenko, G.A., 1969, Accumulation of osmium, ruthenium, and the other platinum-group metals in chrome spinel in platinum-bearing dunites: *Geochem. Int.*, v. 6, p. 546-557.

--------, and Khvostova, V.P., 1965, Concentration and distribution patterns of platinum group metals in ultrabasic and alkalic rocks: *Doklady Akad. Nauk SSSR*, v. 162, p. 207-210.

--------, Khvostova, V.P., and Novikov, V.A., 1965, Platinum metals in the essential and accessory minerals of ultramafic rocks: *Geochem. Int.*, v. 2, n. 1, p. 118-131.

Rice, H.M.A., 1947, Geology and mineral deposits of the Princeton map-area, British Columbia: Geol. Surv. Canada, Mem. 243, 136 p.

Robert, R.V.D., van Wyk, E., and Palmer, R., 1971, Concentration of the noble metals by a fire-assay technique using nickel sulphide as the collector: N.I.M. Report 1371, 16 p.

Robert, R.V.D., and van Wyk, E., 1975, The effects of various matrix elements on the efficiency of the fire-assay procedure using nickel sulphide as the collector: N.I.M. Report 1705, 10 p.

Rucklidge, J.C., 1972, Chlorine in partially serpentinized dunite: *Econ. Geol.*, v. 67, p. 38-40.

--------, and Patterson, G.C., 1977, The role of chlorine in serpentinization: *Contrib. Min. Pet.*, v. 65, p. 39-44.

Smith, D.G.W., and Gold, C.M., 1979, EDATA2: A FORTRAN IV computer program for processing wavelength and/or energy-dispersive electron microprobe data: *Proc. 14th Ann. Conf. Microbeam Anal. Soc.*, San Antonio, Texas, p. 273-278.

Sobolev, S.F., Anoshin, G.N., and Perezhogin, G.A., 1974, Distribution of gold in rocks of ultrabasic and basic formations in Ural: *Int. Geology Rev.*, v. 16, n. 7, p. 800-809.

Stevens, G.T., Hatherly, M., and Bowles, J.S., 1978, The ordered phase fields of the iron-nickel-platinum equilibrium diagram: *J. Mater. Sci.*, v. 13, p. 499-504.

Takeuchi, T., Uehara, S., and Hayashi, T., 1980, Comparisons of several dead time correction methods in the case of a mixture of short- and long-lived nuclides: *J. Radioanal. Chem.*, v. 56, p. 25-35.

Taylor, H.P. Jr., and Noble, J.A., 1960, Origin of the ultramafic complexes in southeastern Alaska: *in* 21st IGC, Section 13, p. 175-187.

Westland, A.D., 1981, Inorganic chemistry of the platinum-group elements: *in* Cabri, L.J., ed., *Platinum-group elements: mineralogy, geology, recovery*: CIM Spec. Vol. 23, p. 5-18.

Wyllie, P.J., 1967, *Ultramafic and related rocks*: John Wiley and Sons, New York, 464 p.

Wyttenbach, A., 1971, Coincidence losses in activation analysis: *J. Radioanal. Chem.*, v. 8, p. 335-343.

Description of the nickel sulfide fire-assay preconcentration technique, including

step-by-step instructions and a discussion of its applicability.

A. Reagents and materials

The following is a list of the reagents and hardware required for the nickel sulfide

fire-assay preconcentration procedure, as used in this study:

Fused, ground sodium borate (Fisher, S-252)
Calcined, dry, purified sodium carbonate (Fisher, S-261)
Silica floated powder, 240 mesh (Fisher, S-153)
Sublimed sulfur (Fisher, S-591)
Nickel carbonyl powder (INCO Metals Co. Ltd., Nickel Powder type 123)
30 gram assay crucibles (Canlab, 8522-30C)
12 M HCl (Fisher, A-144)
Nitrocellulose membrane filters, 47 mm, 5 micron porosity (Schleicher and Schuell, AE98)
800 ml beakers
watch glasses to cover 800 ml beakers
hot plates
pan balance
analytical balance
separatory funnels (at least 250 ml)
ring stand and ring to hold separatory funnels
buchner funnels (43 mm is the size closest to that of the membrane filters that can be
    obtained: the membranes must be cut down to the size of the funnel to be of any
    use)
filter flasks and diaphragms
spoonula
weighing papers
muffle furnace capable of holding at least one assay crucible at a time and able to maintain
    1000° C for extended periods (a Thermolyne 1400 was used in this study with very
    good results)
unglazed porcelain tiles
carbide scriber
stainless steel swing mill
distilled water
4 mil polyethylene sheet
hammer or crow bar to smash crucibles
safety glasses or goggles
long (approximately 0.5 m) furnace tongs
asbestos mittens

There are two points to bear in mind when ordering nickel and membrane filters: the INCO

nickel is a very pure nickel powder, and requires no roasting or other treatment before

use. Whatman cellulose nitrate membrane filters were found to be unsuitable for the

analyses, as they contain gold and high concentrations of bromine. Bromine produces

excessive activity during activation, and increases the background which raises the

detection limits of the PGE during counting. Thus, the membrane filters chosen should be

analyzed by the researcher to ensure that they are low in bromine and contain no noble

metals.

B: Fusion procedure

The fusion procedure is based on the work of Robert et al. (1971, 1975), Hoffman (1978), and Hoffman et al. (1978). It should be emphasized that the fusion procedure given in this appendix *does not adequately fuse samples rich in chromite*. Samples with greater than approximately 20 volume percent chromite must be treated in the manner outlined in Appendix II. Robert et al. (1971, 1975) give procedures which they claim allow this fusion technique to properly fuse chromite-rich samples, *but it is the present author's experience that their method does not work*.

The procedure is as follows: Approximately 25 grams of rock powder are weighed and placed in a clean crucible. This is done twice to give a total sample of approximately 50 grams. Using a pan balance, the reagents are weighed into the crucibles in the following amounts:

    16 g nickel powder
    45 g sodium borate
    22.5 g sodium carbonate
    10 g silica
    6.25 g sulfur

This is the basic mixture that seems to work best for the majority of geological samples. If samples with more sulfur than the typical, sulfide-poor ultramafic rock are being assayed, the amount of sulfur added to the sample must be reduced. For most ultramafic rocks with above average sulfide contents (*i. e.*, with visible sulfides) a reduction in the added sulfur to 5.75 to 6.0 grams should be sufficient.

The reagents are mixed in the crucibles using a spoonula, being careful to avoid losses, and ensuring that any clumps of reagent (especially sulfur and sodium borate) are broken up in the crucibles. The clumps are smeared against the inside walls of the crucibles with a spoonula to break them up.

After the reagents are thoroughly mixed, an unglazed porcelain tile is placed over each of the crucibles. If the tiles are too wide for the furnace, they can be cut by scribing and tapping. The tile covers are important, as they prevent spattering of the flux onto the ceiling of the furnace. If this spattering is not prevented, the furnace elements will burn out.

One crucible is loaded into the furnace, which has been pre-heated to 1000° C. The temperature will drop a few hundred degrees, and when the furnace is again up to 1000° the timing of the fusion begins. The sample is allowed to fuse for 1.25 hours, and is then removed to cool. Upon removal from the furnace the porcelain tile must be taken off the crucible. If this is not done the melt will not convect properly, which will result in incomplete collection of the nickel sulfide.

After the crucible has cooled for at least one hour the button may be removed. The crucible is placed on a clean piece of strong paper, such as absorbant laboratory paper, and is gently tapped along its side, near the base. Care must be exercised at this point, for if the crucible is hit too sharply or if the hammer follow-through is not checked the button can be damaged or destroyed. In the event that a small amount of the button does break away from the rest of the button, a pair of forceps and a magnet can be used to recover it.

Occasionally the button will not be entirely free of slag after it has been released from the crucible. If the amount is slight, on the order of less than one third the area of the button, it can be disregarded. If, however, the amount of slag is enough to cover one third or more of the button it must be removed. If it is not removed it will create a gel during the dissolution stage which will clog the membrane filter. The simplest way to remove the excess slag is to scrape it off the button with a clean spatula or similar object. One must be careful not to damage the button during this procedure.

After the button has been released from the crucible and any excess slag removed, the broken bits of crucible and slag are discarded. The button is weighed, and the weight recorded. If the mixture quoted at the beginning of this section is used, the buttons should weigh between 20 and 21 grams. If they do not, the sample may not have fused properly or else all of the nickel sulfide did not collect. Usually this indicates too much sulfur, and another fusion must be performed with another aliquot of the same sample, with an adjustment in the amount of added sulfur. Other indicators and probable causes of incomplete or poor fusion include the following:

1. A button that shatters on release from the crucible indicates that too much sulfur has been added.

2. Buttons that are marcasite-colored are usually indicative of too much added sulfur.

3. Powder around the button indicates incomplete fusion. At first, it is difficult to determine whether the powder observed is the result of incomplete fusion or has been produced by crushing of the slag and crucible during removal of the button.

4. Areas in the slag that appear white or chalky green indicate that some of the borate or carbonate was not completely crushed before fusion.

5. Small yellow spheres of nickel sulfide suspended in the slag indicate incomplete collection of the sulfide into the button.

6. If samples with large amounts of chromite are assayed, incomplete fusion of the chromite may result. In general, if there are refractory minerals in the sample that have not fused, they will precipitate along with the NiS during cooling, and will form a blanket above the button. Often, this will result in small droplets of NiS being caught by this blanket of material, so that in addition to incomplete fusion of the sample there is also incomplete collection of the NiS.

7. The typical slag is dark green to dark brown in color, and should show signs of convection when the crucible is opened. If the slag is a strange color, or if there is no sign of convection, the sample may not be properly fused.

In general, if any of the above observations are made, it is best to discard the button and produce another from that sample.

C. Crushing, dissolution, and filtration of the buttons

Crushing

After two satisfactory buttons have been produced from a sample the next step is to crush and dissolve them. Each button from a sample is crushed, dissolved, and filtered independently of the other button from that sample.

A stainless steel swing mill, of 14 cm inside diameter with a ring of 12 cm outside diameter and a puck of 7.5 cm diameter, was used for the crushing of the buttons. Tungsten carbide swing mills contribute too much tungsten to the sample, which does not

dissolve in the HCl. Tungsten activates readily during neutron irradiation and due to the increase in background during counting will raise the detection limits for the PGE. The only major elemental contribution from the stainless steel swing mill used in this study is chromium, which presents no significant problems during NAA.

One complete, unbroken button is placed in the mill, between the puck and the ring. The mill is turned on for ten seconds, off, and then on and off for a series of four crushes of five seconds duration each. It is advisable to check the contents of the mill between five second crushings to see if the crushing is complete. When finished the crushings should look like a fine gray dust, with little or no glossy material remaining. It is not wise to crush any longer than specified, as the NiS is sufficiently malleable to smear on parts of the mill, resulting in significant losses. This crushing procedure may not be applicable to other swing mills.

After the material is completely crushed, each piece of the mill is carefully brushed clean onto a clean sheet of paper. The crushings are transferred to a clean 800 ml beaker, ready for dissolution. The swing mill is cleaned using three loads of approximately 50 ml each of 20/30 sandblasting sand. This has been determined to be satisfactory for removing any smeared nickel sulfide from the various pieces of the mill. After the three loads of sand have been crushed, the mill is washed with detergent water and dried with compressed air.

The cleaning procedure was tested by radiotracer tests. Buttons spiked with ^{192}Ir, produced in the SLOWPOKE reactor, were prepared, along with blank buttons. One of the spiked buttons was crushed, the mill cleaned, and then one of the blanks crushed. The crushings from both buttons were transferred to a medium-sized irradiation vial (approximately 7 ml). This size vial fits neatly into the well of a 3" x 3" NaI detector at the SLOWPOKE facility. Counts of 1000 seconds were made on three different test blanks, and no ^{192}Ir activity was observed.

The activity in the spiked buttons was measured before and after crushing by 1000 second counts on the NaI detector. The spiked buttons were first crushed to less than approximately 0.5 cm with a platner mortar and placed in a medium irradiation vial. The activity of the button was recorded over a 1000 second count and then the button was crushed in the swing mill. The crushings were again placed in a medium irradiation vial

and were counted a second time. A comparison of the counts over 1000 seconds before and after crushing in the swing mill indicated that no detectable change in the activity had occurred. This was taken to indicate that the losses due to smearing and incomplete recovery of the crushings are negligible when care is taken in this procedure.

The above method of determining losses through crushing is preferable to weighing the button before and after crushing, as the swing mill often contributes a small amount of steel to the crushings. In most instances, it was found that the crushings weighed more than the original button. Thus, the weight method does not give a true indication of the losses through crushing.

Dissolution of the buttons

The crushed button in the 800 ml beaker is ready for dissolution. 450 ml of concentrated (12 M) HCl are added to the beaker and crushings, and the beaker covered with a watch glass. The beaker is then placed on a hot plate set below the boiling point of HCl. This must be the setting for the first fifteen minutes, or losses due to effervescence will occur. After fifteen minutes the hot plate is turned up to its maximum setting.

Dissolution generally takes two to four hours, and requires the addition of HCl as evaporation occurs. Dissolution is complete when the bubbling of the solution is very slow. At this point the solution should be a dark, clear green color, with very little, if any, dark material on the bottom of the beaker. The solution is allowed to cool for about five minutes in air, and is then given a water bath to hasten cooling.

During dissolution it is important to ensure that the volume of HCl never falls below about 150 ml. If this occurs, the sulfur in solution will precipitate out, and is very difficult to get back into solution. This in turn causes blockage of the pores in the membrane filter during filtration. Another important point to bear in mind is that there should always be H_2S and elemental sulfur immediately observable in the beaker during dissolution. Sulfur is usually observed as a yellow rind deposited at the interface of the beaker and watch glass; and H_2S is easily detected by smell. An excess of sulfur acts as a buffer, preventing the noble metal sulfides from becoming soluble chlorides, which would be lost during filtration. Also, one must be careful not to allow the solution to "bump" during dissolution as an explosion can result from superheated solutions.

Filtration of the solutions

After the solution has been allowed to cool to room temperature, it is poured into a separatory funnel, and the walls of the beaker washed down twice with cold, concentrated HCl. These washings are added to the solution in the separatory funnel. After the two washings, the beaker is held above the separatory funnel and the bottom and sides washed into the separatory funnel, again with cold, concentrated HCl. This is also repeated twice.

It is almost impossible to purchase small buchher funnels that are the same size as the membrane filters available on the market. Thus, a filter cutter fashioned out of stainless steel was used, which when tapped against the brittle filter, cut it to the 43 mm diameter of the buchner funnels. The cut filter is placed in a diaphragm-supported buchner funnel on a filter flask. The vacuum is turned on, the filter washed with cold concentrated HCl, and the stopcock on the separatory funnel slowly opened. It is important to make sure that the solution coming from the funnel is at a rate slow enough to ensure that it does not spread out across the filter to the edges, as some loss may occur if the filter does not fit snugly in the buchner.

When the separatory funnel is empty, it is washed down twice with cold concentrated HCl. A wash bottle (nalgene) works best for washing down the separatory funnel and beakers. After the two HCl washings have filtered, the funnel is again washed, this time with distilled water. The water wash is repeated three times, making sure that all the sides of the separatory funnel are rinsed thoroughly. After the water washes have filtered, the edges of the filter are carefully washed with distilled water. This step takes a bit of practice, as too much water will result in lost material, since the fine colloidal residue on the filter is extremely surface active. The rinsing with the wash bottle is complete when no traces of nickel chloride solution or HCl can be detected on the filter.

The next step involves passing 500 ml of distilled water through the separatory funnel and through the filter. This makes fairly certain that as little chlorine or nickel remain on the filter as possible. These two elements are major contributors to the background activity during NAA, so it is desirable to ensure that as little as possible is included for analysis.

The filters are allowed to dry in the buchner funnels, under covers to prevent dust from possibly contaminating the samples. When dry, the two filters from each sample are carefully unloaded from the buchners using forceps and a spatula. The two filters are stacked one on top of the other and are placed together in a polyethylene envelope. The author made these envelopes by cutting 4 mil polyethylene sheet into strips of 10 cm x 5 cm, folding the strips lengthwise, and heat-sealing the two sides. This leaves the top open to permit the filter papers. It should be noted that the plastic strips had been washed in methanol before heat-sealing, to minimize the risk of contaminants. The envelopes with the two filters from each sample were then heat-sealed, ready for irradiation and counting.

D. Blanks

Analytical blank determinations were made throughout the development and practice of this procedure. Individual blanks of nickel powder, silica, and sulfur were made, and no noble metals were detected. Total blanks, obtained by using silica powder instead of rock powder and treating the resulting buttons as though they were samples, showed no detectable contaminants in any of the reagents or in the crushing, dissolution, or handling of the samples and buttons.

During an investigation into membrane filters with little or no bromine, blanks of two types of membrane filter were analyzed. Whatman membrane filters of nitrocellulose not only contain significant quantities of bromine, but also contain detectable amounts of gold. The Schleicher and Schuell membrane filters used for this study contain low levels of bromine and no detectable noble metals. One of the polyethylene envelopes for irradiation was also analyzed, and no noble metals were detected.

E. Samples not suitable for treatment by the nickel sulfide procedure

During the analysis of Tulameen samples, several rock and ore standards were analyzed, as well as samples of terrestrial sedimentary rocks and one galena sample. Hoffman (1978) gives a formula that can be used to take into account the nickel and sulfur in a sample, so that the amounts of nickel and sulfur added to the sample can be adjusted accordingly. However, it is the author's experience that Hoffman's (1978) corrections

for nickel and sulfur do not work, as the buttons made from the CANMET standard PTC-1, a nickel sulfide flotation concentrate, never came out successfully. Invariably they contained too much sulfur and had large amounts of slag attached to them.

During analyses for Dr. J. Lerbekmo, the author had occasion to analyze some Cretaceous sedimentary rocks. The nickel sulfide fusion procedure was found unsuitable for the fusion of un-ashed coals, and samples rich in bentonitic clays must be thoroughly disaggregated before fusion. If the coals are not ashed before fusion, large amounts of graphite are produced, which causes problems during dissolution and filtration. If the clays are not totally disaggregated, they tend to bake during fusion, and become highly resistant to attack by the flux.

The one galena sample attempted proved to be problematic as well. Although the galena fused completely, the resulting button was very large, weighing almost 60 grams. All of the lead in the galena sample came down as a lead sulfide during cooling, and produced a "lead-nickel" sulfide button. It is the author's belief that samples rich in lead must be dealt with very differently from most samples of rock or ore. Either the lead must be leached from the sample before fusion, or the cooling rate must be slow enough to allow the lead to segregate completely from the nickel after fusion.

IX. APPENDIX II: FIRE-ASSAY USED WITH CHROMITE-RICH SAMPLES.

All samples with approximately 20 volume percent or more chromite were prepared via the procedure described here. Most of the considerations made with regards to the various steps involved in the procedure detailed in Appendix I should be applied to the technique discussed in the present appendix.

A. Reagents and materials

The reagents and hardware used for the chromite-rich procedure are basically the same as those listed in Appendix I. The only difference is the use of lithium tetraborate (Aldrich, Gold Label: 22,253-4) instead of sodium borate as the major component of the flux. Also, it was found to be advantageous to mix the reagents in a 1000 ml beaker as opposed to mixing in the crucibles, for the reasons given subsequently.

B. Fusion procedure

The fusion procedure employed with chromite-rich samples is that of Borthwick and Naldrett (pers. comm.). Approximately 30 g of crushed sample are weighed and placed in a 1000 ml beaker. Borthwick and Naldrett (pers. comm.) give the following masses of reagent required:

    10 g nickel powder
    60 g lithium tetraborate
    30 g sodium carbonate
    6 g silica
    6 g sulfur

The reagents are weighed into the 1000 ml beaker containing the sample, and the contents thoroughly mixed with a spoonula. The analyst must make certain that all clumps of sulfur and lithium tetraborate are broken up during mixing. Mixing cannot be done in the crucibles, as the large amount of reagent plus sample fills the crucibles to the top. As long as clean, dry beakers are used there should be essentially no loss of material as a result of adhesion to the beaker.

After the reagents are mixed in the beaker, the mixture is transferred to a crucible. Some compaction of the material will be required for it all to fit into the crucible. An unglazed porcelain tile is placed on the crucible (as a cover) and the crucible is loaded into a furnace heated to 1000° C. After the furnace returns to 1000° C, the sample is allowed.

to fuse for two hours. The crucible is then removed from the furnace, and the tile cover immediately removed to allow convection to proceed.

After cooling to room temperature the button is removed from the crucible by breaking the crucible with a hammer. Unlike the buttons formed via the sodium borate fusion, the buttons produced by the lithium tetraborate fusion have not been observed by the author to have remnant slag adhering to them. In addition, these buttons have been found to be less likely to chip or crack upon release from the crucibles. The typical button produced via the lithium tetraborate fusion is gun metal blue in color, and weighs about 15 g.

The physical appearance of the slag and the vigorousness of convection upon removal from the furnace appear to be controlled by the amount of chromite in the sample. Samples very rich in chromite (i.e., true chromitites) produce a rough-textured, deep green colored slag with no obvious signs of convection. The melts produced from these high-chromite fusions effervesce violently when the crucibles are removed from the furnace. Samples with lower chromite contents, on the order of 20 to 30 volume percent chromite, produce an emerald green slag that has a smooth glassy texture. These low-chromite melts also effervesce, but not nearly as violently as the high-chromite melts.

C. Crushing, dissolution, and filtration of the buttons

Crushing

As with the procedure outlined in Appendix I, the buttons are crushed in the stainless steel swing mill described in Appendix I. A major difference in the present case is that only one button is produced per sample. This is important in the context of the PGE's as chromite-rich samples often contain very high noble metal concentrations. If a total of 60 g of sample were used, the amount of noble metal recovered would be very high in some instances, causing errors during NAA. Also, the cost of lithium tetraborate is substantial, so one must consider the cost-effectiveness of producing two buttons per sample.

The buttons produced by the lithium tetraborate fusion crush much more readily than those produced via the sodium borate fusion. This is partly due to their smaller size

(15 g as opposed to 21 g) and may also be due to structural/chemical differences. As a result, the author found that one ten-second crush followed by one five-second crush was sufficient for these buttons.

Dissolution of the buttons

The procedure for transferring the crushings to an 800 ml beaker and cleaning of the swing mill are the same as that described in Appendix I. There are basically two major differences in the dissolution procedure used with the present fusion compared with the sodium borate fusion. Firstly, the hot plates are never turned to their highest settings: they are always kept slightly below the boiling point of concentrated HCl. This effectively means that the dissolution is carried out at a simmer. Secondly, it has been found that the buttons require between 0.5 and two hours to dissolve, provided that 450 ml of concentrated HCl and the simmering temperature are used.

Filtration of the solutions

The filtration procedure used is exactly the same as that described in Appendix I. However, one point must be noted: *the noble metal residue is extremely surface active, much more so than the residue from the sodium borate-produced buttons.* Thus, great care must be exercised to keep any losses due to surface active material to a minimum.

Blanks

Total analytical blanks were prepared using silica powder instead of a sample. On analysis, it was found that 0.4±0.1 ppb gold was present in the reagents. Since the blanks from the sodium borate fusion showed no detectable noble metals, the author considers the lithium tetraborate as the source of this contamination. The 0.4 ppb value was taken into account before quoting the results of the analyses from the chromite-rich samples.

X. APPENDIX III: DESCRIPTION OF THE CRUSHING AND SPLITTING METHOD USED IN THIS STUDY

One of the most important considerations facing the analyst when dealing with the noble metals is how to address the crushing and splitting of samples (Harris, 1982). The noble metals commonly occur as grains in the tens of microns, are relatively inert geochemically, and tend to be erratically dispersed throughout a sample (Crocket and Cabri, 1981; Harris, 1982). As a result, one must take steps to make certain that the aliquot analyzed is truly representative of the entire sample.

A. Crushing

The following is a description of the crushing technique used in this study for samples with less than approximately 20 volume percent chromite. The crushing procedure for chromite-rich samples utilized in this study is given in a subsequent section. Each field sample to be analyzed, typically on the order of four to five kilograms, was cut in half with a diamond saw. One half was saved for thin sectioning and as a reserve, while the other half was carefully washed and prepared for crushing. The half for analysis was crushed in a jaw crusher to a chip size of about 1 cm or less. This material was then split by the use of a chute splitter to give two halves. One of these halves was set aside for the final crushing, while the other half was again split with the chute splitter, giving two quarter sections. Each of these quarter sections was run through a tungsten carbide swing mill to ensure that no contaminants from a previous sample, such as smeared PGE or gold, remained on the mill. These were then bagged, sealed, and stored as pulps. The remaining half was then crushed until approximately 200 grams of material that was 96 percent 120 mesh or less, 51 percent of which is 170 mesh or less, was obtained. The remaining material was bagged, sealed, and saved in reserve. The swing mill was then cleaned using 20/30 mesh sandblasting sand, washed with detergent water, and dried with compressed air. It should be noted that tungsten is not collected by the nickel sulfide during the fusion procedure, so a tungsten carbide swing mill can be used to crush the rock samples.

B. Splitting

The 200 gram aliquot was split using the cone and quarter method. A cutter was made for this study, consisting of two pieces of stainless steel welded at right angles to one another, producing a "+" shape in plan view. The 200 gram aliquot, originally placed in a large plastic vial, was dumped onto a clean sheet of paper. This produced a butte-shaped mound of material rather than a true cone. The cutter was placed through the butte, and each quarter swept away with a small brush while the cutter was held firmly in place. The four cuts were individually packed in plastic vials, ready for analysis. Besides resulting in the sample(s) for noble metal assay, 200 mg of the split material were taken for whole rock analysis by INAA. It should be mentioned that all of the samples analyzed for this study were crushed no more than one day in advance of fusion, so the effects of oxidation in the sample were minimized.

In an attempt to determine the representativeness of the splitting technique, a series of experiments was carried out using a bimodal silt sample. A sample of 150 grams, consisting of 90 grams of -140 +160 mesh and 60 grams of -180 +200 mesh material was prepared and homogenized by rolling on a piece of paper. A cone or butte was built on the paper by pouring the silt from a plastic vial, as is done with the actual samples for assay. The quartering tool was then used to obtain one quarter, which was sieved and the two fractions (-140 +160 and -180 +200 mesh) weighed. A total of 20 such experiments was carried out.

The coarse fraction showed a linear decrease from start to finish. This was attributed to abrasion of the material during sieving. In fact, the coarse fraction showed a decrease of 0.62 grams per run on the average, and the fine fraction showed an increase of 0.46 grams per run. Obviously the losses and gains did not equal one another, as we were only concerned with the two grain sizes, and most likely the material unaccounted for was lost to grains not equal to -180 +200 mesh. An average of the percentages of coarse material in each quarter over all 20 runs resulted in 53.23 percent after applying a correction factor for abrasion, with a standard deviation of 2.68. Thus, although the quartering method does apply a slight bias to the samples, it does not appear to be great enough to cause concern.

As a further test of the reliability of the sampling procedure, the first ten samples analyzed for the noble metals were done in triplicate, with each of the three replicates coming from three of the four quarters made from each sample. The results from these analyses are shown in the body of the thesis in Table 7. As was discussed in the text, these results indicate that the quartering method employed does give aliquots that are representative of the sample taken for analysis.

Crushing of samples rich in chromite

The procedure outlined here for the crushing of samples rich in chromite is not by any means required. However, the author had the opportunity to employ this method on a short-term basis, and therefore took advantage of the situation.

Seven samples of massive, or essentially massive, chromite from the Tulameen Complex were collected. These samples typically weighed about one kilogram. All but about 200 grams of this material was crushed in a jaw crusher, with the remainder saved for polished sections. The crushings from the jaw crusher were then crushed to less than 170 mesh using a Brinkman Pulverizer, which was lent to the author by Brinkman Instruments for evaluation. This device consists of a tungsten carbide rotor which spins at between 10,000 and 20,000 r.p.m. inside a tungsten carbide screen of 170 mesh. A catch tray surrounds the screen, and the entire mechanism is contained within a locked-down canister. The jaw crushed material was fed into a hopper on the outside of the canister with the rotor spinning at 20,000 r.p.m. The crushed material is warranted to be 95 percent finer than the mesh of screen used.

The crushings were removed from the catch tray and dumped onto a clean sheet of paper. Sample splitting was the same as that used for the other samples (see previous section in this appendix). The crushing machine was cleaned in the same manner as the swing mill, using 20/30 mesh sandblasting sand followed by detergent water and blow-drying.

Unfortunately, it was found that although the manufacturer of this device claims that it is capable of handling material of hardnesses of approximately Mohs 6.5, this does not appear to be the case. After all seven chromite-rich samples had been crushed, the rotor and screen showed appreciable wear, and even the small amounts of sandblasting

sand used to clean it (approximately 20 ml) could not be crushed in the end.

This crushing instrument was lent to the author approximately four months before the chromite samples were analyzed. Since the machine was on temporary loan for the purposes of testing, the author chose to crush the samples well in advance of the time of fusion. The crushed samples were stored in sealed plastic vials, which should have kept oxidation to a low level.

C. Contaminants

Tests for contaminants arising from the crushing procedure involved the crushing of aliquots of 20/30 mesh sandblasting sand mixed with 240 mesh silica powder. Five 200 milligram samples of this material were taken for NAA before crushing, and the remainder crushed with a tungsten carbide swing mill. Five more 200 milligram samples were then taken for NAA.

The ten samples were analyzed for trace elements, and the weighted mean of the five analyses for each type of sample taken to represent the composition of that sample. The results indicate:

1. Tungsten is contributed to the sample in quantities great enough to result in background activities that are too high for counts to be made after five days of decay.

2. Cobalt is introduced to the sample on the order of 33 ppm.

3. On average, 0.05 ppm scandium is introduced.

4. There is no detectable contribution of Ni, Cr, Fe, Sb, or noble metals to the sample.

As a result of these findings, corrections for Sc and Co were required after data reduction. The average contamination was subtracted from the ppm value given in data reduction so that the values given in this report are more reliable than if the correction was not applied. Also, no counts were made until after two weeks of decay so that the tungsten activity would pose no problem.

One fault of this test is that the sample crushed did not duplicate the hardness of each ultramafic sample crushed. This in turn should make a difference in the true

contamination from sample to sample. However, in the interests of attempting to quantify these effects, it is felt that the method described was sufficient for the analyses performed.

Samples of 20/30 mesh sandblasting sand were also crushed in the Pulverizer, used to crush chromite-rich samples. Samples of this material were analyzed by INAA and shown to contribute no detectable noble metals, and little in the way of Cr, Fe, Sb, Sc, and Ni. However, large quantities of tungsten were contributed to the samples.

XI. APPENDIX IV: NEUTRON ACTIVATION ANALYSIS

Neutron activation analysis (NAA) has been employed in this research, both as a means of quantifying the noble metal contents of Tulameen samples, and as a means of obtaining other elemental data for those samples. The use of NAA for the analyses was chosen mainly because of the high sensitivity of the method, which becomes paramount when working in the parts per billion (ppb) range (Gijbels, 1971; Beamish and Van Loon, 1972; Crocket and Cabri, 1981). This section gives the NAA data and analytical procedures, as well as an account of the standardization and corrections. For a more complete discussion of the theory of NAA and gamma spectroscopy, the reader is referred to Rakovic (1970), Kruger (1971), De Soete et al. (1972), Muecke (1980), and Duke (1983).

A. Nuclear data and standardization

The nuclear reactions and nuclear data for those reactions are presented in the text in Table 4. As is mentioned in Table.4, some of the data were taken from the literature (Nadkarni and Morrison, 1974; Chart of the Nuclides, 1977; Lederer and Shirley, 1978), while others were calculated using standards. The short-lived radionuclides of Rh, Pd, Al, Mn, Mg, V, and Ti were analyzed by comparator NAA. This technique uses the measured counts per μg in a given irradiation-decay-counting scheme from standards as a means of directly comparing the concentration of the element in the standard to its concentration in the sample. Standards for these elements were prepared from a number of dilutions of atomic absorption standards, and the resulting counts per μg calculated after applying corrections for live time / clock time and pulse pile-up effects (see later section in this appendix).

The elements Pt, Au, Ir, Os, and Ru were determined by the absolute method of NAA (Bergerioux et al., 1979). This technique utilizes the basic NAA equation, given below as equation IV.1:

$$m = \frac{\lambda \cdot A \cdot M}{\sigma \cdot \varnothing \cdot N \cdot f \cdot I \cdot E \cdot (1-e^{-\lambda t_i})(e^{-\lambda t_d})(1-e^{-\lambda t_c})} \qquad \ldots\ldots IV.1$$

where

m is the calculated mass of the element of interest

λ is the decay constant of the radionuclide of interest
A is the integrated peak area for the radionuclide
M is the atomic mass of the parent nuclide
σ is the effective cross-section for the reaction
$\emptyset$ is the thermal neutron flux
N is Avogadro's number (6.023×10^{23})
f is the fractional isotopic abundance of the parent nuclide
I is the fractional gamma yield for the photopeak of interest
E is the fractional detector efficiency at the energy of the photopeak of interest
ti is the irradiation time
td is the decay time
tc is the counting time

The only terms in this equation that are not accurately known are the effective cross-section and the detector efficiency, which are factors of the reactor and detector used. In practice, the cross-section of interest is not the thermal cross-section, but the effective cross-section, which incorporates the resonance integral for the reaction. Thus, in order that this method of analysis can be used, the analyst must have accurate determinations of the effective cross-sections and the detector efficiencies for the various photopeaks of interest.

As mentioned earlier in the body of the text, the counting for Pt, Au, Ir, Os, and Ru is done on the 413R Ge(Li). Early on in the development of the technique used in this research it was decided that in order to maintain a constant counting geometry, it would be best to construct a sample holder that held the filters flat over the detector in a well-defined position. This therefore required calculation of the detector efficiency at each of the energies of the photopeaks of interest for the flat 1 cm geometry, as this detector (413R) had been calibrated for efficiency using sources in 1.5 ml vials. This in turn meant that the effective cross-sections be measured before the efficiencies could be calculated. Thus, two sets of standards were prepared. Atomic absorption standards were diluted to 20 μg per ml for each metal, except Os, which was prepared with 100 μl of stock solution of 1041 μg per ml. This was because of the highly poisonous and volatile nature of OsO_4, which is the form in which the Os is prepared for atomic absorption standards.

Ten to twelve standards were prepared for each of the elements: half were prepared by placing 1 ml of the standard solution in 1.5 ml irradiation vials, and half by carefully dropping 1 ml of solution onto membrane filters. In the case of the 1.5 ml vials, this is relatively simple, as all that is required is clean vials and a burette to measure the

1 ml of solution into the vials. Irradiation of volumes greater than about 100 μl is not recommended for extended periods in high neutron fluxes, as radiolytic decomposition of solutions can result in damaged containers and contamination of the irradiation facilities. As a result, the solutions must be evaporated to dryness before the vials can be sealed and irradiated. After irradiation, a hypodermic syringe was used to inject 1 ml of water into the vials. The injection hole was sealed, and the vials allowed to stand for at least one hour to allow the residue to return to solution.

In the case of the membrane filter standards, the procedure was a little more difficult. The filters were suspended on a clean steel ring or cylindrical tube of slightly smaller diameter than the filter over a hot plate. Then, one drop at a time was allowed to fall from the burette onto the membrane filter. After each drop had evaporated another was added, and so on until 1 ml of solution had been placed on the filter. The filters were then placed in polyethylene envelopes, heat-sealed, and irradiated. In the case of Os, the 100 μl of solution were not allowed to dry prior to sealing the envelopes. This was to keep losses through volatilization to a minimum.

The standards in the 1.5 ml vials were counted using the Win[15] Ge(Li) detector, which has been calibrated for efficiency using sources in 1.5 ml vials. The spectra resulting from these standards were peak searched, and the effective cross-sections calculated. The weighted mean of all the effective cross-sections for each reaction was taken as the final value. The filter standards were counted on the 413R Ge(Li), and using the effective cross-sections calculated with the 1.5 ml vial standards, the efficiency for each of the photopeaks of interest was calculated. Again, the weighted mean of all the efficiency determinations for each photopeak was taken as the detector efficiency for that peak.

Membrane filter standards were also prepared for Rh and Pd. Solutions of 0.1, 1, and 20 μg per ml were prepared for Rh, and solutions of 20 and 100 μg per ml for Pd. Six standards of each concentration were made, and since these two elements produce short-lived radionuclides, it was possible to analyze each standard twice. The resulting counts per μg were calculated after corrections for live time/clock time and pulse pile-up effects were made.

Standards for Mn, Mg, Al, Ti, and V were prepared from atomic absorption standards. Since the irradiations for these elements were only four minutes at 1×10^{11} n/cm^2/s, the liquids could be irradiated, with no need to evaporate to dryness. As with Rh and Pd, about five standards on the average were analyzed for each element, and those standards were each analyzed twice. At least two, and sometimes three different concentrations of standard solution were analyzed for each element. Counts per μg for each element were then calculated after applying corrections for live time/clock time and pulse pile-up effects (see later section in this appendix for a discussion of these corrections). The USGS rock standards DTS-1 (dunite), PCC-1 (peridotite), and AGV-1 (andesite) were analyzed for Al, Mn, Mg, Ti, and V to test the standardization and corrections used in these analyses.

Standards for Sc, Cr, and Fe were prepared from atomic absorption standards, and were checked against USGS rock standards (J. Duke, pers. comm., 1983). Ni and Co standards were prepared from both pure metal and atomic absorption standards, were analyzed, and the data obtained compared to USGS rock standards (J. Duke, pers. comm., 1983).

B. Irradiation and counting

The irradiation and counting scheme given in Table 5 in the thesis was chosen on the basis of the nuclear data of the radionuclides of interest. The times and fluxes used in the irradiations were chosen to maximize the activity of the radionuclides produced, while keeping the background activity as low as possible. Thus, elements producing short-lived radionuclides, such as Rh, Pd, Al, Mn, Mg, Ti, and V, were subjected to short irradiations and short counting periods soon after irradiation. Elements producing longer-lived radionuclides required longer irradiations to achieve useful activities, and the counting periods required were longer as well.

Counts for short-lived radionuclides were done with the Win^{15} Ge(Li) in an open geometry (un-shielded). The filter paper holder was used for Rh and Pd, whereas a small irradiation vial holder was used for the whole rock analyses, as the whole rock samples were packaged in 1.5 ml irradiation vials that had been cut in half. Counts for the long-lived radionuclides were done with the Ge(Li) detectors mounted inside a lead cave

with 10 cm thick walls, floor, and ceiling, which is lined with a graded shield of 0.2 cm of copper sheeting and, 0.5 cm of plexiglass sheet. The cave is useful in lowering the environmental background during counting. The lead cave was not necessary for the short-lived work, as those samples tended to have high activities, which would have produced fluorescent lead x-rays if the samples were counted in the cave. These x-rays can be significant contributors to the low energy background while counting.

C. Corrections

Two types of corrections are required for the NAA. The first is the live time / clock time, or dead time correction. This correction adjusts the measured counts for each photopeak for decay occurring while the counting system is busy. The method of Takeuchi et al. (1980) has been employed in this study for the calculation of these corrections. The equation used for the correction is given in equation IV.2:

$$A' = A.(tk / tl)((1-e^{-\lambda tl}) / (1-e^{-\lambda tk})) \qquad \qquad .....IV.2$$

where

A' is the corrected counts
A is the measured counts
tk is the clock time
tl is the live time
λ is the decay constant for the radionuclide of interest

The live time / clock time correction is necessary only when counting short-lived radionuclides, as the live time / clock time effect is essentially negligible when dealing with long-lived isotopes.

The second correction is the pulse pile-up correction. Pulse pile-up, or random summing, results in the loss of counts in photopeaks when two or more photons are summed during detection at high count rates (Wyttenbach, 1971). The method used for this correction is that of Wyttenbach (1971). This correction was found to be necessary only for the short-lived radionuclide work, as much lower count rates were encountered during the counting of long-lived isotopes. One set of corrections was made for the flat geometry used to count samples for Rh and Pd, and another set for the counting of samples for Al, Mn, Mg, Ti, and V.

The procedure for calculating the pulse pile-up correction as described by Wyttenbach (1971) involves the use of a precision pulse generator, or pulser. Fifteen spectra with only the pulser sending signals to the preamplifier and essentially no dead time were obtained to clearly define the rate of the pulser. After these spectra were acquired, 12 to 18 spectra were obtained for each of the two counting geometries with varying dead times using the standards prepared for the comparator work as sources. The correction factors were calculated from best fit lines on plots of dead time versus the ratio of observed pulser counts to true pulser counts (i. e., the actual rate of the pulser as defined with no dead time). These correction factors result from the value of the slope of the best-fit lines, and are used in the purpose-developed data reduction programs DATRED and ALETC.

The live time/clock time and pulse pile-up corrections were applied to the integrated peak areas from the peak searches before the final data reduction. This was done by the data reduction programs, which only required the live time and clock time to make the corrections. Equation IV.2 and the following equation, IV.3, both appear in the main routines of DATRED and ALETC:

$$A''=A'.(1-(-1.481((tk/tl)-1))) \qquad \qquad .....IV.3$$

where

- A" is the final corrected counts
- A' is the corrected counts after the live time/clock time correction has been applied
- tk is the clock time
- tl is the live time
- -1.481 is the slope of the best fit line for the pulse pile-up effect plot

The only difference between the pulse pile-up correction used in DATRED and the one used in ALETC is the slope, which in the case of ALETC is -0.32. The difference in slope is due to the differences in count rate between the two geometries and the differences in the radionuclides counted.

D. Errors

In any analytical technique, there are always sources of error and uncertainty. In this study, the majority of the quantifiable errors result during NAA. This section deals with those errors.

Nuclear data

Uncertainties in the nuclear data are, in this case, the result of the spread in values calculated, and can be traced to measurement errors of various types. Thus, the value obtained for the effective cross-section has a level of uncertainty associated with it, and when this value is used to calculate the detector efficiency for the 413R Ge(Li), it propogates this error. The resultant error from the combined effects of these two sources, when they are multiplied or divided, is calculated by equation IV.4:

$$E = (E_1^2 + E_2^2)^{0.5} \qquad \qquad \text{.....IV.4}$$

where

E is the total percentage error
E_1 is the percentage error from one source
E_2 is the percentage error from another source

This method of calculating the error was used throughout this work.

Pulse pile-up correction

The error imposed by the calculation of the pulse pile-up correction also propagates through the data reduction. This error is the result of a number of factors, including the uncertainty in the actual pulser rate, as well as the uncertainty in the pulser peak, both with dead time superimposed on the pulser spectra and without, as determined during the peak search. These were accounted for during data reduction, where a standard pulse pile-up error factor was calculated. This was done by taking the uncertainty in the pulser rate from the weighted means of all the observed pulser counts, and the error associated with each of the pulser peaks as taken from the peak searches of the spectra of the pulser with dead time.

Counting statistics

A third type of error resulting from NAA which can be quantified is the peak error, as determined during the peak search of the spectra. Because NAA is a statistical form of analysis, the probability of the occurrence of events can invoke errors in the analysis (Knoll, 1979). The best way to minimize the effects of random fluctuations in the occurrence of these events is to increase the total number of counts for any given photopeak. However, an error will still exist when the spectrum is peak searched, as the shape of the peak and the background under that peak will impart an uncertainty in the integrated peak area. This error is noted as the peak error, or uncertainty in the peak area determination, and is given by equation IV.5:

$$E= \frac{A+2B}{A} \times 100\% \qquad .....IV.5$$

where

A is the photopeak area
B is the background under that peak
E is the error

Counting geometry

Counting geometry is the positional relationship between the sample and the detector. The closer the sample is to the detector, the greater the effect of slight deviations in the counting geometry on the counts for each photopeak. Thus, it is extremely important that the samples be placed in as reproducible a position with respect to the detector as possible. The triplicate analyses given in Table 7 and the duplicate analyses given in Table 8, as well as the replicate analyses of SARM 7, given in Table 6, indicate that the geometry used for the analyses gave reproducible results.

Reactor fluctuations

The SLOWPOKE reactor is one of the most inherently stable neutron sources available (Bergerioux et al., 1979). As a result, the day-to-day or hour-to-hour fluctuations in the neutron flux and neutron spectrum are extremely small, even over periods of months. This results in essentially no significant error in the neutron flux as measured at the reactor control console, and very little deviation in the total neutron

spectrum. Thus, it is not necessary to irradiate and count flux monitors and other standards with every batch of samples. In fact, once an analytical scheme has been standardized, no further standardization is required, although most analysts run checks from time-to-time.

Final uncertainty

The final, or total uncertainty, as listed on the output from the data reduction programs, is the square root of the sum of the squares of all the errors discussed above. This total uncertainty is then translated into μg, percent, and ppm values for the final output of data reduction.

Obviously, there are other sources of uncertainty which are not so readily quantified as those mentioned above. Uncertainties in the measurement of mass and time may be considered negligible when compared to the other errors already mentioned, provided that the analyst takes steps to ensure that these measurements are done as carefully as possible.

E. Interferences

There are two main types of interference that are likely to be encountered in NAA: spectral and nuclear. Tables 14, 15, and 16 list the typical interferences that might be expected during the NAA of the samples used in this study. One of the most important considerations in the determination of interferences is the recognition of potential interferences before they occur, or by a careful analysis of typical spectra. This provides a means whereby the analyst is not likely to misinterpret the data acquired.

Spectral interferences

Spectral interferences result when photopeaks of different radionuclides fall close enough to one another in the spectrum so as to be beyond the resolving power of the spectrometry system in use (detector, analogue-to-digital converter, and count rate are all factors to consider). In the case of the PGE assays, spectral interferences are effectively eliminated by the preconcentration procedure, and by careful selection of the photopeaks for analysis. The only spectral interference encountered in this study of the

PGE was the 316 keV ^{192}Ir photopeak and the 320 keV ^{51}Cr photopeak. This problem was circumvented by using the 296, 308, and 468 keV photopeaks of ^{192}Ir for the analysis of Ir. In the whole-rock analyses, three spectral interferences were significant (Table 14). Thus, the analysis of Mn is done with the 1811 keV peak of ^{56}Mn, Mg with the 1014 keV peak of ^{27}Mg, and Sc with the 890 keV peak of ^{46}Sc. This results in little chance of spectral interference in these analyses.

Nuclear interferences

Nuclear interferences result from the production of a radionuclide of interest via reactions that are not of the type required for the analysis, which is usually an (n,γ) reaction in NAA. These other types of reactions may be (n,p), (n,f), or (n,∝) reactions. The nuclear interferences most likely to occur in the PGE analyses used in this research are given in Table 15. The cross-sections for these reactions tend to be small compared to the (n,γ) cross-sections. Also, these reactions tend to be unimportant unless the interfering element makes up the matrix, or is present in a quantity greater than the element of interest in the sample (Gijbels, 1971). This is not the case with the PGE in this study.

In the case of the whole rock analyses, the most important nuclear interference is the ^{28}Si(n,p)^{28}Al reaction. This is because Si is present in much greater abundance than Al in ultramafic rocks. Duke (1983) has shown that in the analysis of the USGS rock standard DTS-1, a dunite with 40.5 percent SiO_2, the (n,p) reaction given above can result in the production of 0.06 percent Al_2O_3. DTS-1 has a recommended value of 0.24 percent Al_2O_3, so the Si-produced Al results in 25 percent of the total Al content of this standard. The only means of correcting for this is to measure the Si content of the rocks and calculate the amount of Al that will be produced from Si.

Another nuclear interference of concern in the whole rock analyses is the ^{27}Al(n,p)^{27}Mg reaction. Using the spectra obtained for the comparator standardization of Al, the author calculated the mass of Mg produced per μg of Al. After converting this value into one applicable to the oxides of these two metals, it was used as a correction factor for the MgO values in all samples with greater than one percent Al_2O_3. Samples with less than one percent Al_2O_3 required no correction, as the contribution of

Table 14: Potential spectral and nuclear interferences that may be encountered during the whole rock NAA in this study (after Duke, 1983).

Analysis Isotope	Potential Spectral Interference	Potential Nuclear Interference
^{28}Al	-----	^{28}Si(n,p)^{28}Al ^{31}P(n,α)^{28}Al
^{56}Mn	^{27}Mg at 844 keV	^{56}Fe(n,p) ^{56}Mn ^{59}Co(n,α)^{56}Mn
^{27}Mg	^{56}Mn at 847 keV ^{152}Eu at 842 keV	^{27}Al(n,p)^{27}Mg ^{30}Si(n,α)^{27}Mg
^{52}V	-----	^{52}Cr(n,p)^{52}V ^{55}Mn(n,α)^{52}V
^{46}Sc	^{182}Ta at 1121 keV	-----

Table 15: Selected primary interference (n,p) and (n,α) reactions (after Gijbels, 1971). (Φ_f and Φ_{th} refer to the fast and thermal neutron fluxes respectively.)

Activation reaction of interest; isotopic abundance and thermal cross-section	Interfering reaction; isotopic abundance and fission cross-section	Interference if $\Phi_f/\Phi_{th}=0.1$ (ppm)	Element determined and matrix
^{102}Ru(n,γ)^{103}Ru 31.35%; 1.3 b	^{106}Pd(n,α)^{103}Ru 27.3%; 2.7μb	0.19	Ru in Pd
^{108}Pd(n,γ)^{109m}Pd 26.75%; 0.19(+11) b	^{109}Ag(n,p)^{109m}Pd 48.65%; 0.2 mb	3.3	Pd in Ag
^{190}Os(n,γ)^{191m}Os 26.4%; 10+3 b	^{191}Ir(n,p)^{191m}Os 38.5%; 0.02 mb	0.23	Os in Ir
^{192}Os(n,γ)^{193}Os 41.0%; 2.0 b	^{193}Ir(n,p)^{193}Os 61.5%; 5μb	4×10^{-4}	Os in Ir
^{191}Ir(n,γ)^{192m}Ir 38.5%; 520+436 b	^{192}Pt(n,p)^{192m}Ir 0.78%; 0.02 mb	4×10^{-5}	Ir in Pt
^{193}Ir(n,γ)^{194}Ir 61.5%; 110 b	^{194}Pt(n,p)^{194}Ir 32.9%; 8μb	4×10^{-3}	Ir in Pt
^{190}Os(n,γ)^{191m}Os 26.4%; 10+3 b	^{194}Pt(n,α)^{191m}Os 32.9%; <0.1μb	$<10^{-3}$	Os in Pt
^{192}Os(n,γ)^{193}Os 41.0%; 2.0 b	^{196}Pt(n,α)^{193}Os 25.2%; <0.1μb	$<3 \times 10^{-5}$	Os in Pt
^{196}Pt(n,γ)^{197m}Pt 25.2%; 0.05+0.9 b	^{197}Au(n,p)^{197m}Pt 100%; 7μb	2.95	Pt in Au
^{193}Ir(n,γ)^{194}Ir 61.5%; 110 b	^{197}Au(n,α)^{194}Ir 100%; 0.1μb	1.5×10^{-4}	Ir in Au

^{27}Al(n,p)^{27}Mg is negligible. The other nuclear interferences given in Table 14 are insignificant in the context of these analyses (Duke, 1983).

Primary interferences from (n,f) reactions can be a major factor when analyzing geological materials. These reactions result from the production of radionuclides of interest via the fission of ^{235}U and to a much lesser extent ^{238}U and ^{232}Th. Gijbels (1971) points out that in cases where the U content of a sample is greater than the noble metal content, reactions such as ^{235}U(n,f)^{103}Ru and ^{235}U(n,f)^{109}Pd can be significant. Fortunately, this is not the case in the analyses performed in this study. The ultramafic rocks have extremely low abundances of U and Th, so the whole rock analyses do not suffer from this type of interference. Also, the preconcentration technique used for the noble metal assays ensures that no U or Th will be present in the samples analyzed.

Second-order interferences result when a radionuclide of interest is produced by coupled (n,γ) reactions. Examples of such interferences, as they apply to the PGE, are given in Table 16. These interferences increase with the neutron flux and irradiation time, which can be chosen to minimize these effects. In general, it is better to increase the flux and decrese the irradiation time as opposed to increasing the irradiation time and decreasing the flux (Gijbels, 1971).

Potential problematic second-order interferences in the analysis of the PGE include:

$$^{197}\text{Au(n,}\gamma\text{)}^{198}\text{Au (n,}\gamma\text{)}^{199}\text{Au}$$

This reaction can result in the apparent loss of Au and increase in Pt during counting, if ^{199}Au is used to determine Pt (see Table 4 and Table 16). Although Au does occur in Tulameen samples, its abundance is low. In addition, this reaction only becomes a serious problem when high fluxes and long irradiation times are used (Nadkarni and Morrison, 1974). During the calculation of the effective cross-section and efficiency for gold, the author never observed the production of ^{199}Au during the four hour irradiations at 1×10^{12} n/cm^2/s, even when 20 μg of gold were present in the standard.

Table 16: Second-order interferences, with an example of the calculated interference of ^{196}Pt on the determination of gold via ^{191}Au at various irradiation periods (t irr.) with thermal neutron flux of 5×10^{10} n/mm^2/s and epithermal neutron flux of 5×10^8 n/mm^2/s (after Gijbels, 1971).

^{102}Ru(n,γ)^{103}Ru(β^-)^{104m}Rh

^{108}Pd(n,γ)^{109}Pd(β^-)^{109}Ag(n,γ)^{110m}Ag

^{107}Ag(n,γ)^{108}Ag(β^-, E.C.)^{108}Pd(n,γ)^{109}Pd

^{190}Os(n,γ)^{191}Os(β^-) ^{191}Ir(n,γ)^{192}Ir

^{192}Os(n,γ)^{193}Os(β^-) ^{193}Ir(n,γ)^{194}Ir

^{191}Ir(n,γ)^{192}Ir(E.C.) ^{192}Os(n,γ)^{193}Os

^{193}Ir(n,γ)^{194}Ir(β^-)^{194}Pt(n,γ)^{195m}Pt

^{190}Pt(n,γ)^{191}Pt(E.C.) ^{191}Ir(n,γ)^{192}Ir

^{196}Pt(n,γ)^{197}Pt(β^-) ^{197}Au(n,γ)^{198}Au

t irr. (hr)=	1.62	6.48	25.93	103.7
ppb Au=	0.135	2.095	30.17	345.4

F. Self-shielding and self-absorption

Errors due to self-shielding result when materials containing isotopes of high capture cross-section are analyzed. Self-absorption effects result when samples contain large quantities of dense elements. In the case of the noble metal assays, the concentrations of the noble metals are always less than 10 ppm, so these two effects are of little importance. Similarly, the small (200 mg) size and the chemistry of the whole rock samples helps to minimize the effects of self-shielding and self-absorption.

In one instance self-shielding and self-absorption may have been a problem during the standardization of gold. The standards for effective cross-section and detector efficiency were originally produced with 20 μg of gold. In an attempt to ensure that the self-shielding and self-absorption effects were not a problem in this case, a second set of standards of 1 μg gold were produced. The results from the 1 μg standards were in good agreement with those of the 20 μg standards, indicating that the effects of self-shielding and self-absorption were insignificant.

G. Data reduction

As stated in the text, three data reduction programs and one peak search program were utilized for the data reduction in this study. The programs DATRED and ALETC were written for offline analysis using the University of Alberta AMDAHL computer. These programs, written in FORTRAN IV, take all their data from the peak searches and irradiation data. NAARUN peak searches and reduces the data online with the ND660 LSI-11 (Apps and Apps, 1981). A listing of the program DATRED is given in Appendix VIII.

Peak searching on the Series 80 MCA is done with built-in functions. Output includes the region of interest, integrated peak area, background counts, counts per second in the region of interest, the uncertainty in the peak (in percent), the full width half maximum (FWHM) of the peak in keV, identifies the peak centroid in keV, and has the capability of using a library for radionuclide identification. Peak searching on the ND660 uses the program PREP10 (Apps, 1978). This program returns all the information given by the Series 80 peak search, without the isotope identification.

The 4096 channel spectra are stored on floppy disks. In the case of NAARUN, peak searching via PREP10 is part of the data reduction routine, so all that is required is

the specification of parameters such as sample identification, mass of sample, irradiation date and time, and counting date and time (Apps and Apps, 1981). For reduction with DATRED and ALETC, the integrated peak areas, peak errors, live time and clock time, irradiation date and time, the date and time of counting, sample identification and sample mass are required. The results from NAARUN and DATRED are given in μg and ppm, those from ALETC in ppm or percent, and as oxides where appropriate. All three programs provide the user with the total calculated uncertainty for each analysis, expressed either in percent of the result for each element (ALETC, NAARUN) or in the units of output, such as ppm (ALETC, NAARUN, DATRED).

XII. APPENDIX V: PGE ASSAY RESULTS FOR TULAMEEN SAMPLES

This section gives a tabulation of all the PGE analyses performed for this study. All results are in ppb at 95 percent confidence limits. Those values that are presented without uncertainty should be considered semi-quantitative, and blank entries indicate that the element was below the limits of quanitification.

Sample	Rh	Pd	Os	Ir	Pt	Au
R3-4	0.9±0.1			0.6±0.1	22.0±9.5	0.2
R3-5	1.9±0.2			0.2±0.1	18.4±6.7	0.1
R3-7	2.4±0.2			0.2±0.1	48.9±7.6	0.2
R3-10#1	3.5±0.3			0.3±0.1	60.0±8.9	0.3
R3-10#2	2.9±0.3			0.2±0.1	75.9±11.7	0.8±0.1
R3-10#3	0.6±0.1			0.2±0.1	62.5±9.6	0.1
R3-11	0.4±0.1			1.5±0.1		0.1
R3-13	1.4±0.2			0.9±0.1	15.4±6.2	0.1
R3-14	1.7±0.2			0.1±0.01	16.5±5.4	0.3
R4-1	0.2±0.1			4.5±0.1	111.1±10.6	0.1
R4-5				0.1±0.01	29.2±6.1	0.1
R4-7					12.8±9.5	0.1
R4-8	0.1±0.1					0.2
R4-9	0.2±0.1	13.3±12.3				
B4-3	0.2±0.1			0.1	18.7±5.7	239.4±6.7
L5-2				0.2±0.01	36.9±7.1	0.3
L5-3		36.0±14.3				0.2
L5-5		41.9±14.1			32.2±6.8	2.9±0.1
L5-13						0.6±0.1

Sample	Rh	Pd	Os	Ir	Pt	Au
T8-1#1	0.8±0.3			1.7±0.1	87.3±10.9	0.2
T8-1#2	1.3±0.1			1.8±0.1	94.1±12.3	0.7±0.1
T8-1#3	1.3±0.2			1.1±0.2	103.7±10.4	0.1
T8-2						0.4
D14-1#1	1.7±0.3			0.7±0.1	18.5±12.9	0.8±0.1
D14-1#2	0.9±0.2			0.7±0.1	19.8±10.7	0.5±0.1
D14-1#3	0.6±0.1			0.5±0.1	18.3±9.4	0.1
D14-7#1	74.7±3.8		29.7±16.9	185.1±0.5	4582.7±79.6	2.2±0.1
D14-7#2	78.7±3.9			204.0±0.6	5224.3±89.8	2.8±0.2
T15-2#1	1.5±0.2			1.0±0.1	106.0±10.2	0.3±0.1
T15-2#2	1.5±0.1			1.2±0.1	112.2±9.6	0.1
T15-2#3	1.6±0.1			1.4±0.1	144.1±10.8	0.1
T15-5	0.7±0.1			1.4±0.1	35.1±7.9	0.3±0.1
T15-7#1	3.7±0.3			4.5±0.1	403.1±18.3	0.3
T15-7#2	3.8±0.3			3.7±0.1	383.5±16.6	0.2±0.1
T15-7#3	3.8±0.3			3.8±0.1	380.2±17.4	0.9±0.1
T15-7 ox	4.1±0.4			3.3±0.1	450.3±25.8	0.6±0.1
T15-7 sp	3.4±0.4			3.5±0.1	490.1±24.8	0.6±0.1
T16-4	1.9±0.2				30.9±8.4	0.3±0.1

Sample	Rh	Pd	Os	Ir	Pt	Au
G16-10#1	0.6±0.1			0.9±0.1	26.1±7.7	0.9±0.1
G16-10#2	0.9±0.1			0.9±0.1	25.4±6.6	0.8±0.1
G16-10#3	0.7±0.1			0.9±0.1	32.3±7.3	0.4±0.1
G16-12#1	6.5±0.5			32.3±0.3	141.4±28.6	1.6±0.1
G16-12#2	5.2±0.5			22.4±0.2	163.8±27.6	1.2±0.1
B18-1	2.2±0.2			1.2±0.1	102.2±8.5	0.2±0.1
G20-1	0.1±0.1	24.5±15.9		0.1±0.01	16.4±5.9	0.3
G20-2	1.0±0.2			0.9±0.1	64.8±8.4	0.1
G20-5	0.7±0.1			0.3±0.1		0.2±0.1
G20-6#1	1.3±0.1			0.7±0.1	41.5±9.6	0.4
G20-6#2	1.1±0.1			0.8±0.1	26.5±10.9	0.1
G20-6#3	1.5±0.2			0.7±0.1	31.2±19.7	0.3±0.1
G20-7				0.1±0.1		0.3±0.1
G20-8#1	2.7±0.2			1.9±0.1	191.1±12.8	0.5±0.1
G20-8#2	2.8±0.2			2.4±0.1	211.0±12.6	0.6±0.1
G20-8#3	2.6±0.2			2.3±0.1	198.9±12.4	0.7±0.1
G20-9	1.3±0.1			0.4±0.1	21.9±7.3	0.3±0.1
G20-10	5.4±0.4		2.7±1.7	6.3±0.1	587.5±16.1	0.2
G20-11				0.7±0.1		0.3

Sample	Rh	Pd	Os	Ir	Pt	Au
G20-12	0.9±0.2		2.6±1.4	0.8±0.1	81.6±9.7	4.6±0.1
G20-13	0.1±0.1			0.6±0.1	20.2±13.4	0.2
G20-14	0.2±0.1			0.5±0.1	22.8±13.5	0.1
L23-1			1.1±0.7		8.1±6.7	0.2
L23-2	0.4±0.1	42.9±17.8			52.3±8.8	2.3±0.1
L24-1					14.0±5.8	0.2
L24-2	1.3±0.2		6.0±1.4	0.4±0.1	64.1±7.4	0.2
G26-4#1	0.9±0.1			8.3±0.1		0.2±0.1
G26-4#2	3.3±0.3			10.1±0.1		1.5±0.1
G26-4#3	2.6±0.3			10.2±0.1		1.9±0.1
G26-4A#1	16.3±1.2			274.2±0.6		3.6±0.2
G26-4A#2	11.8±1.0			74.2±0.4	63.5±44.0	1.99±0.01
G26-6	0.4±0.1	348.3±33.8		0.1±0.01	120.9±8.1	0.6±0.1
G27-3	1.2±0.2			0.8±0.1	76.7±16.3	33.5±0.9
H28-2	0.1±0.1				8.8±6.4	0.1
OM-2#1	2.2±0.3			1.2±0.1	144.8±9.2	0.3±0.1
OM-2#2	2.5±0.2			1.2±0.1	141.1±10.3	0.7±0.1
OM-2#3	2.4±0.2			1.0±0.1	136.6±10.9	0.2±0.1
H3-3A#1	3.7±0.3			13.0±0.2	96.7±22.9	1.5±0.1

Sample	Rh	Pd	Os	Ir	Pt	Au
H3-3A#2	3.8±0.4			13.0±0.2	96.7±22.9	1.5±0.1
H3-3B#1	20.3±1.1		17.1±7.3	74.3±0.4	1425.6±43.3	7.9±0.2
H3-3B#2	24.5±1.5		11.6±7.1	59.1±0.4	1522.2±43.2	11.4±0.4
H4-2A#1	148.9±6.3		78.4±18.4	234.3±0.6	13856.3±90.1	42.4±1.2
H4-2A#2	145.3±62.1		67.4±16.9	235.8±0.6	13826.8±90.4	36.2±1.1
H4-8#1	0.3±0.1			0.2±0.1		0.2±0.1
H4-8#2	0.2±0.1			0.1±0.01		0.1
H4-8#3	0.3±0.1					0.3±0.1
H5-1						0.1
H6-6	0.1±0.1		1.8±1.0			2.8±0.01
S12-2	0.3±0.1		1.9±0.8	0.4±0.01	75.8±7.9	0.1
S12-3	0.2±0.1		1.0±0.7	0.1±0.01	10.2±8.8	0.2
S12-4	0.2±0.1		4.3±1.4	0.6±0.1	63.1±7.7	0.2
S15-7		161.0±24.0			44.3±17.6	12.2±0.4

XIII. APPENDIX VI: RESULTS FOR WHOLE ROCK ANALYSES

All samples assayed for the PGE were analyzed for other elements, both major and trace, via INAA on whole rock samples. The results of these analyses are given here, in ppm or in weight percent where noted. All values are given at 95 percent confidence limits, with blank entries indicating that the element was below the limits of quantification. The values for Al_2O_3 have not been corrected for the contribution from $^{28}Si(n,p)^{28}Al$, so samples low in Al probably have erroneous values of Al_2O_3 recorded. Samples with Al_2O_3 greater than about one percent are reasonably accurate.

Sample	MgO (%)	Al$_2$O$_3$ (%)	Sc	TiO$_2$ (%)	Cr$_2$O$_3$	V$_2$O$_5$	MnO	NiO	FeO (%)	Co
R3-4#2	7.9±0.9	1.13±0.07	23±3	1.28±0.01	235±14	337±7	1090±120		7.8±0.4	33±1
R3-5	47.3±2.7	0.28±0.01	5±1		7065±410	19±3	2090±212	1139±55	10.2±0.4	135±6
R3-7	45.9±2.6	0.23±0.01	4±1		4101±1381	10±2	1696±174	1369±56	8.4±0.4	140±6
R3-10	48.6±2.7	0.34±0.01	4±1		1.11±0.06%	25±3	1967±199	1082±61	8.7±0.4	135±6
R3-11	41.1±2.2	0.23±0.01	3±1		3654±212	16±2	1314±136	1552±53	7.5±0.3	117±5
R3-13	39.1±2.1	0.27±0.01	7±1		1380±80	11±3	1816±188	1351±56	7.7±0.4	112±5
R3-14	46.3±2.6	0.26±0.01	4±1		5906±343	17±3	2232±227	1389±59	11.6±0.4	149±6
R4-1	39.1±2.1	0.25±0.01	4±1		3325±193	15±3	2221±225	1615±62	11.2±0.4	158±7
R4-5	13.1±0.9	0.99±0.14	37±4	0.59±0.08	489±29	562±11	2041±208		10.9±0.5	50±2
R4-7#1	1.8±1.0	14.6±0.1	1.5±0.2	0.18±0.07	26±2	122±10	150±32		1.3±0.1	10±1
R4-7#2	3.9±1.0	1.41±0.03	1.4±0.2	0.16±0.07	19±2	124±12	155±29		1.4±0.1	11±1
R4-8	7.7±1.2	1.31±0.01	41±5	1.3±0.1	20±3	901±4	2062±209		12.1±0.5	40±2
R4-9	13.7±1.2	3.66±0.02	127±15	1.05±0.06	105±8	1077±5	1745±180		14.4±0.8	46±2
B4-3	3.3±1.0	13.6±0.1	15±2	0.51±0.09	21±3	453±9	1818±71		7.6±0.4	27±1
L5-2	16.5±1.2	2.44±0.02	96±12	0.29±0.05	924±54	189±6	1335±138		6.5±0.6	49±2
L5-3	18.6±1.4	1.95±0.02	83±10	0.23±0.05	1327±77	143±6	1107±115		7.8±0.6	56±2
L5-5	2.3±1.1	15.3±0.1	18±2	0.88±0.09	10±2	518±13	1517±157		7.3±0.4	28±1
L5-13#1	11.9±1.2	5.91±0.04	106±13	1.01±0.08	19±4	805±12	1674±173		12.2±0.7	51±2
L5-13#2	13.1±1.2	6.2±0.1	100±12	0.98±0.08	18±4	840±12	1716±178		10.9±0.7	48±2

Sample	MgO (%)	Al₂O₃ (%)	Sc	TiO₂ (%)	Cr₂O₃	V₂O₅	MnO	NiO	FeO (%)	Co
T8-1#1	43.8±2.5	0.57±0.01	5±1	0.04±0.04	4967±289	21±3	1516±157	1377±56	8.2±0.4	119±5
T8-1#2	43.6±2.6	0.57±0.01	5±1	0.04±0.05	5105±297	22±3	1530±159	1380±56	8.4±0.4	122±5
T8-2	7.2±1.2	1.4±0.1	33±4	0.88±0.08	60±5	622±13	1760±182		9.3±0.5	34±1
D14-1#1	47.8±2.7	0.21±0.01	5±1		3655±212	10±3	1927±196	1519±56	10.7±0.4	152±6
D14-1#2	46.8±2.6	0.21±0.01	4±1		3397±201	7±2	1939±197	136±37	9.9±0.4	142±6
D14-7	13.8±1.3	5.99±0.04	12±1	0.76±0.08		901±13	2758±286	4701±108	31.2±0.7	286±12
T15-2	43.3±2.5	0.21±0.01	4±1		2360±137	10±3	1756±182	1203±54	9.5±0.4	128±5
T15-5	39.9±2.3	0.25±0.01	4±1		3529±204	11±3	1421±147	1342±53	9.3±0.4	132±6
T15-7	37.2±1.9	0.29±0.01	5±1		143±9	7±2	1374±141	1119±62	14.3±0.4	160±7
T16-4	18.8±1.2	1.55±0.01	77±9	0.20±0.05	1286±75	86±5	1558±163	223±70	4.8±0.5	40±2
G16-10	45.4±2.6	0.28±0.01	10±1		2706±157	14±3	1686±175	2018±67	8.9±0.4	125±5
G16-12	45.4±2.5	0.77±0.02	4.5±0.5	0.09±0.05	2.91±0.16%	64±4	1828±189	6019±84	10.8±0.4	321±13
B18-1#1	46.5±2.6	0.25±0.01	4±1		6768±392	14±3	1826±189	1474±62	9.4±0.4	137±6
B18-1#2	47.9±2.7	0.28±0.01	4±1		7529±437	15±3	1927±199	1445±57	10.2±0.4	149±6
G20-1	13.2±1.2	9.4±0.1	76±9	1.22±0.07	489±29	801±3	1858±193		12.7±0.6	62±3
G20-2	39.7±2.2	0.56±0.01	18±2		2783±162	28±4	1853±192	1037±67	9.2±0.4	119±7
G20-5	44.7±2.5	0.27±0.01	3±1		5635±327	8±2	1420±147	1851±56	7.2±0.3	121±5
G20-6#1	44.3±2.5	0.81±0.01	7±1		4169±242	42±3	1486±154	1557±59	8.4±0.3	120±5
G20-6#2	44.1±2.5	0.83±0.01	7±1	0.08±0.05	4167±242	45±4	1488±154	1458±57	7.4±0.3	117±5

Sample	MgO (%)	Al$_2$O$_3$ (%)	Sc	TiO$_2$ (%)	Cr$_2$O$_3$	V$_2$O$_3$	MnO	NiO	FeO (%)	Co
G20-7	46.3±2.6	0.25±0.01	4±1		2883±167	9±2	1715±178	1436±59	7.9±0.4	130±6
G20-8#1	39.3±2.2	0.26±0.01	4±1		6730±391	19±3	1809±187	1286±59	9.1±0.3	123±5
G20-8#2	40.6±2.2	0.28±0.01	4±1		7208±418	20±3	1883±192	1388±58	9.8±0.4	130±6
G20-9	40.7±2.2	0.22±0.01	4±1		4292±249	16±3	1628±169	1304±55	9.4±0.4	129±6
G20-10	36.4±2.1	0.18±0.01	4±1		1367±79	6±2	1652±171	1323±56	10.8±0.5	115±5
G20-11	42.1±2.3	0.21±0.01	3±1		3540±205	7±2	1369±142	1827±57	7.7±0.3	122±5
G20-12	43.4±2.5	0.21±0.01	4±1		2245±130	6±3	1797±186	1143±55	9.2±0.4	131±6
G20-13	44.9±2.5	0.31±0.01	4±1		9407±546	20±3	1515±157	2186±63	8.5±0.4	122±5
G20-14	45.9±2.6	0.24±0.01	4±1		1866±108	9±2	1803±187	1794±57	9.7±0.4	124±5
L23-1	12.9±1.2	3.7±0.1	97±12	1.24±0.07	87±7	1174±5	1955±199		22.7±0.7	83±3
L23-2	11.9±1.2	4.38±0.04	94±11	1.50±0.09	22±4	1738±7	2084±212		20.5±0.7	76±3
L24-1	11.4±1.2	3.12±0.02	86±10	1.17±0.07	35±4	1185±5	1958±199		19.9±0.7	67±3
L24-2	9.8±1.2	3.83±0.02	68±8	2.05±0.09	686±40	2229±10	2392±243		36.8±0.8	116±5
G26-4	44.2±2.5	0.42±0.01	4±1		2.8±0.2%	45±3	1764±183	2391±65	10.1±0.4	136±6
G26-4#2	44.2±2.4	0.43±0.01	3.7±0.4		3.11±0.18%	51±3	1823±189	3513±74	10.2±0.4	126±6
G26-4A	17.2±4.1	4.51±0.03	7.7±0.9	0.45±0.08		450±10	3358±342	5046±101	24.5±0.6	341±14
G26-6#1	11.3±1.2	6.19±0.04	82±10	1.48±0.09	12±4	1524±16	1786±185		20.2±0.7	79±3
G26-6#2	10.8±1.2	6.3±0.1	83±10	1.52±0.09	18±4	1562±17	1902±197		20.2±0.7	80±3
G27-3	43.3±2.5	0.25±0.01	4±1		4534±263	10±2	1740±180	1455±52	8.6±0.4	125±5

Sample	MgO (%)	Al$_2$O$_3$ (%)	Sc	TiO$_2$ (%)	Cr$_2$O$_3$	V$_2$O$_3$	MnO	NiO	FeO (%)	Co
H28-2	19.9±1.4	1.23±0.01	62±7	0.17±0.04	1777±103	88±5	1026±106	256±65	3.8±0.5	45±2
OM-2	44.5±2.5	0.25±0.01	4±1		4505±261	14±3	1922±195	1356±57	10.1±0.4	141±6
H3-3A	46.2±2.6	0.52±0.01	4.5±0.5		1.64±0.09%	47±4	2318±240	2989±69	11.4±0.4	154±6
H3-3B	28.7±1.9	3.01±0.02	6.2±0.7	0.33±0.01		291±8	2737±278	3609±94	18.1±0.6	551±23
H4-2A	20.4±1.5	3.99±0.03	1.2±0.1	0.65±0.08		594±11	3593±365	4655±102	30.1±0.6	319±13
H4-8	49.5±2.8	0.21±0.01	4±1		1282±75	3±2	1616±167	1655±55	8.3±0.3	134±6
G5-1	7.6±1.2	1.5±0.1	37±4	1.04±0.06	34±4	793±3	2031±211		11.9±0.5	37±2
H6-6#1		0.41±0.01	0.9±0.1		20±2	17±2	18±5		1.5±0.2	106±4
H6-6#2		0.43±0.01	0.6±0.1		17±2	18±2	17±5		1.3±0.2	98±4
S12-2	11.8±1.2	3.54±0.02	91±11	1.77±0.04	37±5	2009±9	2198±224		27.5±0.2	93±4
S12-3	12.5±1.2	3.59±0.02	101±12	1.28±0.08		1336±2	1867±193		20.2±0.8	83±3
S12-4	13.2±1.2	4.32±0.04	96±12	1.75±0.07	21±2	2024±9	2286±233		25.6±0.8	85±4
S15-7#1	10.9±1.2	3.17±0.02	96±12	1.07±0.09	98±8	1378±15	1795±186		21.9±0.8	190±8
S15-7#2	11.3±1.2	3.18±0.02	88±11	1.10±0.07	88±7	1381±15	1788±185		20.8±0.7	166±7

XIV. APPENDIX VII: MINERAL ASSEMBLAGES OBSERVED IN TULAMEEN SAMPLES

Thin sections, polished thin sections, and polished blocks of all samples analyzed for the PGE were examined. This table gives the mineral assemblages observed by lithology. An explanation of the abbreviations used in this appendix is given before the Introduction of the thesis.

110

Dunite and peridotite mineral assemblages

Sample	ol	sp	cb	cpx	at	tc	mt	ct	py	po	pn	vi	ilm	rt	hm	cp
R3-5	*	*	*	*												
R3-7	*	*	*	*												
R3-10¹	*	*	*		*	*	*	*	*	*	*	*				
R3-13	*	*	*	*												
R3-14	*	*	*	*												
R4-1	*	*	*				*	*	*		*	*				
T8-1²	*	*	*		*		*	*	*	*	*	*	*	*		
D14-1¹	*	*	*					*	*							
T15-2	*	*	*													
G16-10	*	*	*			*										
B18-1	*	*	*		*				*							
G20-5	*	*	*	*	*		*	*								*
G20-6¹	*	*	*	*	*		*	*	*	*	*	*			*	
G20-7¹	*	*	*													
G20-11	*	*	*		*											
G20-13	*	*	*				*	*	*		*	*				
G20-14¹	*	*	*				*	*	*		*	*				
G27-3¹	*	*	*	*								*				

Sample	ol	sp	cb	cpx	at	tc	mt	ct	py	po	pn	vi	ilm	rt	hm	cp
OM-2	*	*	*													

[1]in polished thin section
[2]dunite breccia in polished section

Serpentinite and serpentinite-dunite mineral assemblages

Sample	ol	sp	cb	tc	at	mt	ct	cp	py	pn	vi	ilm	po
R3-11[1]		*	*			*	*	*	*	*	*	*	
T15-5[1]		*	*			*	*		*	*	*		*
T15-7[1]		*	*	*		*	*		*	*	*		
G20-8[1]		*	*			*	*	*	*	*	*		
G20-9	*	*	*		*								
G20-10		*	*										
G20-12	*	*	*										

[1] in polished thin section

Olivine clinopyroxenite and clinopyroxenite mineral assemblages

Sample	ol	sp	cb	cpx	hb	at	mt	ct	py
T16-4[1]	*	*	*	*	*		*	*	*
G20-2	*	*	* |	*		*			
G26-4	*	*	*	*	vi/pn	*	*	*	*
L5-2		*	pl	*	tc	*			
L5-3		*		*	tc	*			

[1]in polished thin section

Hornblende clinopyroxenite and hornblendite mineral assemblages

Sample	cb	cpx	at	pl	qz	hb	cl	ep	sp	bt	rt	mt	py	cp	ilm	Hm
R4-9	*	*	*	*	*	*	*	*				*				
G20-1[1]		*	*	*	*	*	*		*			*	*		*	*
G26-6[1]		*				*										
G5-1	*	*	*	*	*	*	*			*		*	*	*		
L5-13	tc	*	*			*										
S15-7[1]	*	*	*		*	*	*				*	*	*	*	*	*
L23-1		*	*			*						*				
L23-2	tc	*	*	*		*						*				
L24-1	tc	*				*						*				
L24-2	tc	*			*	*			*			*				
S12-2	tc	*	*			*						*				
S12-3	tc		*			*						*				
S12-4	tc															

[1] in polished thin section

Syenogabbro and syenodiorite mineral assemblages

Sample	cpx	at	tc	pl	hb	cl	ep	qz	Kf	cb	mt	py
R4-5	*	*	*	*	*	*	*					
R4-7		*		*		*	*	*	*			
R4-8		*		*	*	*	*	*		*		
B4-3[1]	*		bt	*	*	*	*	*	*		*	*
L5-5	*			*		*	*	*				

[1] in polished thin section

Mineral assemblages for chromitite, Nicola Group, and one quartz vein analyzed

Sample	cpx	at	tc	pl	qz	br	cl	ep	sp	ct	mt	pn	vi	PGM
R3-4[1]	*	*	*	*	*	*	*	*						
H6-6[4]					*		*							
D14-7[?]										cp	py			
G16-12[2]									*	*	*	*	*	*
G26-4A[3]	*	*		*	*	*		*	*	*	*	*	*	
H3-3A[2]									*	*	*	*	*	
H3-3B[2]									*	*				
H4-2A[2]									*	*	*	*	*	*

[1] Nicola Group in thin section
[2] chromitite in polished block
[3] chromitite in polished thin section
[4] quartz vein from the hornblende clinopyroxenite on Olivine Mountain

XV. APPENDIX VIII: SOURCE LISTING OF THE FORTRAN PROGRAM DATRED

This program was written by the author for use in the comparator and absolute NAA of the PGE.

```
 1   C     ***DATRED*** A FORTRAN PROGRAM TO REDUCE NEUTRON ACTIVATION ANALYSIS
 2   C     DATA FOR THE NOBLE METALS. THIS PROGRAM IS BASED ON THE SO-CALLED
 3   C     ABSOLUTE METHOD FOR ALL BUT RH AND PD, WHICH ARE DONE BY COMPARATOR.
 4   C     THE NUCLEAR DATA ARE IN AN MTS FILE CALLED NUCDAT, WHICH IS DEVICE 7.
 5   C     THE RAW DATA FOR REDUCTION ARE IN ANY MTS FILE SPECIFIED AS DEVICE 8
 6   C
 7   C     THIS PROGRAM WRITTEN BY *** ROBERT M. ST. LOUIS ***
 8   C
 9   C     AN EXAMPLE OF THE FORM..THE INPUT DATA IN FILE 8 MUST TAKE
10   C     IS AS FOLLOWS (ASSUME ALL LINES BEGIN IN COLUMN 1):
11   C
12   C
13   C     EXAMPLE UNIT 8          (SAMPLE ID)
14   C     50.00001.44E4           (SAMPLE MASS=50 G., IRRADIATED 4HRS.)
15   C     3600..3604.             (LIVE TIME AND CLOCK TIME IN SEC.)
16   C     211282093000            (INTO REACTOR AT 9:30 A.M. 21DEC82)
17   C     291282134500            (COUNTING BEGAN AT 1:45 P.M. 29DEC82)
18   C     412.000362487.0.3       (412 KEV PEAK, WITH 362487 COUNTS IN
19   C                             AREA, AND 0.3% ERROR ASSOCIATED WITH
20   C                             THIS PEAK)
21   C     (OTHER LINES OF RAW DATA, AS THE ONE STARTING WITH 412 ABOVE)
22   C     777.                    (END OF SAMPLE CHARACTER; IF THIS IS
23   C                             THE LAST SAMPLE, ENTER 999. AT THIS
24   C                             POINT IN THE DATA FILE)
25   C
26   C
27         DATA D/'D'/
28         DATA H/'H'/
29         DATA A/'A'/
30         DIMENSION PAR(20), RESULT(20), GRAMER(20), PPM(20), PPMERR(20)
31         REAL NUCDAT(8,16)
32         REAL LAMBDA
33         REAL KEV
34         INTEGER*4 SAMPID(4)
35   C
36   C     THIS NEXT STEP READS NUCDAT INTO THE ACTIVE FILE
37   C     (NUCDAT IS THE MTS FILE CONTAINING THE NUCLEAR DATA USED IN THE
38   C     CALCULATIONS; IT IS SPECIFIED AS DEVICE 7)
39   C
40         DO 10 JROW=1,8
41         READ(7,500) (NUCDAT(JROW,JCOL),JCOL=1,16)
42     10  CONTINUE
43   C
44   C     READING IN OF RAW DATA BEGINS--SAMPLE ID, ETC.
45   C     (THESE DATA ARE CONTAINED IN ANY MTS FILE SPECIFIED AS DEVICE 8)
46   C
```

```
47          20 READ(8,510) SAMPID
48             READ(8,520) SMPMAS,TACT
49             READ(8,530) TLIVE,TCLOCK
50             BUSY=100.0-((TLIVE/TCLOCK)*100.0)
51   C
52   C   CALCULATION OF COOLING INTERVAL
53   C
54             CALL COOL(TCOOL,IDAYC,MONCT,IYEARC)
55             TCOOL=TCOOL-TACT
56             WRITE(6,580)
57             WRITE(6,540) SAMPID
58             WRITE(6,560) IDAYC,MONCT,IYEARC,TLIVE,BUSY
59             WRITE(6,600)
60             WRITE(6,600)
61             WRITE(6,690)
62             WRITE(6,610)
63             WRITE(6,620)
64   C
65   C   READING IN OF KEV,AREA, AND ERROR BEGINS--TOP OF LOOP
66   C
67             DO 9990 JCNT=1,10
68             READ(8,640) KEV,AREA,ERROR
69   C
70   C   CHECK FOR END OF SAMPLE OR END OF FILE
71   C
72             IF(KEV.EQ.777) GOTO 23
73             IF(KEV.EQ.999) GOTO 23
74             GOTO 29
75   C
76   C   CALCULATION OF WTD. MEANS IF TWO PEAKS FOR SAME NUCLIDE RECORDED
77   C
78          23 ICNT=JCNT-1
79             WRITE(6,600)
80             WRITE(6,670)
81             DO 26 ME=1,ICNT
82             IT=ME+1
83             IF(IT.GT.ICNT) GOTO 28
84          DO 25 MY=IT,ICNT
85             IF(PAR(ME).EQ.PAR(MY)) GOTO 27
86          25 CONTINUE
87             GOTO 26
88          27 R1=RESULT(ME)
89             R2=RESULT(MY)
90             G1=GRAMER(ME)
91             G2=GRAMER(MY)
92             P1=PPM(ME)
```

```
 93        P2=PPM(MY)
 94        E1=PPMERR(ME)
 95        E2=PPMERR(MY)
 96        CALL XBARS(R1,R2,G1,G2,P1,P2,E1,E2,XGRAM,XGMER,XPPM,XPPMER)
 97        WRITE(6,680) PAR(ME),XGRAM,XGMER,XPPM,XPPMER
 98  26    CONTINUE
 99  28    IF(KEV.EQ.999) GOTO 9999
100        GOTO 20
101  C
102  C     NUCLEAR DATA AND VARIABLE ASSIGNMENT BEGINS
103  C
104  29    DO 30 JROW=1,8
105        DO 40 JCOL=8,10
106        IF(KEV.EQ.NUCDAT(JROW,JCOL)) GOTO 50
107  40    CONTINUE
108  30    CONTINUE
109  50    PAR(JCNT)=NUCDAT(JROW,1)
110        ENT=NUCDAT(JROW,2)
111        PABUND=NUCDAT(JROW,3)
112        PMASS=NUCDAT(JROW,4)
113        HAFLIF=NUCDAT(JROW,5)
114        UNITS=NUCDAT(JROW,6)
115        SIGMA=NUCDAT(JROW,7)
116        GAMMA=NUCDAT(JROW,JCOL)
117        NCOL=JCOL+3
118        YIELD=NUCDAT(JROW,NCOL)/100.0
119        MCOL=NCOL+3
120        EFFIC=NUCDAT(JROW,MCOL)/100.0
121        FLUX=1.00E12
122        IF(UNITS.EQ.A) HAFLIF=HAFLIF*(6.00E1)
123        IF(UNITS.EQ.H) HAFLIF=HAFLIF*(3.60E3)
124        IF(UNITS.EQ.D) HAFLIF=HAFLIF*(2.40E1)*(3.60E3)
125  C
126  C     CALCULATION OF NUCLIDE MASS BEGINS
127  C
128        LAMBDA=0.693/HAFLIF
129        TIRR=(1-(EXP(-(LAMBDA*TACT))))
130        COLD=(EXP(-(LAMBDA*TCOOL)))
131        COUNT=(1-(EXP(-(LAMBDA*TCLOCK))))
132  C
133  C     DEAD TIME CORRECTION
134  C
135        CLIVE=(1-(EXP(-(LAMBDA*TLIVE))))
136        CCLOCK=(1-(EXP(-(LAMBDA*TCLOCK))))
137        CAREA=AREA*(TCLOCK/TLIVE)+(CLIVE/CCLOCK)
138        IF(JROW.EQ.6) GOTO 55
```

```
139        IF(JROW.EQ.8) GOTO 55
140        GOTO 60
141  C
142  C  CORRECTION FOR PULSE PILE-UP (RH AND PD ONLY)
143  C
144     55 CAREA=CAREA*(1-(-1.481*((TCLOCK/TLIVE)-1)))
145  C
146        IF(JROW.EQ.6) GOTO 70
147        IF(JROW.EQ.8) GOTO 80
148     60 UPPER=LAMBDA*CAREA*PMASS
149        BOTTOM=SIGMA*FLUX*(6.023E23)*PABUND*YIELD*EFFIC
150        RESULT(JCNT)=UPPER/(BOTTOM*TIRR*COLD*COUNT)
151        RESULT(JCNT)=RESULT(JCNT)*(1.0E6)
152  C
153  C  YIELD CORRECTION FOR OS
154  C
155        IF(KEV.EQ.129) GOTO 63,
156        GOTO 95
157     63 RESULT(JCNT)=RESULT(JCNT)*0.4926
158        GOTO 95
159     70 IF(KEV.EQ.51) GOTO 75
160        IF(KEV.EQ.77) GOTO 77
161        RESULT(JCNT)=CAREA/3401.2
162        GOTO 92
163     75 RESULT(JCNT)=CAREA/50193.8
164        GOTO 90
165     77 RESULT(JCNT)=CAREA/3300.0
166        GOTO 93
167     80 RESULT(JCNT)=CAREA/455.245
168  C
169  C  YIELD CORRECTION FOR PD
170  C
171        RESULT(JCNT)=RESULT(JCNT)*1.4056
172        GOTO 94
173  C
174  C  CALCULATION OF ERRORS IN GRAMS AND PPM
175  C
176  C
177  C  TOTAL ERROR FOR RH AT 51 KEV
178  C
179     90 TTLERR=1.96*(SQRT((0.04)+(3.306**2.0)+(ERROR**2.0)))
180        GOTO 160
181  C
182  C  TOTAL ERROR FOR RH AT 97 KEV
183  C
184     92 TTLERR=1.96*(SQRT((1.4**2.0)+(3.306**2.0)+(ERROR**2.0)))
```

```
185  C        GOTO 160
186  C
187  C  TOTAL ERROR FOR RH AT 77 KEV
188  C
189  93  TTLERR=1.96*(SQRT((1.2**2.0)+(3.306**2.0)+(ERROR**2.0)))
190      GOTO 160
191  C
192  C  TOTAL ERROR FOR PD
193  C
194  94  TTLERR=1.96*(SQRT((0.5**2.0)+(3.306**2.0)+(ERROR**2.0)
195      /+(4.37)))
196      GOTO 160
197  95  IF(KEV.EQ.158) GOTO 100
198      IF(KEV.EQ.208) GOTO 110
199      IF(KEV.EQ.308) GOTO 120
200      IF(KEV.EQ.296) GOTO 125
201      IF(KEV.EQ.468) GOTO 130
202      IF(KEV.EQ.412) GOTO 140
203      IF(KEV.EQ.129) GOTO 150
204      GOTO 160
205  C
206  C  RU TOTAL ERROR
207  C
208      TTLERR=1.96*(SQRT((ERROR**2.0)+(0.014**2.0)))
209      GOTO 160
210  C
211  C  PT TOTAL ERROR AT 158 KEV
212  C
213  100 TTLERR=1.96*(SQRT((ERROR**2.0)+0.029))
214      GOTO 160
215  C
216  C  PT TOTAL ERROR AT 208 KEV
217  C
218  110 TTLERR=1.96*(SQRT((ERROR**2.0)+0.078))
219      GOTO 160
220  C
221  C  IR TOTAL ERROR AT 308 KEV
222  C
223  120 TTLERR=1.96*(SQRT((ERROR**2.0)+(0.011**2.0)))
224      GOTO 160
225  C
226  C  IR TOTAL ERROR AT 296 KEV
227  C
228  125 TTLERR=1.96*(SQRT((ERROR**2.0)+(0.013**2.0)))
229      GOTO 160
230  C  IR TOTAL ERROR AT 468 KEV
```

```
231  C
232  130 TTLERR=1.96*(SQRT((ERROR**2.0)+(0.005**2.0)))
233      GOTO 160
234  C
235  C   AU TOTAL ERROR
236  C
237  140 TTLERR=1.96*(SQRT((ERROR**2.0)+(0.003**2.0)+(2.0**2.0)))
238      GOTO 160
239  C
240  C   DS TOTAL ERROR
241  C
242  150 TTLERR=1.96*(SQRT((ERROR**2.0)+(0.050**2.0)+(116.42)))
243  160 GRAMER(JCNT)=RESULT(JCNT)*TTLERR*0.01
244      BIGERG=BIGERG+(GRAMER(JCNT)**2.0)
245      PPM(JCNT)=(RESULT(JCNT)/SMPMAS)
246      PPMERR(JCNT)=PPM(JCNT)*TTLERR*0.01
247      BIGERP=BIGERP+(PPMERR(JCNT)**2.0)
248  C
249  C   WRITE RESULT FOR THE INDIVIDUAL LINE OF INPUT DATA
250  C   AND GO BACK TO READ THE NEXT LINE OF INPUT DATA
251  C
252  190 IAREA=AREA
253      MAREA=CAREA
254      WRITE(6,660) PAR(JCNT),ENT,KEV,RESULT(JCNT),GRAMER(JCNT),
255     /PPM(JCNT),PPMERR(JCNT),IAREA,MAREA
256  9990 CONTINUE
257  9999 WRITE(6,580)
258      STOP
259  500 FORMAT(2A4,F5.3,F9.5,F5.2,A1,E8.6,3F5.1,3F4.1,3F5.3)
260  510 FORMAT(4A4)
261  520 FORMAT(F7.4,E8:6)
262  530 FORMAT(2F7.1)
263  540 FORMAT(T2,'SAMPLE:',T12,4A4)
264  560 FORMAT(T2,'COUNTED ON',T13,I2,T15,'/',T16,I2,T18,'/',
265     CT19,I2,T22,'FOR',T26,F6.0,T33,'SECONDS',T41,'WITH BUSY=',
266     CT52,F5.2,T58,'%')
267  580 FORMAT('1')
268  600 FORMAT(' ')
269  610 FORMAT(T66,'COUNTS')
270  620 FORMAT(T2,'ISOTOPE',T12,'KEV',T24,'MASS (UG)',T45,
271     /'PPM',T61,'RAW',T71,'CORRECTED')
272  640 FORMAT(F4.0,F10.0,F4.1)
273  660 FORMAT(T2,2A3,T12,F4.0,T19,F7.2,T27,'+/-',T30,F5.2,
274     CT37,F7.4,T45,'+/-',T49,F6.4,T58,I9,T71,I9)
275  670 FORMAT(T2,'WTD. MEANS FOR DUAL PEAKS ARE GIVEN BELOW:')
276  680 FORMAT(T2,A3,T19,F7.2,T27,'+/-',T30,F5.2,T37,F7.4,
```

```
277         /T45,'+/-',T49,F6.4)
278   690 FORMAT(T23,'RESULTS AT 95% CONFIDENCE LIMITS')
279       END
280   C
281   C   SUBROUTINE TO CALCULATE COOLING INTERVAL FROM DATES AND
282   C   TIMES OF IRRADIATION AND COUNTING (RETURNS VALUE IN SEC.)
283   C
284       SUBROUTINE COOL(CHILL,IDAYC,MONCT,IYEARC)
285       MONTH1=0
286       MONTH2=0
287       MONTHS=0
288       DIMENSION MONTH(12)
289   C
290   C   READS IN DATES AND TIMES OF IRRADIATION AND COUNTING
291   C
292       READ(8,60) IDAY,MONIR,IYEAR,IHOUR,IMIN,ISEC
293       READ(8,60) IDAYC,MONCT,IYEARC,IHOURC,IMINC,ISECC
294       MYEAR=IYEARC-IYEAR
295       IF(MONIR.EQ.1) MONLEN=31
296       IF(MONIR.EQ.2) MONLEN=29
297       IF(MONIR.EQ.3) MONLEN=31
298       IF(MONIR.EQ.4) MONLEN=30
299       IF(MONIR.EQ.5) MONLEN=31
300       IF(MONIR.EQ.6) MONLEN=30
301       IF(MONIR.EQ.7) MONLEN=31
302       IF(MONIR.EQ.8) MONLEN=31
303       IF(MONIR.EQ.9) MONLEN=30
304       IF(MONIR.EQ.10) MONLEN=31
305       IF(MONIR.EQ.11) MONLEN=30
306       IF(MONIR.EQ.12) MONLEN=31
307       MONTH(1)=31
308       MONTH(2)=29
309       MONTH(3)=31
310       MONTH(4)=30
311       MONTH(5)=31
312       MONTH(6)=30
313       MONTH(7)=31
314       MONTH(8)=31
315       MONTH(9)=30
316       MONTH(10)=31
317       MONTH(11)=30
318       MONTH(12)=31
319       IF(MONIR.EQ.MONCT) GOTO 20
320       IDAYCT=MONLEN-IDAY
321       J=MONCT-1
322       IF(J.EQ.0) J=13
```

```
323        K=MONIR+1
324        IF(K.EQ.J) GOTO 20
325        MT=J-K
326        IF(MT.EQ.-1) GOTO 30
327        IF(MT.LE.O) GOTO 20
328        IF(K.EQ.13) K=1
329        DO 10 M=K,J
330        MONTHS=MONTHS+MONTH(M)
331     10 CONTINUE
332        GOTO 30
333     20 MONTHS=0
334        IT=MONCT-MONIR
335        IF(IT.EQ.-11) GOTO 25
336        IDAYS=(IDAYC-1)-IDAY
337        GOTO 40
338     30 IDAYS=MONTHS+IDAYCT+(IDAYC-1)
339     25 IDAYS=(IDAYC-1)+(MONLEN-IDAY)
340     40 SECOND=IDAYS*(2.40E1)+(3.60E3)
341     50 HOURIR=(23-IHOUR)*(3.60E3)
342        MINIR=(59-IMIN)*(6.00E1)
343        MINCT=IMINC*(6.00E1)
344        SECIR=(60-ISEC)*(1.00EO)
345        SECCT=ISECC*(1.00EO)
346        DAYIR=HOURIR+MINIR+SECIR
347        DAYCT=HOURCT+MINCT+SECCT
348        CHILL=DAYIR+DAYCT+SECOND
349        RETURN
350     60 FORMAT(3I2,3I2)
351        END
352
353     C
354     C  SUBROUTINE TO CALCULATE WEIGHTED MEANS FROM TWO PEAKS FOR SAME
355     C  NUCLIDE (I.E., 158 AND 208 KEV FOR 199 AU)
356     C
357        SUBROUTINE XBARS(R1,R2,G1,G2,P1,P2,E1,E2,XGRAM,XGMER,XPPM,
358       /XPPMER)
359        GE1=(1/(G1**2.0))
360        GE2=(1/(G2**2.0))
361        PE1=(1/(E1**2.0))
362        PE2=(1/(E2**2.0))
363        SUMGE=GE1+GE2
364        SUMPE=PE1+PE2
365        WR1=R1*GE1
366        WR2=R2*GE2
367        WP1=P1*PE1
368        WP2=P2*PE2
```

```
369     SUMWR=WR1+WR2
370     SUMWP=WP1+WP2
371     XGMER=SQRT(1/SUMGE)
372     XPPMER=SQRT(1/SUMPE)
373     XGRAM=SUMWR/SUMGE
374     XPPM=SUMWP/SUMPE
375     RETURN
376     END
```

End of file

XVI. APPENDIX IX: OVERLAP COEFFICIENTS GENERATED FOR USE WITH ENERGY DISPERSIVE MICROPROBE ANALYSIS OF THE PGMs

The overlap coefficients given in this appendix were generated using pure element spectra via the program EDATA2 (Smith and Gold, 1979). An element that appears along the x-axis of the table is overlapped by an element on the y-axis by n percent (i. e., Pt is overlapped by S by 5.51 percent; M(a), L(a), and K(a) refer to $M\alpha$, $L\alpha$, and $K\alpha$ X-rays respectively).

	Pt M(a)	Ir M(a)	Os M(a)	Pd L(a)	Rh L(a)	Ru L(a)
Pt M(a)	100	97.97	42.48	1.28	1.54	2.16
Ir M(a)	50.29	100	94.34	1.17	1.37	2.02
Os M(a)	14.28	51.64	100	1.02	1.25	1.79
Pd L(a)	0.10	-----	-----	100	64.30	16.04
Rh L(a)	0.98	0.50	-----	13.98	100	65.07
Ru L(a)	0.27	0.88	0.66	5.64	15.12	100
Sb L(a)	0.24	0.29	0.18	1.01	0.06	0.08
As L(a)	1.35	1.92	2.36	0.32	0.30	0.45
S K(a)	5.51	2.67	0.72	1.68	4.10	6.70
Fe K(a)	0.08	0.18	0.07	0.06	0.08	0.11
Ni K(a)	0.03	0.10	0.05	0.04	0.02	----
Cu K(a)	0.14	0.46	0.09	0.04	0.04	0.01
Cr K(a)	0.17	0.24	0.16	0.11	0.19	0.13
Mn K(a)	0.15	0.22	0.12	0.21	0.10	0.04